

1-1-1984

A model for the climatic behavior of water on Mars.

Stephen Mark Clifford
University of Massachusetts Amherst

Follow this and additional works at: https://scholarworks.umass.edu/dissertations_1

Recommended Citation

Clifford, Stephen Mark, "A model for the climatic behavior of water on Mars." (1984). *Doctoral Dissertations 1896 - February 2014*. 1781.
https://scholarworks.umass.edu/dissertations_1/1781

This Open Access Dissertation is brought to you for free and open access by ScholarWorks@UMass Amherst. It has been accepted for inclusion in Doctoral Dissertations 1896 - February 2014 by an authorized administrator of ScholarWorks@UMass Amherst. For more information, please contact scholarworks@library.umass.edu.

UMASS/AMHERST



312066 0024 4060 1

A MODEL FOR THE CLIMATIC BEHAVIOR
OF WATER ON MARS.

A Dissertation Presented

By

STEPHEN MARK CLIFFORD

Submitted to the Graduate School of the
University of Massachusetts in partial fulfillment
of the requirements for the degree of

DOCTOR OF PHILOSOPHY

May 1984

Department of Physics and Astronomy



Stephen Mark Clifford

All Rights Reserved

National Aeronautics and Space Administration

NSG 7405

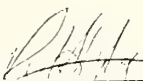
A MODEL FOR THE CLIMATIC BEHAVIOR
OF WATER ON MARS.

A Dissertation Presented

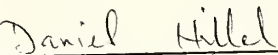
By

STEPHEN MARK CLIFFORD

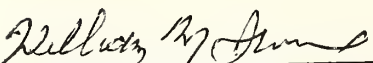
Approved as to style and content by:



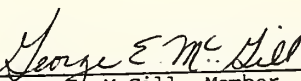
Robert L. Huguenin
Chairperson of Committee



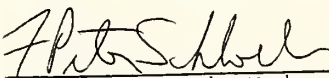
Daniel Hillel, Member




William M. Irvine, Member



George E. McGill, Member



F. Peter Schloerb, Member



LeRoy F. Cook, Department Head
Department of Physics
and Astronomy

DEDICATION

To my wife, Julie, without whose love and support I would have given all this up long ago.

ACKNOWLEDGEMENTS

I am deeply indebted to Professor Robert Huguenin, who stimulated and encouraged much of my graduate research. His creativity, support, guidance, and friendship, provided the kind of environment that made this dissertation possible.

I thank Professor Daniel Hillel who provided me with the tools of a soil physicist. Despite his having inflicted me with what are, without question, some of the world's most ghastly puns, he is a much respected friend.

I am grateful to Professors George McGill, William Irvine, Peter Schloerb, and Donald Wise, for having given me the opportunity to learn something of the diversity of disciplines encompassed by planetary science. Their consideration, encouragement, and advice, has been much appreciated throughout my graduate education. I would also like to express my gratitude to Professor David Van Blerkhom whose personal interest and advocacy helped save much time, anguish, and very likely a scientific career.

Thanks are due Lee Allison, Michael Carr, Mark Cintala, Fraser Fanale, Tom Gold, Matt Golembek, Wendy Hale, John Hollin, Laurie Johansen, Karen Miller, Mary Ellen Miller, Robert Miller, Peter Mouginiis-Mark, Rick Newton, David Ostendorf, Lisa Rossbacher, Peter Schultz, and Jose Valdez, for providing much inspiration, many helpful conversations, and reviews of some of the chapters contained in this dissertation. Additional thanks go to both Elliot Morris (at USGS

Flagstaff) and the National Space Science Data Center for providing a number of the photographs used in this work. I am also indebted to Kevin Burke and the staff of the Lunar and Planetary Institute, whose financial and technical support was much appreciated during the preparation of the final draft of this dissertation.

Throughout my long and somewhat tortuous academic career my parents have given me much love and encouragement. I hope that this dissertation is at least a partial reward for their unending confidence and patience.

In ancient days two aviators procured to themselves wings. Daedalus flew safely through the middle air and was duly honored on his landing. Icarus soared upwards to the sun till the wax melted which bound his wings and his flight ended in fiasco The classical authorities tell us, of course, that he was only 'doing a stunt'; but I prefer to think of him as the man who brought to light a serious constructional defect in the flying-machines of his day.

So, too, in science. Cautious Daedalus will apply his theories where he feels confident they will safely go Icarus will strain his theories to the breaking-point till the weak joints gape. For the mere adventure? Perhaps partly, that is human nature. But if he is destined not yet to reach the sun and solve finally the riddle of its construction, we may at least hope to learn from his journey some hints to build a better machine.

Sir Arthur Eddington

ABSTRACT

A Model for the Climatic Behavior of Water on Mars

May, 1984

Stephen M. Clifford, B.A., Windham College

M.S., University of Massachusetts

Ph.D., University of Massachusetts

Directed by: Professor Robert L. Huguenin

Present climatic conditions on Mars preclude the existence of ground ice in equilibrium with the atmosphere within the latitude band of $\pm 40^\circ$. Yet, various lines of morphologic evidence suggest that substantial quantities of H_2O have survived in the equatorial regolith for billions of years. The popular explanation for this apparent contradiction has been that equatorial ground ice is a relic of a substantially different climate that existed very early in Martian geologic history. To evaluate this hypothesis, the stability of equatorial ground ice is examined on the basis of our current understanding of the physical properties of the Martian regolith. The results of this analysis suggest that any ground ice, emplaced earlier than 3.5 billion years ago, may have long since been lost by sublimation to the atmosphere. In light of these results, alternative explanations for the long-term survival of equatorial ground ice are considered. Chief among these is the possibility of replenishment from

subsurface sources of H_2O . Such replenishment may occur in response to the Martian geothermal gradient, whereby H_2O is driven from the warmer (higher vapor pressure) depths to the colder (lower vapor pressure) near-surface regolith. In addition to ground ice replenishment, the ultimate fate of H_2O sublimed from equatorial ground ice is also considered. Since mean annual equatorial temperatures exceed the frost-point temperature of the atmosphere by ≥ 20 K, any excess H_2O released to the atmosphere will eventually be cold-trapped at the poles. Should the deposition of this H_2O continue, the polar deposits may eventually reach the thickness required for geothermal melting to begin at their base. Given a planetary inventory of H_2O sufficient to result in the formation of a global-scale subpermafrost groundwater system, the deep percolation of basal meltwater will result in the rise of the subpolar water table in the form of a groundwater mound. The gradient in hydraulic head created by the presence of the groundwater mound may then drive the flow of groundwater to the equator, thus providing the source from which equatorial ground ice may ultimately be replenished.

TABLE OF CONTENTS

DEDICATION	iv
ACKNOWLEDGEMENTS	v
ABSTRACT	viii
LIST OF TABLES	xii
LIST OF ILLUSTRATIONS	xiii
CHAPTER	
I. INTRODUCTION	1
II. THE STABILITY OF GROUND ICE IN THE EQUATORIAL REGION OF MARS	6
A. Introduction	6
B. The Regolith Model	10
1. The origin and extent of the Martian megaregolith	11
2. Particle and aggregate sizes	12
3. Porosity and pore size distribution	19
4. The pore size distribution model	27
C. The Diffusion Model	30
D. Initial Assumptions and Numerical Procedure	39
E. Results and Analysis	45
1. Temperature effects	48
2. Pore size effects	49
F. Discussion	56
1. Depth of burial and the Martian geothermal gradient	56
2. Porosity	60
3. Adsorption and surface diffusion	64
4. Climatic change	72
G. Summary	73
H. Conclusion	78
I. Notation	79
III. MECHANISMS FOR THE SUBSURFACE REPLENISHMENT OF EQUATORIAL GROUND ICE ON MARS	82
A. Introduction	82
B. Possible evidence of ground ice replenishment	84
C. Processes of replenishment	95
1. Hydrothermal convection	96
2. Shock-induced transport	96
3. Thermal moisture movement	101
E. Conclusion	111

IV. POLAR BASAL MELTING ON MARS	114
A. Introduction	114
B. A geologic summary of the Martian polar terrains	117
1. Composition	117
2. Geology	120
3. Origin and evolution	125
C. Basal Melting	132
1. Thermal calculations	136
2. Flow calculations	143
D. Discussion	161
1. Storage of a primitive Martian ice sheet	161
2. Origin of Chasma Boreale	163
3. Polar basal lakes as possible isolated habitats of primitive Martian life	174
4. Basal melting at temperate latitudes	176
5. The mass balance of the polar terrains	181
6. A model for the climatic behavior of H ₂ O	186
E. Conclusion	187
F. Notation	191
V. A MODEL FOR THE CLIMATIC BEHAVIOR OF WATER ON MARS	193
A. Introduction	193
1. The atmospheric equilibrium model	194
2. The fossil ground ice model	197
3. The subpermafrost groundwater model	200
B. The Martian Megaregolith	203
1. Origin and structure	203
2. Porosity profile and total pore volume	205
C. Regolith H ₂ O on Mars	212
1. The emplacement of regolith H ₂ O	212
2. Extent of the cryosphere	215
3. Saturated thickness of groundwater	220
D. The Occurrence of Groundwater and the Permeability of the Earth's Crust	229
E. The Physical Requirements of Global Groundwater Flow	235
1. The growth of the groundwater mound	238
F. Conclusions	252
G. Notation	254
BIBLIOGRAPHY	256

LIST OF TABLES

2.1	Terrestrial Examples of Pore Size Distribution Models . . .	26
2.2	Model Pore Size Distribution Parameters	29
2.3	Lifetimes of a Buried Ground Ice Layer	47
4.1	Basal Melting Thicknesses	139
5.1	Latitudinal Variation of Cryosphere Thickness	217
5.2	Pore Volumes of Cryosphere for Various Combinations of Regolith Porosity and Melting Isotherm Temperature	218
5.3	Groundwater Mound Heights as a Function of Time	241
5.4	Minimum Regolith Permeability Requirements for Steady-State Flow	249

LIST OF ILLUSTRATIONS

2.1	Specific Surface Area and Equivalent Diameter of Fine Soil Component	17
2.2	Pore Size Distribution Models	23
2.3	Effective Diffusion Coefficient of H ₂ O in a Single Capillary Pore	37
2.4	Regolith-Ice Layer Model	41
2.5	Saturated Vapor Pressure of H ₂ O as a Function of Temperature	44
2.6	Differential and Cumulative Flux Curves for Pore Size Distribution Models	52
2.7	Temperature and H ₂ O Vapor Pressure as a Function of Regolith Depth	62
2.8	H ₂ O Surface Diffusion Coefficients as a Function of Heat Adsorption and Ambient Temperature	69
3.1	Martian Rampart Crater	86
3.2	Ground Ice Distribution Resulting from a Major Impact	88
3.3	A Rampart Crater within Two Earlier and Concentric Impact Features	91
3.4	A Rampart Crater along the Cratered Highland Boundary	94
3.5a	Possible Site of Hydrothermal Activity West of Olympus Mons	98
3.5b	Example of the Martian Valley Networks	100
3.6	Example of Water and Sediment Ejection from the Great Alaskan Earthquake of 1964	103
3.7	Philip and de Vries Model of Thermal Moisture Movement	106
3.8	Subpermafrost Convective Transport Driven by the Presence of a Geothermal Gradient	110
3.9	Subsurface Replenishment of Ground Ice within a Crater Interior	113
4.1	Extent of the Martian Cryosphere	116
4.2	Martian North Polar Cap as Seen by Viking	123
4.3	Mean Annual Polar Surface Temperatures as a Function of Obliquity	131
4.4	Possible Time Evolution of Basal Melting	134
4.5	Necessary Depths for Basal Melting	141
4.6	Frictional Heat Generated by Basal Sliding	145
4.7	Variation of Flow Law Constant with Temperature	149
4.8	Stress-Strain Relationships for Ice at 273 K and 263 K	151
4.9	Orowan Profiles of the Martian North and South Polar Caps	154
4.10	Effect of Basal Temperature on Polar Cap Profiles	156
4.11	Weertman Profiles of the Martian North and South Polar Caps	160
4.12	Model for the Removal and Storage of a Primitive Martian Ice Sheet	165
4.13a	Viking Photograph of Chasma Boreale (85°N, 0°W)	171
4.13b	Viking Photograph of Riva Valis (2°N, 43°W)	172

4.14	Basal Melting at Temperate Latitudes	179
4.15	Model for the Climatic Behavior of Water on Mars	189
5.1a	Atmospheric Equilibrium Model	196
5.1b	Fossil Ground Ice Model	199
5.1c	Subpermafrost Groundwater Model	201
5.2	Idealized Stratigraphic Column of the Martian	207
5.3	Theoretical Porosity Profiles of the Martian Crust	210
5.4	Saturated Thicknesses of Groundwater	220
5.5	Potential Latitudinal Variation and Relationship between Surface Topography, Ground Ice, and Groundwater	225
5.6	Possible Areal Distribution of Global Groundwater System	227
5.7	Groundwater Mound Created by Basal Melting	237
5.8	Unconfined Steady-State Well Flow	244
5.9	Confined Steady-State Well Flow	246
5.10	Relative Permeabilities of Various Rocks	251

CHAPTER I

INTRODUCTION

The relative abundance of various constituents in the Martian atmosphere, viewed in the light of current models for the evolution of the primitive solar nebula, suggests that Mars has outgassed a quantity of H_2O equivalent to a globally averaged layer of liquid 10^2 - 10^3 m deep (McElroy et al., 1977; Pollack and Black, 1979; J. S. Lewis, personal communication, 1980). At present, only the equivalent of some 10 m of H_2O is stored in the Martian polar caps, while a few tens of precipitable microns exists as water vapor in the Martian atmosphere. Of the remaining inventory, a portion may have been lost through exospheric escape (Fanale, 1976; Walker, 1977) or by chemical incorporation in the regolith (Fanale, 1976; Huguenin, 1976); but what of the rest? Probably the most reasonable explanation is that this 'missing' H_2O is stored as ground ice, and possibly as groundwater, within the Martian crust (Leighton and Murray, 1966; Fanale, 1976; Rossbacher and Judson, 1981).

Under current climatic conditions the occurrence of ground ice in equilibrium with the water vapor content of the atmosphere is restricted to the colder latitudes poleward of $\pm 40^\circ$ (Leighton and Murray, 1966; Fanale, 1976; Farmer and Doms, 1979). Yet, there is a growing body of morphologic evidence that indicates that substantial quantities of ground ice may have been present in the equatorial regolith throughout much of Martian geologic history. To resolve this

apparent contradiction necessitates that we understand something of the processes that govern both the transport and climatic behavior of water on Mars.

To date, much of the research relating to the climatic behavior of H_2O has focussed on the potential for insolation-driven exchange between the Martian atmosphere, polar caps, and near-surface regolith, with particular emphasis given to the role played by adsorption (Leighton and Murray, 1966; Fanale and Cannon, 1974; Toon et al., 1980; Fanale et al., 1982). This dissertation differs from these earlier studies in that it specifically concentrates on aspects of the long-term behavior of water on Mars that have so far received little or no attention. The discussion is divided into four major sections:

1. In Chapter II, the stability of equatorial ground ice on Mars is examined in light of our current understanding of the physical properties of the Martian regolith. Specifically, the lifetime of a 200-m layer of ground ice, buried below 100 m of ice-free regolith, is examined for the latitudes between $\pm 30^\circ$. Twelve model pore size distributions, representative of silt- and clay-type soils found on Earth, are selected to simulate the pore structure of the Martian regolith. The parallel pore model of gaseous diffusion is then used to calculate the flux of escaping H_2O molecules from the buried ground ice layer. The potential effects of such factors as depth of burial, the Martian geothermal gradient, regolith porosity, adsorption, surface diffusion, and climatic change are also considered.

2. One explanation for the long-term survival of equatorial

ground ice is that it has undergone a process of continuous or episodic replenishment. Photographic evidence in support of this possibility is presented in Chapter III. The evidence is based on the occurrence of rampart craters (whose distinct morphology is thought to originate from an impact into an ice-rich regolith) within the theoretically ice-free interiors of numerous larger impact features. If the current conditions of atmospheric pressure and surface temperature on Mars are representative of the planet's climatic history, then ground ice replenishment from the atmosphere, either by cold-trapping or by direct precipitation as snow or rain, is prohibited. However, subsurface replenishment, from juvenile water or from an established subpermafrost groundwater system, appears to be a viable alternative. In this regard, several mechanisms by which H_2O may be vertically transported from a deeply buried source region to the base of a near-surface layer of ground ice are discussed.

3. The ultimate fate of H_2O sublimed from equatorial ground ice is considered in Chapter IV. Thermodynamic considerations suggest that if the pore volume of the Martian cryosphere is saturated anywhere with ice, it will most likely be at the poles. Given this condition, the annual deposition of dust and H_2O in the polar regions will result in a situation where the equilibrium depth to the melting isotherm has been exceeded; thus, melting at the base of the cryosphere will begin and continue until such time as the equilibrium depth is once again established. Should deposition persist at the poles, the polar caps may ultimately reach a thickness where the melting isotherm will rise

and contact their actual base. At this point, the thickness of the polar ice may reach a state of equilibrium, where deposition at the surface is balanced by geothermal melting at the base. The potential importance of basal melting on Mars is illustrated through a discussion of six examples: (1) the storage of a primitive ice sheet, (2) the origin of the major polar reentrants, (3) the existence of polar basal lakes as possible isolated habitats of Martian life, (4) the possibility of basal melting at temperate latitudes, (5) the mass balance of the polar terrains, and (6) the climatic cycling of H_2O .

4. In Chapter V, the results and processes discussed in the preceding chapters are considered as part of an integrated model for the climatic behavior of H_2O on Mars. Previous climatic studies have implicitly assumed that the Martian atmosphere is the sole pathway available for volatile exchange. However, should the planetary inventory of H_2O exceed by more than a few percent the quantity required to saturate the pore volume of the Martian cryosphere, then a subpermafrost groundwater system of global extent will result. The existence of such a system raises the possibility that subsurface H_2O transport may complement long-term atmospheric exchange. In particular, a pole-to-equator movement of groundwater may result from the gradient in hydraulic head created by the onset of basal melting at polar and temperate latitudes. The physical requirements for such flow, and its implications for the long-term cycling of H_2O between the Martian atmosphere, polar caps, and deep regolith, are considered in detail.

It should be noted that with an eye towards eventual publication, each chapter in this dissertation has been written as a self-contained discussion. Therefore, of necessity, a certain amount of repetition and overlap exists between chapters.

Chapter II has previously been published in the Journal of Geophysical Research (Clifford and Hillel, 1983); while Chapter IV is currently in review in that same journal. Portions of Chapter III and V have previously appeared as abstracts and short papers written for various meetings and conferences.

CHAPTER I I

THE STABILITY OF GROUND ICE IN THE EQUATORIAL REGION OF MARS

A. Introduction

Photographs taken by Mariner and the Viking spacecrafts have provided considerable geomorphologic evidence in support of the idea that sizable quantities of water might be stored as ground ice within the Martian crust. Much of this evidence is based on the identification of Martian analogs to cold-climate features found on the Earth, such as patterned ground, debris flows, and thermokarst. These findings have been reviewed and analyzed by a number of investigators (Sharp, 1973a,b; Carr and Schaber, 1977; Soderblom and Wenner, 1978; Rossbacher and Judson, 1981; Luchitta, 1981; and others); their common conclusion has been that of the possible mechanisms which might explain the presence of these features on Mars, those involving ground ice appear to be the most reasonable. The occurrence of rampart craters on Mars has also been suggested as evidence for the presence of regolith H_2O ; the distinctive lobate nature of the ejecta blankets which surround these craters is thought to originate from the fluidization of ejecta material during an impact into a water- or ice-rich regolith (Carr et al., 1977; Johansen, 1978, 1981; Mougini-Mark, 1979; Allen, 1979; and Blasius and Cutts, 1981). The geologic evidence for the widespread occurrence of ground ice is in accord with theoretical estimates of the global inventory of H_2O on Mars; these estimates

suggest that an amount of H_2O equal to or greater than a 100 meter layer of ice averaged over the planet's surface may be stored within the crust (McElroy et al., 1977; Pollack and Black, 1979).

Earth-based measurements of the water vapor content of the Martian atmosphere and the detailed observations made by the Viking Orbiter Mars Atmospheric Water Detectors (MAWD) indicate a global frost point temperature of approximately 198 K (Farmer, 1977; Farmer and Doms, 1979). Therefore, the existence of ground ice in equilibrium with the water vapor content of the Martian atmosphere is restricted to the colder latitudes poleward of $+40^\circ$ (Leighton and Murray, 1966; Fanale, 1976; Farmer and Doms, 1979).

However, there is a growing body of morphologic evidence which indicates that substantial quantities of ground ice may have existed throughout Martian geologic history in the comparatively warm equatorial regolith (Johansen, 1978, 1981; Allen, 1979; Rossbacher and Judson, 1981). This evidence presents a major problem, for it is difficult to account for both the initial origin and the continued survival of ground ice in a region where present mean annual surface temperatures exceed the frost point temperature of the atmosphere by more than 20 K. As noted by Flasar and Goody (1976), Farmer (1977), and others, the present atmospheric conditions of temperature and pressure on Mars prohibit the equatorial regolith from acting as a net annual sink for atmospheric H_2O . Indeed, ground ice which exists in disequilibrium with the atmosphere should experience a net annual depletion - resulting in a preferential transfer of H_2O from the

"hot" equatorial region to the colder latitudes poleward of $\pm 40^\circ$ (Flasar and Goody, 1976). This problem is apparently compounded by results from a recent study of the climatic history of Mars (Toon et al., 1980) which suggest that the mean annual surface temperatures near the equator have not varied substantially since the formation of Tharsis - an event which Wise et al. (1979) have dated at some 3.5 to 4 billion years ago.

How then is it possible to account for the existence of ground ice within the equatorial regolith? The most popular explanation for this apparent contradiction appears to be that the H_2O found near the equator is a relic, emplaced very early in Martian geologic history and under substantially different climatic conditions. Evidence in support of just such a climatic period comes from the existence of the Martian valley networks (Pieri, 1979, 1980; Carr and Clow, 1981). The occurrence of these features, which bear a close resemblance to runoff channels found on Earth, appears restricted to the heavily cratered terrain of Mars (Masursky et al., 1977; Pieri, 1979, 1980; Carr and Clow, 1981). This association has led investigators to suggest that the climatic conditions responsible for the formation of the valley networks probably did not persist much beyond the beginning of the decline in the planetary cratering rate which is thought to have occurred some 3.9 billion years ago (Pieri, 1979, 1980; Carr and Clow, 1981).

If, as the valley networks suggest, conditions on early Mars were suitable for the global distribution of water within the near surface

regolith, it follows that significant reservoirs of ground ice may then have formed as the climate gradually cooled. However, the question still remains as to how this ground ice has managed to survive for 3.5 to 4 billion years in disequilibrium with the Martian atmosphere. Those who have addressed this question often suggest that the depletion of a fossil ground ice layer on Mars could be substantially retarded by the diffusion limiting properties of a relatively shallow layer of fine-grained regolith (Soderblom and Wenner, 1978; Arvidson et al., 1980, Luchitta, 1981; Rossbacher and Judson, 1981). This explanation is based on an extrapolation of the work of Smoluchowski (1967, 1968), who showed that under certain limited conditions of porosity, pore size, temperature, and depth of burial, a 10 meter thick layer of ground ice in disequilibrium with the atmosphere might survive for as long as a billion years.

Of course, given few constraints, one could easily create a model of the Martian regolith with physical properties sufficient to preserve a buried layer of ground ice for an indefinite period of time; however, while such a model may be physically possible, it may also bear very little resemblance to reality. A decade of intensive exploration by Mariner and Viking spacecrafts has provided us with considerably more information regarding the nature of the Martian regolith than was available when the survival of a buried ground ice layer on Mars was first considered by Smoluchowski (1967, 1968). Therefore, in light of our present understanding of the physical and chemical properties of the Martian regolith and of the magnitude of climatic change on Mars,

we have reconsidered the lifetime of an unreplenished layer of ground ice lying in the equatorial band of $\pm 30^\circ$. The results of this study suggest the possibility that the lifetime of ground ice within this latitude band may be considerably shorter than was previously thought.

B. The Regolith Model

The stability of ground ice in the equatorial region of Mars is governed by the rate at which H_2O molecules can diffuse through the regolith and into the Martian atmosphere. To calculate the magnitude of this loss, it is first necessary to characterize the physical properties of the porous medium through which that diffusion occurs. Knowledge of such factors as the particle size distribution of the soil, its specific surface area, and overall porosity can help to determine the relative importance of the various diffusive processes by which molecular transport can occur within the regolith (*i.e.*, ordinary molecular diffusion, Knudsen diffusion, and surface diffusion).

Observations made by orbiting Mariner and Viking spacecrafts and the results of the limited physical investigations of the Martian surface carried out by the Viking Landers have given us at least a rudimentary understanding of the origin, extent, and structure of the Martian regolith. In addition, we can to some extent supplement this information by drawing on our knowledge of terrestrial and lunar soils. It is from this combined base of information that we have attempted in

the following discussion to define the range of physical properties which are likely to characterize the Martian regolith on a global scale. We will conclude this section by presenting twelve model pore size distributions that we believe are consistent with our present understanding of the Martian regolith and that are used as the basis for the calculations presented later in this paper.

1. The origin and extent of the Martian megaregolith. Impact processes have obviously played a major role in the structural evolution of the Martian crust (Soderblom et al., 1974; Gurnis, 1981). Field studies of terrestrial impact craters (Dence et al., 1977; Pohl et al.; 1977) and theoretical models of the cratering process (Melosh, 1980; O'Keefe and Ahrens, 1981) have shown that impacts modify the structure of a planetary surface in at least two important ways: (1) by the production and dispersal of large quantities of ejecta, and (2) through the intense fracturing of the surrounding and underlying basement. Fanale (1976) has calculated that over the course of Martian geologic history, the volume of ejecta produced by impacts was probably sufficient to have created a blanket of unconsolidated material averaging 2 km thick over the planet's surface. As noted by Carr (1979), it is likely that volcanic flows and various forms of sedimentary deposits are interbedded with this crater ejecta. On the Moon, which has experienced a similar cratering history (Neukum and Wise, 1976), studies of the seismic propagation characteristics of the outer layer of the lunar crust suggest that it is brecciated to a depth of roughly 20 km

(Toksoz, 1979; Binder, 1980; Binder and Lange, 1980). Gravitationally scaling these lunar results to Mars indicates that the regolith may remain porous down to a depth of approximately 10 km (Clifford, 1981b); this calculation supports the earlier suggestion of Carr (1979) that the porous nature of the outer layer of the Martian crust may extend to considerable depth.

2. Particle and aggregate sizes. The repeated bombardment of the lunar crust has created a regolith whose particle size distribution represents a balance between the comminution of surface materials by larger impacts and its agglomeration by the molten spatter of smaller impacts (King et al., 1971, 1972; Carrier, 1973). Analysis of the samples returned by the Apollo astronauts indicates that the resulting particle distribution of the lunar soil has a median size lying somewhere between 40 and 130 microns (Carrier, 1973). Were impacts the only process by which the Martian regolith was produced, one might logically expect that the Martian soil would possess a particle size distribution similar to that found on the Moon; however, on Mars, the presence of an atmosphere and the probable existence of thin films of adsorbed water on mineral surfaces (Anderson et al., 1967, 1978; Anderson and Tice, 1979; Fanale and Cannon, 1974) suggest the occurrence of a variety of possible weathering processes (e.g., Malin, 1974; Huguenin, 1976; Gooding, 1978), whose net effect may be to reduce the overall particle size of the soil still further.

Several different approaches have been used to obtain information

about the particle size distribution of the Martian regolith. Based on laboratory measurements of the thermal conductivity of silicate particles at 6mb pressure (Wechsler and Glaser, 1965), thermal inertia observations of Mars made by Mariner and Viking spacecrafts have been used to infer an equivalent uniform particle size range of from 60 to 5000 microns over much of the Martian surface (Neugebauer et al., 1971; Kieffer et al., 1977). In discussing these results, Kieffer (1976) has pointed out that the bonding of smaller particles into aggregates might well produce thermal inertias indicative of a much larger effective particle size; thus, individual particle sizes on Mars could be smaller than indicated on the basis of the thermal observations alone.

Aggregates can form in soils through a number of physical and chemical processes. Greeley (1979) has presented experimental evidence which suggests that sand-size aggregates (roughly 160 microns in diameter) may be generated on Mars by the electrostatic bonding of silt and clay sized particles. Alternatively, Huguenin (1974) has suggested that adsorbed H_2O could play an important role in aggregate formation. In either case, however, it is likely that the bonding strength of such aggregates is sufficiently low that they would remain stable only at comparatively shallow depths of burial. However, cementing agents such as iron and aluminum oxides, chlorides, carbonates, and sulfates can significantly enhance aggregate formation and stability (Fuller and Hargraves, 1978; Hillel, 1980; Johansen, 1980; Nummendal, 1981). Such substances appear to be abundant in the Martian regolith (Toulmin et al., 1977; Clark, 1978). On Earth,

processes such as freezing and thawing (Chamberlain and Gow, 1978) and desiccation (Hillel, 1980) can also play an important role in the formation of soil aggregates; these processes may have an influence in determining the structure of Martian soils as well.

The existence of soil aggregates on Mars was apparently confirmed by the mechanical analysis of surface materials performed by the Viking Landers. The results of these investigations suggest that the soil is composed of silt-size (<100 micron) or smaller particles which bond together to form a variety of stable assemblages (Shorthill et al., 1976a, 1976b; Moore et al., 1977, 1979). Evidence for the existence of a fine-grained component in the regolith is also supported by the results of several studies which have shown that the light scattering properties of the dust suspended in the Martian atmosphere are indicative of particles with diameters in the range 0.2 - 2.5 microns (Pang et al., 1976; Pollack et al., 1979; Chylek and Grams, 1978). Presently, the most direct evidence for a fine-grained soil comes from Ballou et al. (1978), who have reported that the amount of gas desorbed from surface samples analyzed by the Viking Lander gas exchange experiment (GEX) is consistent with a soil having a specific surface area of approximately $17 \text{ m}^2/\text{g}$ - a measurement that Moore et al. (1979) have suggested is indicative of clay-size particles with a uniform diameter of 0.14 microns.

For a soil with a uniform spherical grain size, the specific surface area per unit mass S_m is related to the particle diameter d by the relation:

$$d = 6/\rho_s S_m \quad (\text{II.1})$$

where ρ_s is the mean particle density, usually assumed to have a value of 2.65 g/cm^3 for silicate particles (Hillel, 1980). It is unusual, however, for a naturally occurring particle population to be represented by a single particle size (Irani and Callis, 1963). Indeed, both lunar and terrestrial soils generally exhibit broad particle size distributions (Carrier, 1973; Hillel, 1980); given the regolith forming processes that have been at work on Mars, it seems reasonable to expect that the particle size distribution of Martian soils should also cover a wide range.

Figure 2.1 illustrates how a soil with a measured specific surface area of $17 \text{ m}^2/\text{g}$ could result from a combination of both a coarse- and fine-grained component in the Martian regolith. The coarse component could consist of particles with diameters >2 microns, which generally have specific surface areas less than $1 \text{ m}^2/\text{g}$, while the fine component might consist of clays with large specific surface areas whose equivalent mean particle diameters are given by Equation (II.1). In this regard it is interesting to note that, based on a mineralogical interpretation of the elemental composition of Martian soil samples, smectite clays have been proposed as a major constituent of the regolith (Baird et al., 1976; Toulmin et al., 1977). Such clays generally exhibit very high specific surface areas, usually $>100 \text{ m}^2/\text{g}$ (Alymore et al., 1970; Anderson et al., 1978; Hillel, 1980). If such clays are present at all in the Martian regolith, then Figure 2.1 would

Figure 2.1. A soil with a constant specific surface area of $17 \text{ m}^2/\text{g}$ can result from a combination of both coarse- and fine-grained components. In this figure, such a soil is shown as a function of its content by weight of the fine-grained high specific surface area component. The equivalent diameter of a uniform soil composed of spherically shaped particles is given along the top margin. If the surface area determination of the Martian regolith made by Ballou et al. (1978) is accurate, then this result would appear to suggest that high specific surface area clays constitute only a small fraction of the regolith by weight.

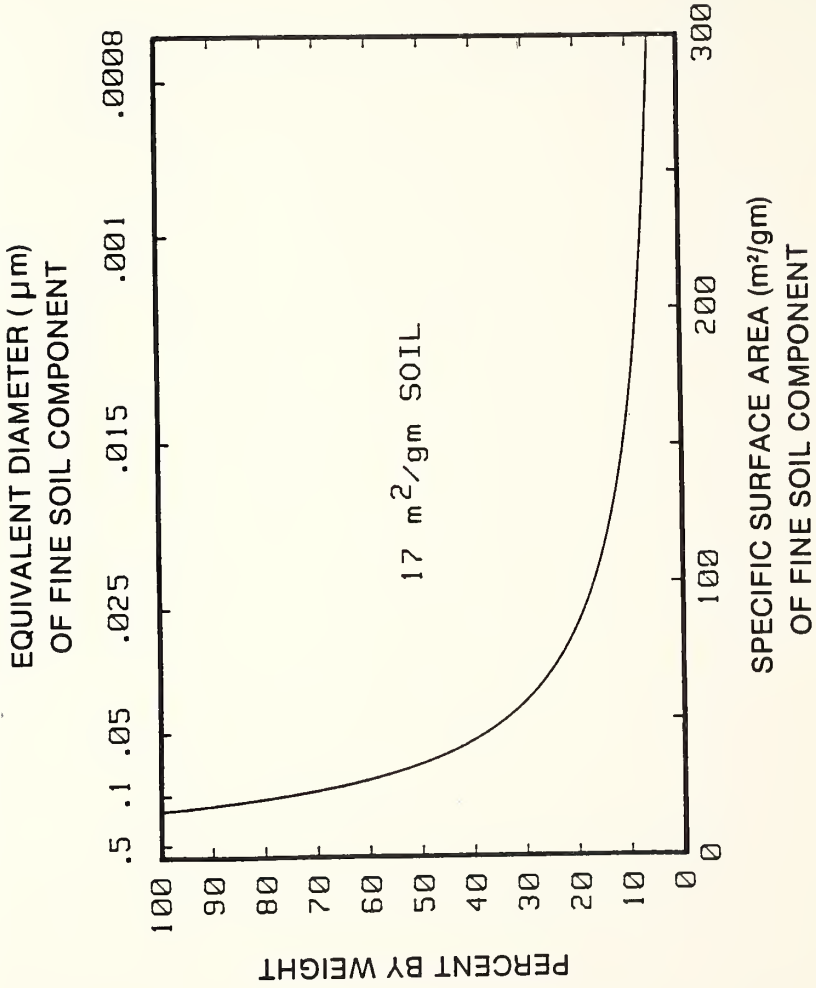


Figure 2.1

seem to suggest that their total contribution must be small. For example, a clay with a specific surface area greater than $100 \text{ m}^2/\text{g}$ is limited to less than 17% of the Martian soil by weight if the soil as a whole is to have a total specific surface area consistent with the $17 \text{ m}^2/\text{g}$ figure obtained by Ballou et al. (1978).

It should be noted, however, that the specific surface area of $17 \text{ m}^2/\text{g}$ calculated from the GEX data is by no means an unambiguous result. In particular, specific surface areas determined from measurements of N_2 and CO_2 adsorption are often significantly less than those estimated from H_2O adsorption data (Puri and Murari, 1963; Aylmore et al., 1970; Fanale and Cannon, 1979). This difference is due to the fact that small polar molecules like H_2O are able to penetrate the interlayer region in sheet silicates such as montmorillonite. The intrusion of H_2O into this region causes the crystal structure of the clay to expand, thus exposing internal adsorption sites that significantly increase the clay's measured specific surface area (Hillel, 1980). Since the GEX results were based on the quantity of N_2 , O_2 , CO_2 , and Ar/CO desorbed from the Martian soil, the possibility exists that the inferred specific surface area of $17 \text{ m}^2/\text{g}$ may underestimate that which might have been obtained from H_2O measurements. On the other hand, the relative inability of these larger molecules to penetrate the interlayer region also implies a more accurate measure of the particle's true external surface area; this, in turn, may provide a more accurate indication of actual particle size.

In summary, it appears that the Martian regolith, like its

terrestrial and lunar counterparts, is probably composed of soil with a broad spectrum of particle sizes. Furthermore, whereas the dominant size fraction may be silt size or smaller, the available spacecraft evidence appears to suggest that particle aggregation has played an important role in determining the structure of the regolith over much of the planet.

3. Porosity and pore size distribution. Clark et al. (1976) have estimated that the bulk porosities of the Martian surface samples analyzed by the Viking Landers were between 45 and 75%; porosities which, on the Earth, are typical of soils and sedimentary rock units composed predominantly of silt and clay size particles (Morris and Johnson, 1967; Hillel, 1980). Of course, the local bulk porosity of the regolith is likely to display considerable heterogeneity over the surface of the planet; however, for the purposes of this paper, we are concerned only with its globally averaged value. Faced with a similar consideration, Toon et al. (1980) assumed that the regolith had a mean column porosity of 50%; for lack of a better estimate, we have adopted this same value for our present study.

It has often been said that the effective pore size of a soil with a broad spectrum of particle sizes is determined by the smallest particle size present in the soil (Smoluchowski, 1968; Farmer, 1976). However, this applies only to the very limited case where the structure of the soil is single grained and where the volume fraction of small particles is sufficient to fill the voids between the larger particles.

For aggregated soils the effective pore size can be significantly greater and is determined primarily by the presence of the much larger interaggregate pores (Hillel, 1980). In general, the higher the clay content of the soil the more likely it is that aggregation will be an important factor in determining the soil's physical structure. As a result, pore sizes in terrestrial soils can cover an enormous range extending from 10^{-9} to 10^{-3} m. To predict successfully the amount of molecular transport which occurs in such soils, we must be able to construct a model of the pore system which accurately reflects this potentially broad distribution in pore size.

Fortunately, the nature of most porous solids is such that their pore systems are readily modeled by a lognormal distribution (Diamond and Dolch, 1972). This approach has two major advantages: (1) it permits a concise and unambiguous description of the pore system, and (2) it is easily incorporated in a numerical model. The lognormal distribution has long been used to describe the size range of various particle populations (Irani and Callis, 1963; Cadle, 1965); as a result, a number of techniques have been developed to tailor the distribution function to any given application (Irani and Callis, 1963; Rowel and Levit, 1970; Ross, 1978). These generalized forms can be readily adapted for use in describing the pore size distribution of a particular soil; however, for our purposes, we found that the standard form could be used to provide a satisfactory agreement with most of the published soil pore size distributions which we considered in this study. The lognormal distribution function, $f(r)$, is given by:

$$f(r) = \frac{1}{\sigma\sqrt{2\pi}} \exp\left(-\frac{1}{2\sigma^2} (\ln r - \ln r_m)^2\right) \quad (\text{II.2})$$

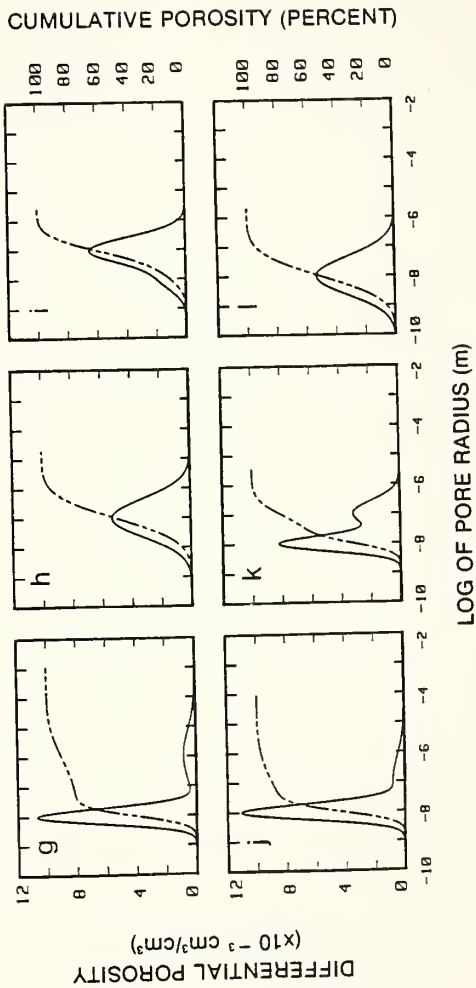
where σ is the standard deviation, and $f(r)$ is the probability that a pore of radius r occurs about some geometric mean pore size r_m .

While no direct measurements of the pore size distribution of the Martian soil were made by the Viking Landers, a likely range of distributions can be inferred by taking into account what is known of the physical properties of the Martian regolith and comparing these properties with soils on Earth that possess similar characteristics. A review of the available literature suggests that for fine-grained soils with specific surface areas $\sim 17 \text{ m}^2/\text{g}$, and porosities of 50%, the range of geologically reasonable pore sizes is covered by the twelve distributions illustrated in Figures 2.2a-2.2l.

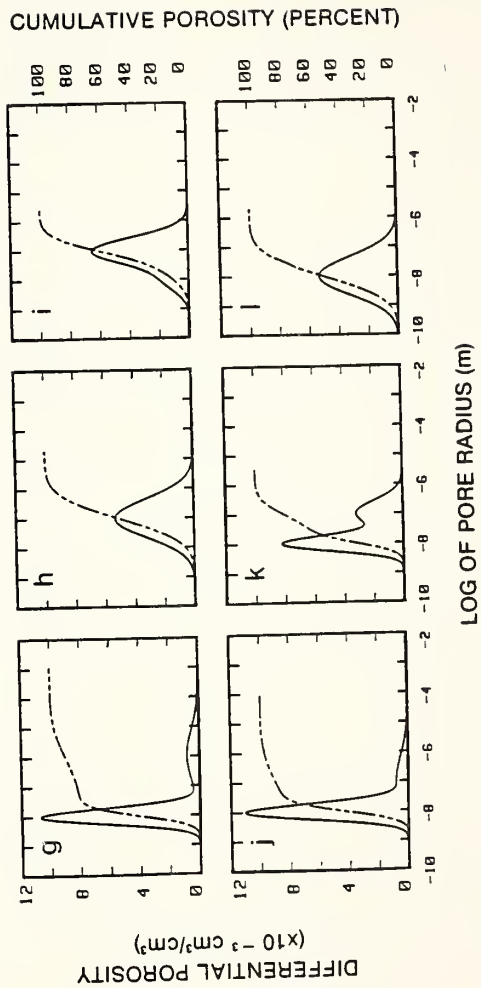
The porosity curves presented in Figure 2.2 are modeled after distributions which have previously appeared in the literature. Since there can be considerable variability in the fine structure of similar soils, these models are not intended to be exact replicas of the pore size distribution of any particular soil but are meant to portray the general characteristics of a number of similar soil types (see Table 2.1). Some distributions are modeled after actual terrestrial silt- and clay-type soils which have been sampled as they occur in the field, while others represent the pore size distribution of just the separated clay-size (< 2 micron) fraction, or represent the distribution obtained from a mixture of clay minerals generated in the laboratory.

Among the examples cited in Table 2.1, sample preparations

Figure 2.2. Twelve pore size distributions, modeled after the measured distributions of terrestrial silt- and clay-type soils (see Table 2.1), are illustrated. The parameters used in Equation (II.4) to model these distributions are listed in Table 2.2. The dashed lines represent the cumulative porosity, while the solid lines represent the differential porosity.



Figures 2.2a-2.2f.



Figures 2.2g-2.2l.

differed substantially; a few were analyzed in the state in which they were obtained from the field, while others were subjected to a number of mechanical, thermal, and chemical treatments. Virtually all of the soils listed in Table 2.1 were oven-dried as part of their preparation. In soils, a well-known side effect of oven drying is that it commonly results in the collapse of many of the larger pores naturally present in the pore system (Diamond, 1970, 1971; Lawrence et al., 1979). As will be discussed later in this paper, the diffusive loss of ground ice is strongly dependent on the total amount of soil porosity which lies in these larger pores. It must be kept in mind, therefore, that the pore models illustrated in Figure 2.2 are likely to underestimate the permeability of the actual soils on which the pore models are based.

It should be emphasized that the terrestrial soils cited in Table 2.1 are extremely fine-grained, as is evident by the fact that even the coarsest of these soils has a mean particle size that is considerably smaller than the mean particle size of sampled lunar soils. However, a comparison between the soils in Table 2.1 and the pore models in Figure 2.2 shows that this small particle size does not necessarily translate into small pore size. As noted earlier, particle size is only one of a number of potential factors which can influence soil structure. Among some of the other factors are particle shape and orientation, the extent and scale of aggregation, and the degree of soil compaction. As a result of the interplay between these various elements, it is not uncommon for a relatively fine-grained illite or nontronite soil to have a pore size distribution which closely resembles that of a coarse-

Table 2.1. Terrestrial examples of pore size distribution models.*

Pore Size Distribution	Terrestrial Examples
a	Packed kaolinite clay [Alzaydi <i>et al.</i> , 1978, Figure 2]; fox silt loam, oven-dried [Diamond, 1970, Figure 6]
b	'Grundite', a poorly crystallized illite clay, dispersed, sedimented and oven-dried [Diamond, 1970, Figure 7] Compacted 'Grundite' at 11% moisture content, oven-dried [Diamond, 1971, Figure 4] 'Clay 3', a clay soil, chemically treated and oven-dried [Quirk and Parsholke, 1962, Figure 3].
c	Garfield nontronite, oven-dried [Diamond, 1970, Figure 4]; 'Edgar Plastic' kaolinite, dispersed, sedimented, and oven-dried [Diamond, 1970, Figure 7]. Compton Beauchamp, a clay soil, chemically treated and oven-dried [Lawrence <i>et al.</i> , 1979, Figure 8].
d	Georgia kaolinite, flocculated, sedimented, and oven-dried with $T = 274^{\circ}\text{C}$ and $P = 216.4$ bars [Diamond, 1970, Figure 11].
e	Hypothetical distribution.
f	'Grundite', flocculated, sedimented, and oven-dried [Diamond, 1970, Figure 7], and 'Edgar Plastic' kaolinite, dispersed, sedimented, and oven-dried [Diamond, 1970, Figure 7]. Compacted 'Grundite', 19% moisture content [Diamond, 1971, Figure 4].
g	Same as distribution 'c', but pore sizes have been reduced by a factor of 10. Macon kaolinite [Diamond, 1970, Figure 4], compacted 'Edgar Plastic' kaolinite [Diamond, 1970, Figure 10], and Leda clay, oven-dried with $T = 274^{\circ}\text{C}$ and $P = 216.4$ bars [Diamond, 1970, Figure 12]. Drayton soil, a clay soil, chemically treated and oven-dried [Lawrence <i>et al.</i> , 1979, Figure 8]. Hanslope soil, a clay soil sampled at a depth of 42-74 cm, oven-dried [Newman and Thomsson, 1979, Figure 7], Ragdale soil—a clay soil sampled at 23-57 cm, oven-dried [Newman and Thomsson, 1979, Figure 7]. Evesham soil—a clay soil sampled at 40-56 cm, oven-dried [Newman and Thomsson, 1979, Figure 9].
h	Same as distribution 'a', but pore sizes have been reduced by a factor of 10.
i	Macon kaolinite [Diamond, 1970, Figure 3]; 'Edgar Plastic' kaolinite, flocculated, sedimented, and oven-dried [Diamond, 1970, Figure 7].
j	Clay Spur montmorillonite, oven-dried [Diamond, 1970, Figure 4].
k	Hypothetical distribution.
l	Same distribution as 'a' (reduced by 100) and 'h' (reduced by 10). Interpolating from Figure 2 of Silts <i>et al.</i> [1973], this pore size distribution might result from a mixture of 28% illite and 72% kaolinite.

Terrestrial examples were selected on the basis of the resemblance between their published differential or cumulative porosity curves and the pore models illustrated in Figure 2. All porosities were normalized to 50%.

*From Clifford and Hillel (1983).

grained kaolinite (e.g., see Figures 2.2b, 2.2c, and 2.2f).

A diversity of potential soil structures is represented by the pore size distribution models illustrated in Figure 2.2. The pore size distributions range from those typical of well-aggregated soils (Figures 2.2b-2.2g) to soils displaying little or no aggregation (Figures 2.2h-2.2l). The general trend illustrated in Figures 2.2a-2.2l is of pore size distributions which are gradually shifted to progressively smaller pores. Where discontinuities occurred in the range of pore sizes covered by the published distributions, model pore size distributions were created to fill in the gaps. These hypothetical distributions are also identified in Table 2.1. The smallest pore sizes generally exhibited by naturally occurring subsoils, as sampled in the field, are represented by Figure 2.2g. The three finest pore models, illustrated in Figures 2.2j-2.2l, are examples of essentially single-grained clay soils that have specific surface areas many times that determined for the Martian regolith. In the event that our basic assumptions regarding the nature of the Martian regolith are wrong, these three distributions may provide some indication as to the potential effect that unaggregated regolith, dominated by fine clay-size particles, would have on the stability of equatorial ground ice.

4. The pore size distribution model. For a unimodal distribution of soil pores, such as illustrated by Figures 2.2a, 2.2h, and 2.2l, the differential porosity $\Delta\epsilon(r)$, which occurs in the pore interval $\Delta \ln(r)$,

is given by:

$$\Delta\epsilon(r) = E f(r) \Delta \ln(r) \quad (\text{II.3})$$

where E is the total porosity of the soil and $f(r)$ is the lognormal distribution function given by Equation (II.2). However, most of the pore size distributions shown in Figure 2.2 are bimodal; this type of structure arises primarily in aggregated, or partially aggregated, soils where there exists a fine network of pores within the aggregates and a set of larger pores between the aggregates. Thus, the differential porosity for most of the twelve distributions in Figure 2.2 is expressed in the more general form:

$$\Delta\epsilon(r) = \frac{\Delta \ln(r)}{\sqrt{2\pi}} \left[\frac{E_1}{\sigma_1} \exp\left\{-\frac{1}{2\sigma_1^2} (\ln(r) - \ln(r_{m1}))^2\right\} + \frac{E_2}{\sigma_2} \exp\left\{-\frac{1}{2\sigma_2^2} (\ln(r) - \ln(r_{m2}))^2\right\} \right] \quad (\text{II.4})$$

where E_1 , r_{m1} , and σ_1 , are the micropore porosity, median micropore size, and micropore standard deviation respectively, and where E_2 , r_{m2} , and σ_2 , are the macropore counterparts. The actual values of these parameters for each distribution are listed in Table 2.2. Note that the terms "micropore" and "macropore" are used here only to describe the relative division of pore sizes within a single distribution and are not intended to connote actual quantitative differences between distributions. Where a given distribution is unimodal, the

Table 2.2. Model pore size distribution parameters.*

Pore Size Distribution	Micropores			Macropores		
	Median Pore Size r_{m1}, m	Standard Deviation σ_1	Porosity E_1	Median Pore Size r_{m2}, m	Standard Deviation σ_2	Porosity E_2
a	10^{-6}	1.5	0.5
b	10^{-8}	1.0	0.1	10^{-6}	1.0	0.4
c	10^{-7}	0.6	0.4	10^{-5}	2.0	0.1
d	10^{-7}	0.6	0.3	10^{-6}	2.0	0.2
e	10^{-8}	1.0	0.25	10^{-6}	1.0	0.25
f	10^{-7}	1.0	0.4	10^{-6}	1.5	0.1
g	10^{-8}	0.6	0.4	10^{-6}	2.0	0.1
h	10^{-7}	1.5	0.5
i	10^{-8}	1.0	0.1	10^{-7}	1.0	0.4
j	10^{-8}	0.6	0.4	10^{-7}	2.0	0.1
k	10^{-8}	0.6	0.3	10^{-7}	1.0	0.2
l	10^{-8}	1.5	0.5

*From Clifford and Hillel (1983).

appropriate parameters are listed under the macropore heading.

Having defined the likely range of physical properties that characterize the Martian regolith, we can now proceed to examine in detail the mechanisms by which molecular transport through this medium is likely to occur.

C. The Diffusion Model

Molecular transport through porous media can occur via three diffusive processes: ordinary molecular diffusion, Knudsen diffusion, and surface diffusion. In discussing the transport of H_2O through the Martian regolith, all three of these diffusive processes may be important. Unfortunately, there is at present no completely predictive model of surface diffusion; nor have any experimental studies of this process under simulated Martian conditions yet been reported. Because of this uncertainty, we limited our initial investigation to consideration of the gas phase transport only. Our failure to include the potential contribution made by surface diffusion means that our final calculations should overestimate the lifetime of a buried ground ice layer by some undetermined margin. Later in this paper, we shall attempt to estimate the size of this margin by making use of a correlation discovered by Sladek (1967), which has been remarkably successful in predicting adsorbate diffusion coefficients in a wide variety of adsorbate-adsorbent systems.

Ordinary molecular diffusion and Knudsen diffusion are the two

processes by which gaseous transport can occur through a porous solid. The factors that influence which of these two diffusive processes will dominate within a pore are: (1) the size of the pore, and (2) the mean free path of the diffusing molecules. In pores where the ratio of the pore radius, r , to the mean free path, λ , is large ($r/\lambda > 10$), ordinary molecular diffusion will be the dominant mode of transport. Therefore, in these larger pores, diffusion is simply governed by the repeated collisions which occur among the molecules present in the pore system. However, when molecular transport occurs in very small pores ($r/\lambda < 0.1$), collisions between the diffusing molecules and the pore walls far outnumber the collisions that occur with other molecules; this is the region of Knudsen diffusion. Since the boundary between ordinary molecular diffusion and Knudsen diffusion is not distinct, the contributions of both processes must be considered when attempting to calculate the amount of transport that occurs in pores of intermediate size ($0.1 < r/\lambda < 10$).

On Mars, the mean free path of H_2O molecules in the atmosphere is about 8 microns (Farmer, 1976). In light of this fact, and in light of the broad range of pore sizes covered by the regolith models in Figure 2.2, it was necessary to adopt a diffusion model capable of predicting the molecular flux of H_2O over the full range of gaseous diffusion processes. Currently, there are essentially four models that are used to describe and predict the transport of gases through a porous solid (Youngquist, 1970). They are the parallel pore model (Wheeler, 1955; Johnson and Stewart, 1965), the random pore model

(Wakao and Smith, 1962), the converging-diverging pore model (Foster and Butt, 1966), and the dusty-gas model (Evans et al., 1961; Mason et al., 1967). For the purposes of this study we chose to use the parallel pore model, both for its relative simplicity and because of its well-documented success in predicting diffusion and flow through porous solids with broad pore size distributions (Youngquist, 1970; Satterfield, 1970; Pandey et al., 1974; Alzadi et al., 1978).

In the parallel pore model a porous solid is viewed as a collection of parallel cylindrical pores of constant radii (Satterfield, 1970). For the case of a binary gas mixture in the region of ordinary molecular diffusion, the flux of component A through component B in a single capillary pore, under isobaric-isothermal conditions, is given by:

$$J_A = -D_{AB} \frac{dn_A}{dz} + \frac{n_A}{n} (J_A + J_B) \quad (\text{II.5})$$

where D_{AB} is the binary molecular diffusion coefficient, n_A is the molecular concentration of component A, n is the total molecular concentration ($n = n_A + n_B$), and dz is the differential length of the capillary pore. It has been shown by Mason et al. (1967), Youngquist (1970), and others, that the flux ratio for a binary gas is described by:

$$J_B/J_A = -(M_A/M_B)^{1/2} \quad (\text{II.6})$$

where M_A and M_B are the molecular weights of components A and B respectively. If we now make the following substitution:

$$\alpha = 1 - (M_A/M_B)^{1/2} \quad (\text{II.7})$$

we can rewrite Equation (II.5) to obtain:

$$J_A = \frac{-D_{AB}}{\left(1 - \frac{n_A}{n} \alpha\right)} \frac{dn_A}{dz} \quad (\text{II.8})$$

For the steady-state case Equation (II.8) can be integrated with respect to z and n_A , to yield:

$$J_A = \frac{D_{AB} n}{z \alpha} \ln \left(\frac{1 - \alpha y_{AZ}}{1 - \alpha y_{A0}} \right) \quad (\text{II.9})$$

where $y_{A0} = n_{A0}/n$ at $z=0$ and $y_{AZ} = n_{AZ}/n$ at $z=z$. From the equation of state for an ideal gas we note that $n=P/kT$, where P is the total pressure, k is the Boltzmann constant, and T is the temperature. Thus, Equation (II.9) can now be written as:

$$J_A = \frac{D_{AB} P}{kTz \alpha} \ln \left(\frac{1 - \alpha y_{AZ}}{1 - \alpha y_{A0}} \right) \quad (\text{II.10})$$

In the smaller pores where Knudsen diffusion becomes important, Equation (II.10) no longer applies. However, based on a momentum transfer analysis, Scott and Dullien (1962) and Rothfield (1963) have derived a similar expression that can be used to predict the gas phase

transport through virtually any size pore. We obtain this expression by dividing the right side of Equation (II.5) by $(1 + D_{AB}/D_{KA})$, where D_{KA} is the Knudsen diffusion coefficient of component A. Integrating the resulting expression in the same manner as before, we find that the gaseous flux of component A for any pore size is given by:

$$J_A = \frac{D_{AB} P}{kTz \alpha} \ln \left(\frac{1 - \alpha Y_{AZ} + D_{AB}/D_{KA}}{1 - \alpha Y_{A0} + D_{AB}/D_{KA}} \right) \quad (\text{II.11})$$

The accuracy of this theoretical equation has been experimentally verified by a number of investigators in the three regions of Knudsen, intermediate, and ordinary molecular diffusion (Johnson and Stewart, 1965; Satterfield and Cadle, 1968; Remick and Geankoplis, 1973; Alzaydi *et al.*, 1978).

The ordinary molecular diffusion coefficient of H_2O in a CO_2 atmosphere is calculated using the expression derived by Wallace and Sagan (1979) on the basis of the experimental results of Schwertz and Brow (1951):

$$D_{AB} = 0.1654 (T/273.15)^{3/2} (1.013 \times 10^6/P) \quad (\text{II.12})$$

Unfortunately, calculating the value of the Knudsen diffusion coefficient D_{KA} is complicated by the fact that the exact form of the equation is dependent on the shape of the pore through which the diffusion occurs (Eldridge and Brown, 1976; Matsun and Quinn, 1977).

For the simple case of a straight cylindrical pore of radius r , we have:

$$D_{KA} = \frac{2}{3} r \left(\frac{8TR}{\pi M_A} \right)^{1/2} \quad (\text{II.13})$$

where R is the universal gas constant.

Using the above relations, we can now define an effective diffusion coefficient D_{eff} by rewriting Equation (II.11) in a form similar to Equation (II.10), that is:

$$J_A = \frac{D_{\text{eff}} P}{kTz \alpha} \ln \left(\frac{1 - \alpha y_{AZ}}{1 - \alpha y_{A0}} \right) \quad (\text{II.14})$$

Following the procedure of Remick and Geankoplis (1973), we can use Equations (II.11) and (II.14) to solve for D_{eff} ; doing so, we obtain:

$$D_{\text{eff}} = \frac{D_{AB}}{\ln \left(\frac{1 - \alpha y_{AZ}}{1 - \alpha y_{A0}} \right)} \ln \left(\frac{1 - \alpha y_{AZ} + D_{AB}/D_{KA}}{1 - \alpha y_{A0} + D_{AB}/D_{KA}} \right) \quad (\text{II.15})$$

In Figure 2.3, D_{eff} is graphed as a function of pore size for H_2O molecules under typical Martian conditions of temperature and pressure. The general shape of the graph is consistent with an 8 micron mean free path for an H_2O molecule in the Martian atmosphere (Farmer, 1976). For pores with radii less than about 0.8 microns, the value of the effective diffusion coefficient falls rapidly with decreasing pore size; this is the region of Knudsen diffusion. For

Figure 2.3. A graph of the effective diffusion coefficient of H_2O in a single capillary pore. The sloping part of the graph represents the Knudsen region, while the horizontal branch on the right side of the graph depicts the region of ordinary molecular diffusion.

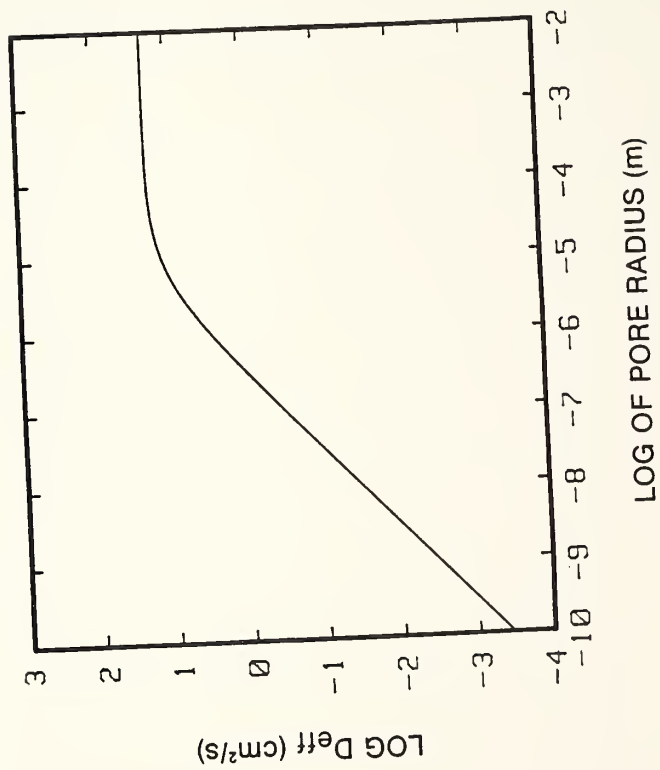


Figure 2.3

pore radii greater than 80 microns, the domain of ordinary molecular diffusion, the diffusion coefficient is independent of pore size since molecular transport in these larger pores is determined almost entirely by intermolecular collisions. As noted earlier, both Knudsen and ordinary molecular diffusion will occur in the transition region which, in this instance, spans the gap between 0.8 and 80 microns.

As it stands, Equation (II.11) only describes the diffusive flux through a single capillary pore. To apply this equation to the case of a porous solid with a broad pore size distribution, the individual contributions must be summed over the entire pore range. After Satterfield and Cadle (1968) and Youngquist (1970) the total flux through a porous solid can be calculated from:

$$J_A = \frac{D_{AB} P}{kTzq\alpha} \sum_{r_{\min}}^{r_{\max}} \ln \left(\frac{1 - \alpha y_{AZ} + D_{AB}/D_{KA}}{1 - \alpha y_{A0} + D_{AB}/D_{KA}} \right) \Delta\epsilon(r) \quad (\text{II.16})$$

where $\Delta\epsilon(r)$ is the porosity in the pore interval Δr , and where q , the tortuosity factor, is included in the equation to account for both the presence of dead-end pore space and the fact that the diffusion path length is often substantially greater than the straight line distance through the porous solid (Youngquist, 1970). In theory, the tortuosity factor is a function of porosity; that is, the lower the porosity of the porous medium, the more tortuous the path of diffusing molecules. Thus, an increase in tortuosity is reflected in a higher numerical value of the tortuosity constant. For a soil with a porosity of 50%, q typically has a value of ~ 5 (Smoluchowski, 1967, 1968; Satterfield,

1970).

In the present application, $\Delta\epsilon(r)$ is given by Equation (II.4); by this substitution the total flux arising from each successive pore interval $\Delta\ln(r)$ can be readily determined. Thus, Equations (II.4) and (II.16), in conjunction with the pore size distribution models described in the previous section, form the basis for our theoretical investigation into the stability of equatorial ground ice on Mars.

D. Initial Assumptions and Numerical Procedure

To calculate the lifetime of an unreplenished layer of ground ice in the equatorial region of Mars, it was necessary to make several initial assumptions regarding the quantity and vertical distribution of ice within the regolith. Based on the estimate of Pollack and Black (1979) that the global inventory of H_2O on Mars is equivalent to a 100 meter layer of ice averaged over the surface of the planet, the amount of ice contained in a vertical column of the regolith was taken to be 10^4 g/cm². It was further assumed that this ice occupied the available pore space in a single massive layer that initially extended from a depth of 100 to 300 meters (Figure 2.4). It is important to note that these figures represent a tenfold increase over both the quantity of ice and the depth of burial originally considered by Smoluchowski (1967, 1968).

To maximize the lifetime of the buried ice layer, the top 300 meters of the regolith were assumed to be isothermal and maintained at

Figure 2.4. The regolith model assumes a 200 meter layer of ground ice buried beneath 100 meters of ice-free regolith; the overall porosity was taken to be 50%.

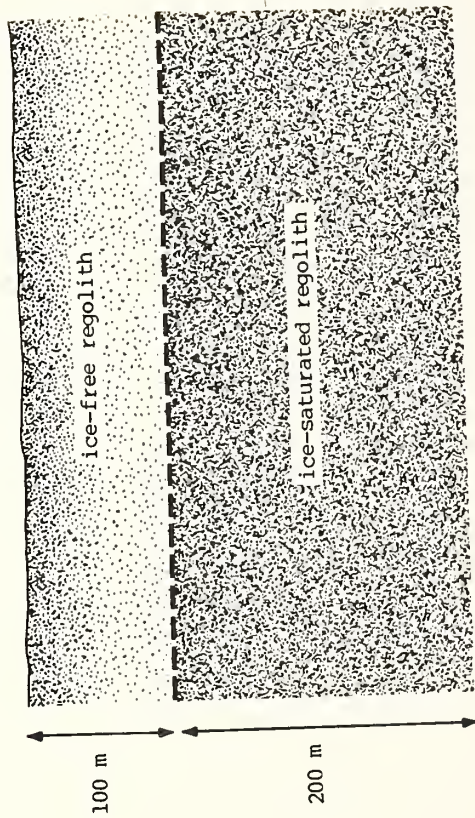


Figure 2.4

a temperature equal to the mean annual surface temperature. For the latitude band between $\pm 30^\circ$, mean annual surface temperatures range from 215 K to 225 K (Fanale, 1976); however, temperatures as low as 210 K and as high as 230 K were also considered in this study to examine the possible effect that minor temperature variations may have had over the course of Martian climatic history.

The equilibrium vapor pressure of H_2O just above the surface of the buried ice layer was calculated using the equation presented by Lebofsky (1975), where:

$$P_{H_2O} = 1.333 \times 10^3 \exp(-5631.1206/T + 18.95304 \log(T) - 0.03861574 T + 2.77494 \times 10^{-5} T^2 - 15.55896) \quad (II.17)$$

Using the above equation, the equilibrium vapor pressure of H_2O over ice has been plotted in Figure 2.5 for the temperature range of 210-230 K.

To determine the partial pressure of H_2O in the Martian atmosphere we used the data obtained by the Viking MAWD experiment during its almost three years of continuous operation. The highest measured, latitudinally-averaged, mean annual column abundance of H_2O within the latitude band of $\pm 30^\circ$ was approximately 15 precipitable microns (Jakosky and Farmer, 1982). Again, in an attempt to maximize the lifetime of the model ice layer, we assumed that this column abundance was representative of the entire equatorial region. The partial pressure of H_2O at the Martian surface was then

Figure 2.5. The saturated vapor pressure of H_2O as a function of temperature.

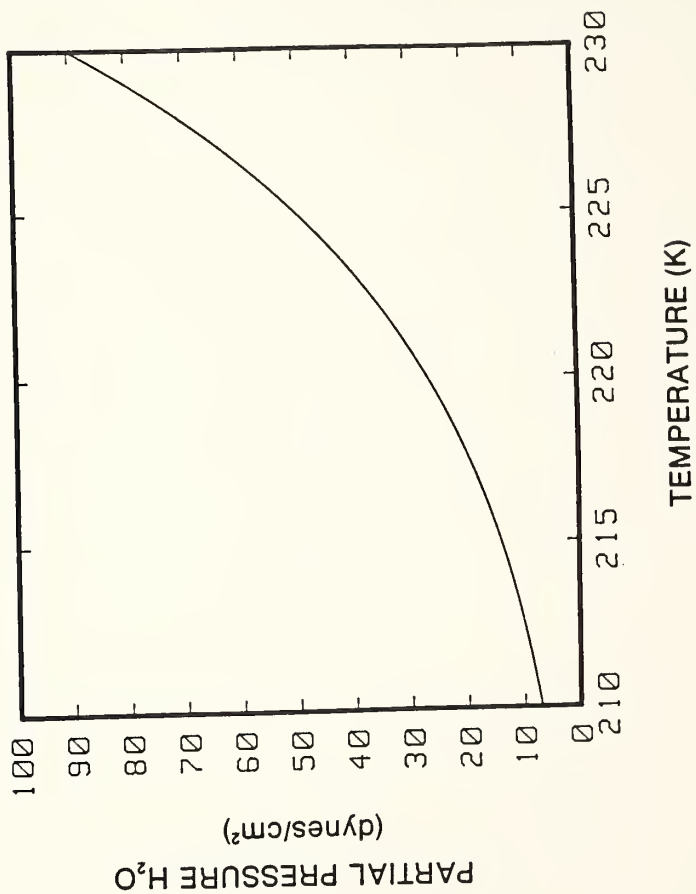


Figure 2.5

calculated based on the conclusion of Davies (1979) that the water vapor present in the Martian atmosphere is uniformly mixed to an altitude of 10 km.

As noted in the previous section, the flux of escaping H_2O molecules from the buried ice layer was calculated from Equation (II.16) for the twelve pore size distributions illustrated in Figure 2.2. The differential porosity $\Delta\epsilon(r)$ was given by Equation (II.4) with the parameters appropriate to each distribution listed in Table 2.2. The recession of the evaporating upper surface of the ground ice from an initial depth of 100 meters to a final depth of 300 meters was taken into account by calculating the diffusive loss of ground ice at 1 meter intervals. For the 50 g/cm^2 of H_2O contained in each 1 meter thickness of regolith, the lifetime, $d\tau$, was calculated from:

$$d\tau = \frac{50}{J_{H_2O}} \frac{N_O}{M_{H_2O}} \quad (\text{II.18})$$

where J_{H_2O} and M_{H_2O} are the molecular flux and molecular weight of H_2O , respectively, and where N_O is Avagadro's number. The total lifetime of the buried ice layer was determined from the sum of these individual contributions.

E. Results and Analysis

For the range of pore sizes and temperatures considered in this study, calculated lifetimes for a 200 meter thick layer of ground ice

buried below 100 meters of ice-free regolith span almost three orders of magnitude - from a low of 166 million years to a high of 114 billion years (Table 2.3). For purposes of comparison between the various pore models, we have presented the lifetimes in Table 2.3 to three decimal places; however, it should be cautioned that the inherent level of accuracy probably does not extend much beyond the first. Therefore, to minimize the effect of this uncertainty on our final conclusions, we have, as noted earlier, attempted to select our model parameters in such a way that the results should consistently overestimate the lifetime of equatorial ground ice.

If ground ice in the equatorial region of Mars is a fossil remnant of a more clement pre-Tharsis climate, then, as discussed earlier in this paper, it appears that that ground ice must have a minimum age of between 3.5 to 4 billion years. If we examine the results of Table 2.3 in light of this minimum lifetime, we find that at 210 K a total of 11 of the regolith models were able to preserve the model ground ice layer for a minimum of 3.5 billion years. However, when the temperature was increased to 230 K, only one of the pore size distributions, illustrated by Figure 2.21, had a permeability low enough to permit the model ice layer to survive beyond the 3.5 billion year limit.

As one might expect, the two trends that are most apparent from the data are that low temperature and small pore size greatly enhance the ability of ground ice to exist in disequilibrium with the Martian atmosphere. Less apparent, however, is the great sensitivity of the results to slight changes in either of these two variables.

Table 2.3. Lifetimes of buried ground ice layer.†

Pore Size Distribution	Mean Surface Temperature, K										
	210	212.5	215	217.5	220	222.5	225	227.5	230	230	230
a	2.63	1.73	1.18	0.822	0.583	0.419	0.305	0.224	0.166		
b	3.86	2.55	1.74	1.22	0.863	0.621	0.453	0.333	0.247		
c	4.38	2.88	1.96	1.36	0.962	0.690	0.500	0.367	0.271		
d	5.10	3.36	2.29	1.59	1.13	0.812	0.590	0.434	0.321		
e	6.11	4.04	2.75	1.92	1.37	0.983	0.716	0.527	0.391		
f	8.82	5.82	3.97	2.77	1.97	1.42	1.03	0.760	0.564		
g	11.1	7.29	4.96	3.45	2.45	1.76	1.28	0.938	0.694		
h	13.8	9.10	6.22	4.35	3.09	2.23	1.63	1.20	0.892		
i	26.3	17.4	11.9	8.33	5.93	4.29	3.13	2.31	1.72		
j*	39.4	26.0	17.8	12.4	8.81	6.35	4.63	3.41	2.53		
k*	48.3	32.0	21.9	15.3	10.9	7.88	5.76	4.25	3.16		
l*	113.5	75.2	51.5	36.0	25.7	18.6	13.6	10.0	7.45		

In billions of years.

*Pore size distributions that are indicative of clay soils which display little or no large-scale aggregation and have specific surface areas that substantially exceed the figure inferred for the Martian regolith [Ballou *et al.*, 1978].

†From Clifford and Hillel (1983).

1. Temperature effects. The ice layer lifetimes presented in Table 2.3 were calculated at 2.5 K intervals for the temperature range of 210-230 K. Over this temperature range, ice layer lifetimes fall by more than an order of magnitude. Indeed, a temperature increase of just a few degrees is sufficient to reduce the lifetime of the ground ice model by 25%. As first noted by Smoluchowski (1967, 1968), this decrease in ice layer lifetimes is due almost entirely to the strong temperature dependence of the equilibrium vapor pressure of H_2O over ice. This is clearly seen in Figure 2.5 where the partial pressure of H_2O in equilibrium with ice is ~ 7 dynes/cm² at 210 K, whereas it is over 90 dynes/cm² at 230 K.

For the temperature range that characterizes the latitudes lying within the band of $\pm 30^\circ$ (215-225 K), Figure 2.5 shows that there is a corresponding increase of more than 300% in the saturated vapor pressure of H_2O over an ice layer surface. This increase in vapor pressure is sufficient to cause a 70% drop in ice layer lifetimes between the coldest and warmest latitudes within the equatorial band.

For the range of present mean annual equatorial temperatures, the results presented in Table 2.3 effectively divide the 12 model pore size distributions into three distinct groups:

1. For distributions in Figures 2.2a-2.2e, the pore sizes are sufficiently coarse that, even at the lower temperature limit of 215 K, they are unable to preserve the ground ice model for more than 2.75 billion years.

2. All of the distributions pictured in Figures 2.2f-2.2i are

capable of protecting the model ice layer for 3.5 billion years at a temperature of 215 K, but only one (distribution in Figure 2.2i) manages to do so for a temperature above 217.5 K. Ultimately, the distribution in Figure 2.2i fails when the temperature is increased to 225 K.

3. Distributions in Figures 2.2j-2.2l are the only pore models examined in this study able to preserve the model ground ice layer at the present maximum Martian mean annual surface temperature of 225 K. As noted earlier, these last three distributions are indicative of clay soils that display little or no large-scale aggregation and that have specific surface areas substantially exceeding the figure inferred for the Martian regolith.

2. Pore size effects. As noted before, the progress of a diffusing water molecule through the Martian regolith is severely constrained when pore sizes fall below 1 micron, a fact which is clearly evident from the graph of the effective diffusion coefficient seen in Figure 2.3. Therefore, it is not surprising that by reducing the overall pore size of the regolith we can significantly enhance the stability of a buried ice layer.

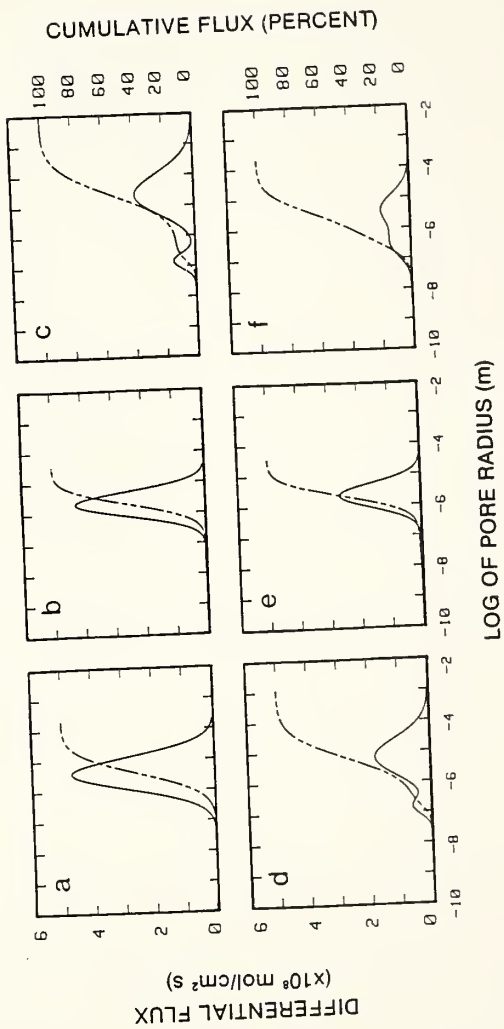
For example, consider the pore size distributions pictured in Figures 2.2a, 2.2h, and 2.2l; the median pore sizes of these otherwise identical distributions are 1 micron, 0.1 microns, and 0.01 microns, respectively. The order of magnitude decrease in median pore size between Figures 2.2a and 2.2h results in a fivefold increase in the

survival time of the model ice layer (Table 2.3); however, reducing the median pore size by two orders of magnitude (to that depicted in Figure 2.21), results in an over fortyfold increase in ice layer lifetimes.

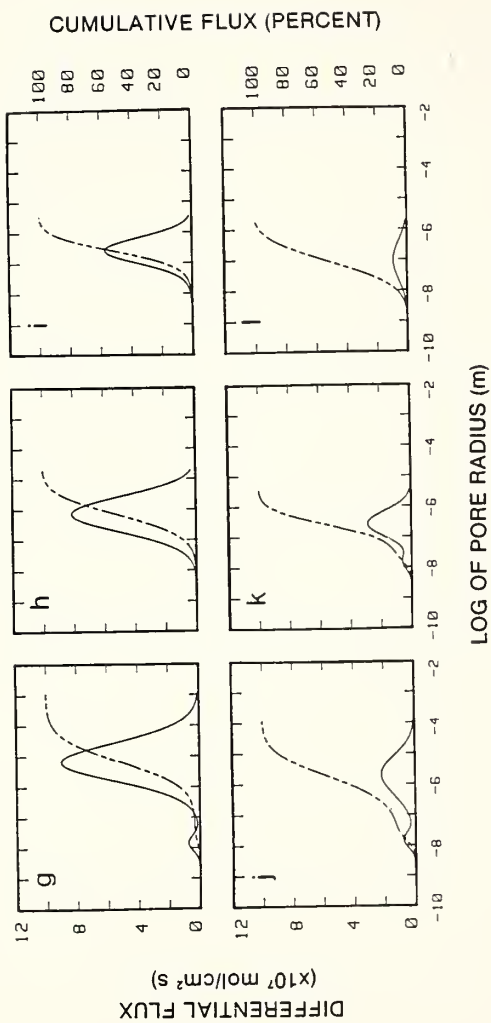
To examine the effect of pore size more closely, we have plotted in Figure 2.6 both the differential and cumulative flux of H_2O molecules through each of the 12 pore size distributions illustrated in Figure 2.2. A one-to-one comparison between Figure 2.2 and Figure 2.6 graphically illustrates the point that gaseous diffusion occurs preferentially within the larger pores of any given distribution.

For instance, consider the pore size distribution in Figure 2.2c and its respective flux curve in Figure 2.6c. While approximately 80% of this distribution's total porosity lies in pores with radii of less than one micron, over 80% of the total flux occurs in the 20% fraction of pores that are micron size or larger. At still smaller pore sizes, where most of the transport falls in the Knudsen domain, this asymmetry becomes even more pronounced. The distribution pictured in Figure 2.2g is identical to that of Figure 2.2c except that the pore sizes in Figure 2.2g have been reduced by an order of magnitude. In this instance about 92% of the total porosity is derived from pores with radii of less than one micron. However, these same pores account for less than 10% of the total flux (Figure 2.6g). This behavior can be understood by once again referring to the plot of the effective diffusion coefficient in Figure 2.3. At larger pore sizes, such as those covered by the distribution pictured in Figure 2.2c, the contrast in the value of the effective diffusion coefficient between the largest

Figure 2.6. The differential flux of H₂O molecules through the twelve pore size distribution models illustrated in Figure 2.2. The cumulative flux and differential flux are given by the dashed and solid lines respectively. The calculations were made at an ice layer depth of 100 meters and a regolith temperature of 220 K. Note the scale change in the differential flux between the distributions in Figures 2.6a-2.6f and 2.6g-2.6l.



Figures 2.6a-2.6f.



Figures 2.6g-2.6l.

and smallest pores within the distribution is mitigated by the fact that the ordinary molecular diffusion coefficient begins to level off for pores with radii greater than about one micron. As more of the total porosity is shifted to smaller pore sizes (e.g., Figure 2.2g), the difference in the effective diffusion coefficient between the largest and smallest pores within the distribution increases because of the explicit dependence of the Knudsen diffusion coefficient on pore size.

As is evident by an examination of Figure 2.6 and the lifetimes presented in Table 2.3, the factor that has the greatest influence on the stability of ground ice, for any given distribution, is the amount of porosity contained in the larger (≥ 1 micron) soil pores. This fact is illustrated by the pore size distributions presented in Figures 2.2g and 2.2h. In the distribution in Figure 2.2g, approximately 18% of the total porosity lies in pores with radii greater than 0.1 microns, as opposed to a figure of 55% for the distribution in Figure 2.2h. Despite this fact, the lifetime of a buried ice layer is actually shorter for the distribution in Figure 2.2g than it is for Figure 2.2h. The important difference is that while the distribution in Figure 2.2g has less total porosity in the larger pores, that porosity is distributed in such a way that it actually has a greater porosity in the very largest pores.

The data in Table 2.3 further suggests that at a mean annual temperature between 215 and 225 K, a regolith with a porosity of more than a few percent in pores large enough for ordinary molecular

diffusion (~ 10 microns) will be unable to preserve the model ice layer for as long as 3.5 billion years. This is an important point because, as noted earlier, a naturally occurring subsoil commonly has a small fraction of its total porosity in pores much larger than those modeled in Figure 2.2. For example, four of the soils which were cited in Table 2.1 as terrestrial examples of the distribution in Figure 2.2g, the Hanslope, Ragdale, Evesham, and Flint soils, had porosities of several percent or more in the pore size range of 10^2 - 10^3 microns (Bullock and Thomasson, 1979). We chose not to include these larger pores because of our uncertainty as to whether such pores would remain stable when subjected to an overburden pressure of 100 or more meters of Martian regolith. If these larger pores are in fact stable at moderate depths of burial, their inclusion in the pore size distributions illustrated in Figure 2.2 would result in lifetimes significantly shorter than those presented in Table 2.3.

In summary, for the warmer equatorial latitudes that have mean annual temperatures in excess of ~ 217.5 K, the results presented in Table 2.3 suggest that it is unlikely that a regolith with a porosity of 50% and a specific surface area of $17 \text{ m}^2/\text{g}$ could preserve a 200 meter thick layer of ground ice buried below 100 meters of ice-free regolith for as long as 3.5 billion years. However, for lower temperatures (≤ 217.5 K), there may well exist a range of geologically reasonable pore size distributions capable of extending the model ice layer lifetime beyond the 3.5 billion year minimum. Only in the improbable circumstance of an essentially single-grained regolith

composed of very fine clay-size particles would our model ground ice layer be preserved at the very highest mean annual surface temperatures that presently occur on Mars.

Because the above conclusions are based on a very specific and limited set of regolith models, we will now attempt to place the results of this study into better perspective by reexamining the legitimacy of some of our initial assumptions. We shall also discuss several additional factors, such as surface diffusion and climatic change, whose affects were not considered in our original model. Finally, we will present what we believe are the principal arguments both for and against the long-term survival of a fossil ground ice layer in the equatorial region of Mars.

F. Discussion

1. Depth of burial and the Martian geothermal gradient. As discussed earlier, the diffusive flux of a gas through a porous medium is directly proportional to its concentration gradient. For a buried ice layer on Mars, the concentration gradient of H_2O in the regolith can be affected in one of two ways: (1) by changing the regolith temperature, and thus the vapor pressure at the ice layer surface, or (2) by changing the depth of ice layer burial. If our goal is to extend the lifetime of ground ice in the equatorial region of Mars, then the range of present mean annual surface temperatures for this latitude band effectively constrains the minimum temperature (and thus

minimum vapor pressure) that can be considered; however, since we have previously argued that Mars may possess a regolith of considerable extent, it would appear that we are relatively unconstrained in discussing the depth of ice layer burial. Indeed, one might be tempted to ask: if burial of an ice layer under 100 meters of regolith is sufficient to preserve it for hundreds of millions of years, then why not consider burial at even greater depths?

The problem is that at some point we will eventually reach a depth where any realistic discussion of the stability of ground ice must include the effect of the Martian geothermal gradient on regolith temperatures. For example, if we attempt to extend the lifetime of a ground ice layer by arbitrarily locating it at some depth below that at which the geothermal gradient begins to take effect, then not only must we consider the reduction in the overall H_2O concentration gradient which occurs as the result of the increased depth of burial, but we must also take into account the increase in the concentration gradient brought on by the higher geothermal temperatures and their associated higher saturated vapor pressures at the ice layer surface.

Of course, the actual depth at which the geothermal gradient might begin to express itself on Mars is unknown. In the calculations presented earlier in this paper, we assumed that the temperature of the Martian regolith was unaffected by the planet's internal heat flux down to a depth of 300 meters. But is such an assumption reasonable?

On the Earth, the geothermal heat flux generally begins to have a measurable effect on subsurface temperatures at depths between 100 and

300 meters (Jaeger, 1965; Lee and Uyeda, 1965). At shallower depths, the geothermal contribution to subsurface temperatures is overwhelmed by the influence of a variety of other factors, the most important of which are the presence and circulation of near-surface groundwater, and past climatic temperature changes (Jaeger, 1965; Lee and Uyeda, 1965). However, on Mars, the potential importance of these factors on near-surface regolith temperatures appears considerably reduced. For example, present mean annual surface temperatures on Mars restrict the occurrence of any large body of groundwater to depths of a kilometer or more, where geothermal heating may elevate regolith temperatures above the freezing point of water (Fanale, 1976; Clifford and Huguenin, 1980; Clifford 1980, 1981a; Rossbacher and Judson, 1981). Likewise, past climatic surface temperature variations in the equatorial region of Mars appear to have been relatively minor, of the order of ± 5 K (Toon et al., 1980). In the absence of these external influences, it seems likely that higher regolith temperatures on Mars, resulting from geothermal heating, would begin to occur at shallower depths than on Earth. On the Moon, where the near-surface temperature environment has apparently remained stable for billions of years, various lines of evidence suggest that the lunar geothermal heat flux begins to have a measurable effect on regolith temperatures at depths as shallow as several meters (Keihm and Langseth, 1975; Langseth et al., 1976). On Mars, with a surface environment that is roughly intermediate between that of the Earth and Moon, a more reasonable estimate of the onset depth might be on the order of ten meters.

Even a small geothermal gradient can have a significant effect on the stability of equatorial ground ice. The existence of a temperature gradient in the regolith will produce a corresponding gradient in the saturated vapor pressure of H_2O . Therefore, any H_2O present at great depth on Mars, either as a liquid or as ice, will undergo a continuous process of depletion as the thermally induced vapor pressure gradient drives the transport of H_2O from the warmer (higher vapor pressure) depths to the colder (lower vapor pressure) near-surface regolith (Philip and deVries, 1957; Clifford, 1980, 1982). This process will continue until either the available pore space in the near-surface regolith is saturated with ice, or the reservoir of deeply buried H_2O is finally exhausted. In either case, any regolith H_2O is ultimately transported to the very coldest, and thus the very shallowest, depths within the regolith, the region where it is most susceptible to sublimation to the Martian atmosphere.

This argument suggests that the calculated ground ice lifetimes presented earlier in this paper may overestimate the actual lifetimes of equatorial ground ice by almost an order of magnitude. This potential reduction in ice layer lifetimes results from a combination of two effects. First, if the Martian geothermal heat flux does begin to elevate regolith temperatures at depths as shallow as 10 meters, then, as noted above, the near-surface regolith will act as a cold-trap for any H_2O present in the regolith. This suggests that a more realistic estimate of the initial depth of ground ice burial would have been on the order of 10 meters, and not the 100 meter figure assumed

earlier in this study. Second, as the ground ice layer is depleted, the sublimation front will recede deeper into the regolith where higher geothermal temperatures will result in higher vapor pressures at the ice layer surface (Figure 2.7). The corresponding increase in the H_2O concentration gradient will result in a substantially higher flux of H_2O out of the regolith than predicted by the isothermal model of diffusion used in the present study. A more detailed analysis of the thermal transport of H_2O in the Martian regolith, and its relation to the stability of equatorial ground ice, is in preparation.

2. Porosity. The lifetimes presented in Table 2.3 were calculated assuming a regolith porosity of 50%. As noted earlier, this figure was chosen because it lies within the range of porosities inferred from the investigations of the Viking Landers, and because it is consistent with estimates made by previous investigators (Fanale, 1976; Toon et al., 1980). However, one might reasonably question whether a porosity of 50%, measured at the Martian surface, can be considered a realistic representation of the porosity of the regolith over a depth of several hundred meters.

On Earth, the porosity of the crust declines with depth as the result of three principal processes: compaction, cementation, and igneous reconsolidation. Within 500 meters of the surface, the lithostatic compaction of nonindurated sediments generally results in a only a 5-20% reduction in near-surface porosity (Maxwell, 1964; Rieke and Chilingarian, 1974; Pettijohn, 1975); on Mars, the potential

Figure 2.7. Regolith temperatures and associated saturated vapor pressures of H₂O are shown as a function of depth for four possible geothermal gradients. Calculations made by Fanale (1976) and Toksoz and Hsui (1978) suggest that the present-day Martian geothermal heat flux is of the order of 35 ergs/cm². Based on the thermal conductivity of a variety of terrestrial rocks and minerals, this heat flux estimate has led investigators to suggest that the geothermal gradient on Mars probably lies somewhere within the range of 15-45 K/km (Fanale, 1976; Soderblom and Wenner, 1978; Schultz and Glicken, 1978; Rossbacher and Judson, 1981). At a depth of 300 meters the regolith temperatures resulting from these gradients have associated H₂O vapor pressures that range from 2 to 5 times higher than that associated with the mean annual surface temperature assumed in this example. At a depth of 1 km, vapor pressures may be as much as 6 to 100 times their near-surface value.

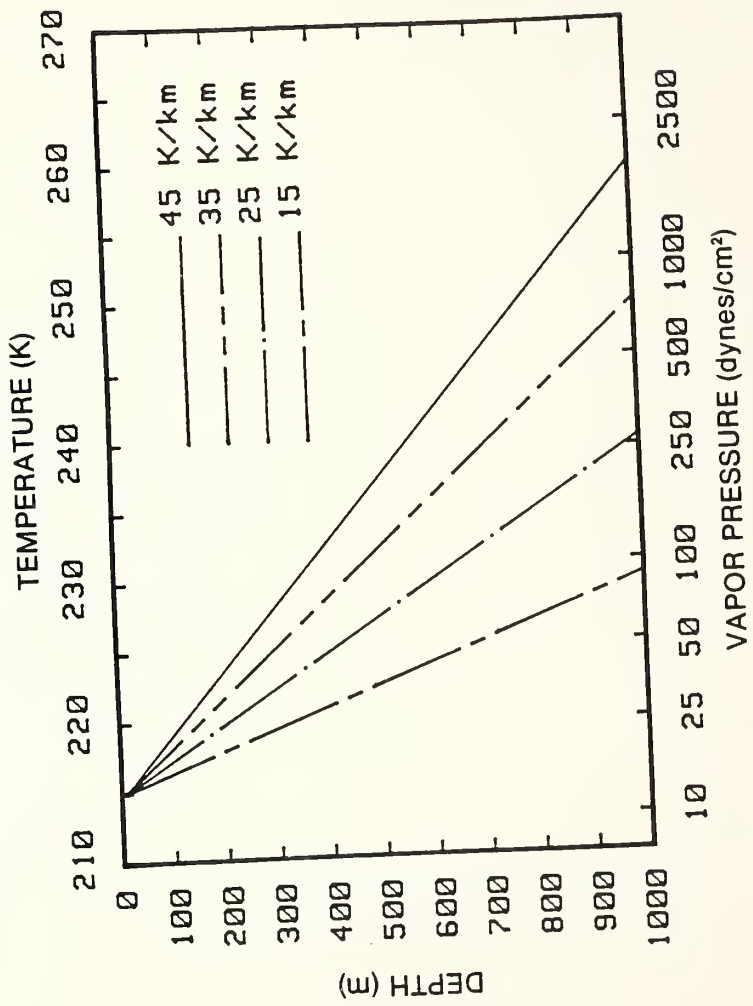


Figure 2.7

importance of this process is further diminished by the planet's low surface gravity. The possible lithification of the Martian regolith by cementation has been discussed by Soderblom and Wenner (1978) and Fuller and Hargraves (1978); however, since extensive cementation generally requires conditions of high temperature, high pressure, and the presence of liquid water (Maxwell, 1964; Rieke and Chilingarian, 1974; Pettijohn, 1975), the widespread occurrence of this process within a few hundred meters of the Martian surface appears unlikely, at least under current climatic conditions. Finally, the photogeologic evidence for extensive volcanism on Mars (Greeley and Spudis, 1981) suggests that lava flows and igneous intrusions may have played an important role in modifying the structure of the near-surface regolith. If so, then the net effect on the overall porosity of the Martian regolith will depend on such factors as the degree of inherent vesicularity in the lava flows and the amount of secondary porosity generated by subsequent fracturing and weathering.

Should the globally averaged near-surface porosity of the Martian regolith be significantly less than 50%, then it will affect our calculated ice layer lifetimes in two ways. First, a reduction in regolith porosity corresponds to an effective reduction in the cross-sectional area of the regolith that is available for molecular transport. Second, in order to store the same volume of ground ice, any loss in storage capacity due to a reduction in regolith porosity must be compensated for by an increase in the total thickness of the regolith over which the ground ice is distributed. The combined

effects of the reduced cross-sectional area and extended depth of storage can add up to a considerable extension of ice layer lifetimes. For an isothermal regolith with a porosity of 25%, the resulting increase in ice layer lifetimes, over those listed in Table 2.3, could be as much as 300%. It should be noted, however, that the presence of even a small geothermal gradient may be sufficient to negate the increase in ice layer lifetimes that would result from any reasonable reduction in regolith porosity.

3. Adsorption and surface diffusion. The likely presence of adsorbed H_2O in the Martian regolith has been discussed by Anderson et al. (1967, 1978), Fanale and Cannon (1971, 1974), Toon et al. (1980), and others. Since the amount of H_2O which is adsorbed in the regolith is a function of both the temperature and the local partial pressure of H_2O within the soil pores, the diurnal and seasonal fluctuations of these conditions can produce substantial changes in the adsorptive capacity of the top few meters of the regolith. As a result, the diffusive transport of H_2O through the pore system of the near-surface regolith can be significantly damped. Although these diurnal and seasonal changes affect the adsorptive capacity of only the top few meters of regolith, it nonetheless raises the question as to the possible role adsorption might play in the diffusion of H_2O from much greater depths.

To understand the effect of adsorption on ice layer lifetimes, consider a layer of ground ice which is buried instantaneously beneath

a thick layer of desiccated regolith. Since there is no H_2O present in the overlying regolith, an enormous initial concentration gradient of H_2O is created just above the surface of the ground ice. As a result of this gradient, H_2O molecules rapidly evaporate from the ice layer surface, filling the adsorptive capacity of the nearby regolith material. When the adsorptive capacity of the entire regolith is finally saturated, the concentration gradient (and thus the evaporation rate) reaches its minimum value. Therefore, the amount of H_2O required to saturate the adsorptive capacity of an initially desiccated layer of regolith must necessarily evaporate faster than an equivalent amount of H_2O which is transported completely through the regolith once the regolith's adsorptive capacity has been filled. Based on this argument, and the assumption that the adsorptive capacity of a 100 meter thick regolith is approximately 10^2 g H_2O/cm^2 (Fanale and Cannon, 1974), the time required to saturate this adsorptive capacity amounts to less than 1% of the ice layer lifetimes presented in Table 2.3. Of course, once the adsorptive capacity of the regolith has been saturated, adsorption will no longer play a role in retarding the flux of H_2O molecules. That is, for every instance a molecule is adsorbed on a pore-wall another must be desorbed; therefore at any instant in time a steady-state condition prevails.

While adsorption may not significantly impede the evaporative loss of deeply buried ground ice, it might very well accelerate the process. As noted earlier, where there is significant adsorption of the diffusing species within a porous solid, diffusion in the adsorbed

layer can occur at the gas-solid interface of the pore wall. In an effort to describe this process, a number of surface transport models have been proposed in the literature; however, most of these fall into one of three general categories: (1) the mechanistic model, where migration of individual molecules proceeds by a hopping process from one lattice site to the next, (2) the hydrodynamic model, where the adsorbed phase is treated as a fluid, and (3) a Fick's law model, where surface transport is viewed in terms of two-dimensional diffusion along a concentration gradient. Aspects of these models have been discussed by Barrer (1967), Satterfield (1970), Horiguchi et al. (1971), Gilliland et al. (1974), Ponzi et al. (1977), Thakur et al. (1980), and numerous others.

As good as the various models of surface transport may be, there is as yet no completely predictive model of surface diffusion. This fact, combined with the lack of any experimental studies of surface diffusion under simulated Martian conditions, makes it extremely difficult to assess the importance of this process to the transport of H_2O through the Martian regolith. However, by using a correlation discovered by Sladek (1967), it is at least possible to make an order of magnitude estimate of this potential contribution.

After Satterfield (1970), we shall describe the transport that occurs in the adsorbed phase by a Fick's law relation, such that the surface flux, J_s , per unit cross section of regolith is given by:

$$J_s = - \frac{D_s}{q_s} \rho_s S_m \frac{dc_s}{dz} \quad (II.19)$$

where D_s is the surface diffusion coefficient, q_s is the surface tortuosity, ρ_s is the particle density, S_m is the specific surface area of the regolith, and c_s is the surface concentration of H_2O molecules.

Sladek (1967) found that the surface diffusivities of various adsorbates correlated well with their heats of adsorption, as long as such factors as temperature, the electrical conduction properties of the adsorbent, and the type of surface bond responsible for the adsorption were also taken into account. In a further analysis of this correlation, Sladek et al. (1974) have presented an equation by which the surface diffusion coefficient of an adsorbate on virtually any surface can be predicted with reasonable accuracy; this equation is:

$$D_s = 1.6 \times 10^{-2} \exp(-0.45 Q/mRT) \quad (\text{II.20})$$

where Q is the heat of adsorption and m is an adjustable parameter with a value of 1, 2, or 3, depending on both the nature of the adsorbent and the surface bond. For a polar adsorbate which is bonded by Van der Waals and electrostatic forces to an insulating material such as a clay, m has a value of 1. Therefore, by knowing the heat of adsorption, Equation (II.20) can be used to obtain a reasonable estimate of the surface diffusion coefficient of water adsorbed on virtually any mineral surface.

In Figure 2.8 we have plotted Equation (II.20) as a function of the heat of adsorption of H_2O for two different temperatures, 296 K and

Figure 2.8. Theoretical and experimentally derived H_2O surface diffusion are shown as a function of their H_2O heat of adsorption. The experimentally determined diffusivities at 296 K were reported by Adams et al. (1979) (open circles) and Laughlin (1977) (solid circles) for H_2O diffusion on monmorillonite; the corresponding H_2O heats of adsorption were taken from the desorption measurements of Mooney et al. (1952). The theoretical curves at 296 K and 220 K were predicted using the correlation (given by Equation (II.20)) reported by Sladek (1967) and Sladek et al. (1974). The agreement between the measured and predicted H_2O diffusivities at 296 K suggest that this correlation can also be used with reasonable confidence to predict D_s at other temperatures. Since the H_2O heat of adsorption on mineral soils is roughly constant per unit surface area (Puri and Murari, 1963), the applicability of Equation (II.20) should be independent of actual soil composition.

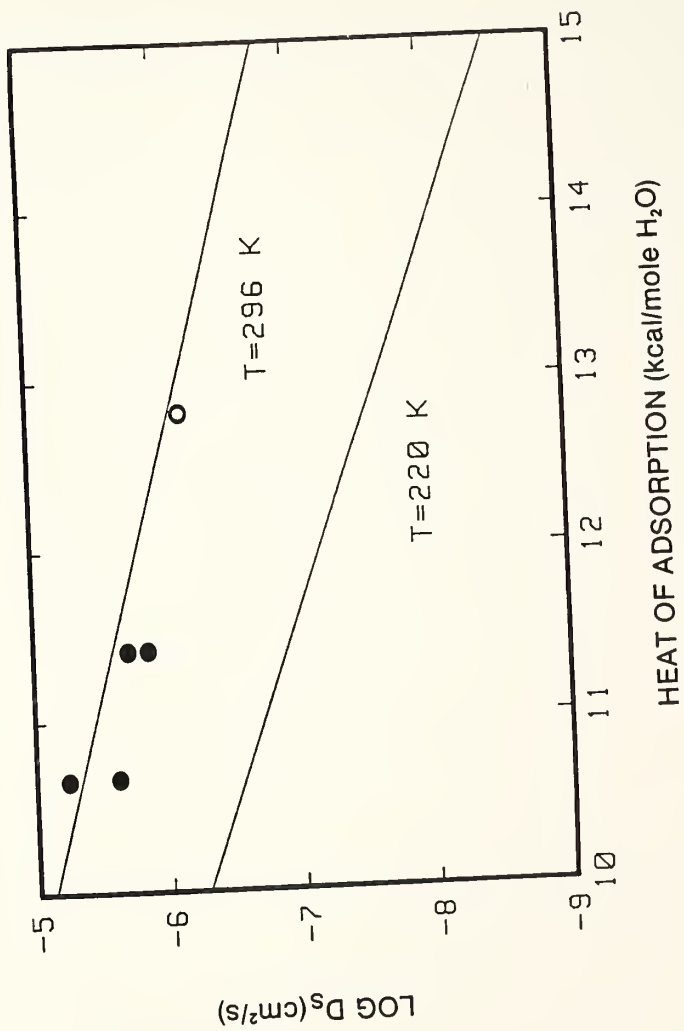


Figure 2.8

can now estimate the surface flux of H_2O through the Martian regolith.

Since we are only interested in making an order of magnitude estimate of J_s , we will assume that the surface tortuosity factor, q_s , is equal to the gaseous value of 5. As before, ρ_s and S_m will be taken to be 2.65 g/cm^3 and $17 \text{ m}^2/\text{g}$ respectively. Just above the buried ice layer, the surface concentration of H_2O molecules is taken to be $6.3 \times 10^{14} \text{ molecules/cm}^2$, a figure which is appropriate for a surface coverage of between one and two monolayers. At the Martian surface, due to the low relative humidity of the atmosphere, we assume that the concentration of adsorbed H_2O molecules falls to zero. Substituting these values into Equation (II.19), we find that the surface flux of H_2O molecules from the model ice layer is approximately $6.2 \times 10^8 \text{ molecules/cm}^2\text{-sec}$. While this flux results in an almost negligible reduction in the shorter lifetimes presented in Table 2.3, it limits maximum ice layer lifetimes to roughly 10^{10} years.

However, if the actual specific surface area of the Martian regolith is as high as several hundred square-meters per gram, then the surface flux of H_2O could be well over $10^{10} \text{ molecules/cm}^2\text{-sec}$. Such a high surface flux would exceed the gaseous flux for many of the pore size distributions considered in this study. The resulting maximum ice layer lifetime would then be between 10^8 to 10^9 years, a result that is entirely independent of how small the actual pore sizes of the regolith might be.

can now estimate the surface flux of H_2O through the Martian regolith.

Since we are only interested in making an order of magnitude estimate of J_s , we will assume that the surface tortuosity factor, q_s , is equal to the gaseous value of 5. As before, ρ_s and S_m will be taken to be 2.65 g/cm^3 and $17 \text{ m}^2/\text{g}$ respectively. Just above the buried ice layer, the surface concentration of H_2O molecules is taken to be $6.3 \times 10^{14} \text{ molecules/cm}^2$, a figure which is appropriate for a surface coverage of between one and two monolayers. At the Martian surface, due to the low relative humidity of the atmosphere, we assume that the concentration of adsorbed H_2O molecules falls to zero. Substituting these values into Equation (II.19), we find that the surface flux of H_2O molecules from the model ice layer is approximately $6.2 \times 10^8 \text{ molecules/cm}^2\text{-sec}$. While this flux results in an almost negligible reduction in the shorter lifetimes presented in Table 2.3, it limits maximum ice layer lifetimes to roughly 10^{10} years.

However, if the actual specific surface area of the Martian regolith is as high as several hundred square-meters per gram, then the surface flux of H_2O could be well over $10^{10} \text{ molecules/cm}^2\text{-sec}$. Such a high surface flux would exceed the gaseous flux for many of the pore size distributions considered in this study. The resulting maximum ice layer lifetime would then be between 10^8 to 10^9 years, a result that is entirely independent of how small the actual pore sizes of the regolith might be.

4. Climatic change. Changes in the Martian climate, which may have occurred since the formation of Tharsis, could potentially affect the stability of a fossil ground ice layer in two distinct ways. First, a long term ($\geq 10^5$ year) oscillation in regolith surface temperatures about their present mean annual values could reduce the lifetime of a buried ice layer by periodically increasing the H_2O vapor pressure above the ice layer surface. Due to the highly non-linear dependence of the saturated vapor pressure of H_2O on temperature, the amount of ground ice that is lost during the high temperature half of such a periodic variation will always exceed the amount that is preserved by the low temperature part of the cycle. Therefore, the greater the amplitude of the temperature change, the greater the reduction in ice layer lifetimes. For a climatic variation in regolith temperature of ± 5 K, the figure obtained by Toon et al. (1980) for the equatorial latitudes, the decrease in ice layer lifetimes presented in Table 2.3 is of the order of 10%.

A second climatic process, suggested by Fanale (1977), is potentially of far greater importance. Climatic fluctuations in both regolith temperature and atmospheric pressure will strongly influence the amount of CO_2 which is adsorbed within the Martian regolith. Indeed, Fanale and Cannon (1979) have estimated that climatic fluctuations may drive a periodic exchange of as much as 10^{20} g of CO_2 between the regolith, atmosphere, and seasonal polar caps. Fanale (1977) has suggested that the CO_2 desorbed from the regolith during this exchange may act as a carrier gas, effectively flushing the

regolith pores of diffusing H_2O molecules. The periodic nature of the obliquity and orbital variations that drive climatic change on Mars implies that the cycle of regolith CO_2 adsorption/desorption has been repeated many hundreds of times throughout Martian geologic history (Fanale and Cannon, 1979; Toon et al., 1980). Unfortunately, our current diffusion model lacks the sophistication to quantify the actual net reduction in ice layer lifetimes that may result from this exchange. However, if the removal of diffusing H_2O molecules is accomplished with even moderate efficiency, then it appears that the climatic cycling of CO_2 will considerably shorten the lifetime of equatorial ground ice.

G. Summary

Using a model based on the present best estimates of the physical properties of the Martian regolith, we have investigated the stability of a buried ground ice layer in the equatorial region of Mars. Consideration of the lifetimes calculated for this regolith-ice layer model and the potential effects of the additional factors discussed below suggests that on a global scale it is by no means obvious that an unreplenished layer of equatorial ground ice could have survived in disequilibrium with the atmosphere for as long as 3.5 billion years. The most important factors affecting the stability of equatorial ground ice appear to be (1) the pore structure of the regolith, (2) the geothermal gradient, and (3) the climatic desorption of regolith CO_2 .

Specifically,

1. Various lines of evidence indicate that the structure of the Martian regolith may be similar to that of aggregated terrestrial silt- and clay-type soils. If so, the regolith's pore size distribution is likely to be very broad, and may contain a number of interaggregate pores with radii greater than 10 microns. Our calculations indicate that a porosity of more than a few percent in these larger pores will substantially reduce the effectiveness of the regolith as a long term diffusive barrier to H_2O . For this reason, most of the fine-grained terrestrial soils considered in this study were unable to preserve a 200- meter-thick layer of ground ice buried beneath 100 meters of ice-free regolith for as long as 3.5 billion years. A more coarsley textured regolith, such as lunar soil, would have resulted in even shorter lifetimes. The results of this study clearly demonstrate that a soil's gaseous permeability cannot be determined on the basis of particle size and porosity alone. Since a well-aggregated fine-grained soil commonly possesses individual pores as large as those typically found in a more coarsley textured single-grained soil, simulations of volatile exchange on Mars that ignore the effect of soil structure may seriously underestimate the extent of diffusive transport that can occur within the regolith.

2. The calculations presented in this study were based on the assumption that the Martian regolith could be considered isothermal down to a depth of 300 meters; however, it appears likely that the Martian geothermal heat flux may begin to elevate subsurface

temperatures at much shallower depths. The presence of even a small geothermal gradient may result in a significant reduction in ice layer lifetimes by (1) thermally driving the transport of H_2O to the colder near-surface regolith, and by (2) increasing the vapor pressure at the ice layer surface as the sublimation front propagates deeper into the Martian crust.

3. Although no attempt was made in the present study to quantitatively assess the importance of CO_2 desorption on the stability of equatorial ground ice, Fanale (1977) has proposed that the climatic exchange of CO_2 between the regolith, atmosphere, and seasonal polar caps, could significantly accelerate the evaporative loss of Martian ground ice by actively flushing the regolith pores of diffusing H_2O molecules. A more detailed examination of the effects of thermal gradients and CO_2 desorption on the stability of equatorial ground ice is in preparation.

If the lifetime of a fossil ground ice layer in the equatorial region of Mars is less than 3.5 billion years, then the fundamental problem that originally motivated this study still remains: how does one account for the seemingly abundant morphologic evidence that substantial quantities of ground ice have existed within the equatorial regolith throughout most of Martian geologic history? The possible answers appear to be as follows:

1. The accepted interpretation of certain Martian surface features as morphologic indicators of ground ice may be in error. The existence of equatorial ground ice is supported by the interpretation

and distribution of a variety of Martian landforms (Johansen, 1978, 1981; Rossbacher and Judson, 1981). Unfortunately, several of the generally accepted morphologic indicators of ground ice, such as rampart craters, are far more common than the others (Allen, 1979). Should ongoing research reveal tenable alternative explanations for the origin of these features, which do not require the presence of regolith H_2O , then the evidence for the widespread occurrence of equatorial ground ice will be seriously weakened.

2. The actual physical characteristics of the Martian regolith, including the quantity of H_2O stored in the regolith as ground ice, may differ substantially from the model parameters chosen for this study. While we have attempted to base our study on a realistic model of the Martian regolith, the possibility that one or more of the model parameters was incorrectly chosen cannot be ignored. For example, our calculations indicate that the lifetime of a fossil ground ice layer could be considerably extended by an extremely fine-grained and essentially structureless regolith. However, should the specific surface area of the Martian regolith exceed several hundred square-meters per gram (as it would if the regolith contained a large quantity of smectite clay), then the surface flux of H_2O might well negate any extension of ice layer lifetimes achieved by the smaller pores of a clay-dominated single-grained regolith.

A longer ground ice lifetime might also result if the geothermal gradient on Mars were extremely small. Without a strong thermally-induced vapor pressure gradient to redistribute H_2O to shallower

depths, equatorial ground ice might easily survive beneath a kilometer thick blanket of regolith throughout Martian geologic time.

Finally, the inventory of ground ice on Mars may be substantially greater than the 10^4 g/cm² figure assumed in this study. Indeed, J. S. Lewis (personal communication, 1980) has argued that the primitive solar nebula was sufficiently enriched with H₂O at the distance of Mars that the planet may easily possess an inventory of water which exceeds an equivalent layer 1000 meters deep averaged over its surface. While such an inventory would do nothing to reduce the rate of ice layer depletion, it could substantially extend the period of time that ice was actually present in the equatorial regolith.

3. Equatorial ground ice may have been replenished. If this replenishment has occurred atmospherically during the past 3.5 billion years, either by cold-trapping or by direct precipitation as snow or rain, then it may suggest one of two possibilities: (1) that the climatic model of Toon et al. (1980) is somehow in error, or (2) that the formation of Tharsis occurred at a time considerably more recent than the estimate of Wise et al. (1979). Subsurface replenishment, from juvenile water or from an established subpermafrost groundwater system, would avoid both of these conflicts. Clifford (1980, 1982) has reviewed several mechanisms by which the transport of H₂O from a deeply buried source region to the near-surface regolith could occur within the Martian regolith; probably the most important of these is the process of thermal moisture transfer discussed by Philip and de Vries (1957). By this process, a geothermal gradient of 45 K/km could

vertically transport enough H_2O through the regolith to replenish a layer of ground ice nearly 1.7 km thick over the course of Martian geologic history (Clifford, 1982).

H. Conclusion

As first demonstrated by Smoluchowski (1967, 1968), given appropriate conditions of porosity, pore size, temperature, and depth of burial, ground ice in disequilibrium with the water vapor content of the Martian atmosphere may survive for billions of years. Indeed, in view of the likely range of geologic environments to be found on Mars, the necessary conditions for the long-term survival of equatorial ground ice undoubtedly exist in isolated regions. However, on a global basis, the physical properties of the Martian regolith inferred from recent spacecraft observations, combined with the results of the calculations presented in this study, suggest that it is unlikely that a fossil layer of equatorial ground ice has been preserved throughout Martian geologic history. The morphologic evidence indicating the presence of ground ice in this region for such a time span may imply that equatorial ground ice has undergone a process of continuous or periodic replenishment.

I. Notation

c_s	surface concentration, molecules/cm ² .
d	particle diameter, cm.
D_{AB}	ordinary molecular diffusion coefficient, cm ² /sec.
D_{KA}	Knudsen diffusion coefficient for A, cm ² /sec.
D_{eff}	effective diffusion coefficient, cm ² /sec.
D_s	surface diffusion coefficient, cm ² /sec.
E	total regolith porosity, cm ³ /cm ³ .
E_1	micropore porosity, cm ³ /cm ³ .
E_2	macropore porosity, cm ³ /cm ³ .
$f(r)$	lognormal distribution function defined by Equation (II.2).
J_A	gaseous flux of A, molecules/cm ² -sec.
J_B	gaseous flux of B, molecules/cm ² -sec.
J_{H_2O}	gaseous flux of H ₂ O, molecules/cm ² -sec.
J_s	surface flux, molecules/cm ² -sec.
k	Boltzmann's constant, 1.38×10^{-16} erg/K.
M_A	molecular weight of A, g/mole.
M_B	molecular weight of B, g/mole.
M_{H_2O}	molecular weight of H ₂ O = 18 g/mole.
n	total gas concentration = $n_A + n_B$, molecules/cm ³ .
n_A	gas concentration of A, molecules/cm ³ .
n_B	gas concentration of B, molecules/cm ³ .
N_O	Avagadro's number, 1 mole = 6.02×10^{23} molecules.
P	total pore pressure, dynes/cm ² .

P_{H_2O}	partial pressure of H_2O , dynes/cm ² .
q	gaseous tortuosity factor (assumed to be = 5).
Q	heat of adsorption, kcal/mole.
q_s	surface tortuosity factor (assumed to be = 5).
r	pore radius, cm.
r_m	median pore size of lognormal distribution, cm.
r_{m1}	median pore size of micropores, cm.
r_{m2}	median pore size of macropores, cm.
r_{max}	maximum pore size in a distribution, cm.
r_{min}	minimum pore size in a distribution, cm.
R	universal gas constant = 8.314×10^7 erg/K-mole = 1.9865 calories/K-mole.
S_m	specific surface area of regolith, cm ² /g.
T	temperature, K.
Y_{A0}	relative concentration of A to B at $z=0$.
Y_{AZ}	relative concentration of A to B at $z=Z$.
z	depth from surface, cm.
Z	depth of ice layer surface, cm.

Greek letters:

α	$= (M_A/M_B)^{1/2}$
$\Delta \epsilon(r)$	differential porosity in $\Delta \ln(r)$, cm ³ /cm ³ .
$\Delta \ln(r)$	lognormal pore interval.
λ	mean free path of H_2O molecules in Martian atmosphere = 8 microns.

- ρ_s mean particle density, g/cm³.
 σ standard deviation.
 σ_1 micropore standard deviation.
 σ_2 macropore standard deviation.
 $d\tau$ lifetime for 50 g H₂O ice at depth Z, sec.

CHAPTER III

MECHANISMS FOR THE SUBSURFACE REPLENISHMENT OF EQUATORIAL GROUND ICE ON MARS

A. Introduction

Under current climatic conditions on Mars, the occurrence of ground ice in equilibrium with the water vapor content of the atmosphere is restricted to the colder latitudes poleward of $\pm 40^\circ$ (Leighton and Murray, 1966; Fanale, 1976; Farmer and Doms, 1979). However, various lines of geomorphologic evidence suggest that substantial quantities of ground ice have existed in the equatorial regolith of Mars throughout most of its geologic history (e.g., Johansen, 1978; Allen, 1979a; Rossbacher and Judson, 1981).

To account for this evidence, it has been proposed that equatorial ground ice was emplaced very early in Martian geologic history and under substantially different climatic conditions (Soderblom and Wenner, 1978; Arvidson et al., 1980; Luchitta, 1981; Rossbacher and Judson, 1981). The survival of equatorial ground ice to the present day is commonly attributed to the diffusion-limiting properties of a fine-grained regolith. This explanation is based on the work of Smoluchowski (1968) who showed that under certain limited conditions of regolith porosity, pore size, temperature, and depth of burial, ground ice in disequilibrium with the Martian atmosphere might survive for billions of years.

While the physical properties necessary for the long-term survival of equatorial ground ice may exist in isolated regions, data obtained during the Mariner and Viking missions to Mars suggests that it is unlikely that such properties characterize the Martian regolith on a global scale. If this analysis is correct, then any ground ice emplaced earlier than 3.5 billion years ago has long since been lost by sublimation to the atmosphere (Clifford and Hillel, 1983).

We are therefore left with a fundamental problem: how does one account for the seemingly abundant geomorphologic evidence that substantial quantities of ground ice have existed within the equatorial regolith for billions of years? One possible solution may be that equatorial ground ice has undergone a process of continuous or periodic replenishment. Yet, under present climatic conditions, the atmospheric loss of ground ice from the equatorial regolith appears irreversible--once ground ice has evaporated, or been removed by some other process, it is difficult to see how it could be replenished by any atmospheric means (Flasar and Goody, 1976). As discussed by Clifford (1980d; 1982a; 1983), this difficulty may be avoided if equatorial ground ice has been replenished by subsurface sources of H_2O .

Given the possibility of subsurface replenishment, by what processes can H_2O be vertically transported from a deeply buried source region to the near-surface regolith? Further, while theoretical arguments may indicate the need to consider the possibility of ground ice replenishment, is there any physical evidence that such replenishment has in fact occurred? In an effort to address these

questions, the geomorphic evidence for the replenishment of ground ice, and several possible mechanisms for the vertical transport of H_2O , will be presented in the following discussion. These processes appear viable, even where the vertical distances separating the source region from the base of the ground ice layer are measured in kilometers.

B. Possible Evidence of Ground Ice Replenishment

Evidence for the replenishment of equatorial ground ice on Mars is based on the popularly accepted origin of Martian rampart craters (Figure 3.1), whereby the distinctive lobate nature of the ejecta blankets which surround these craters is thought to originate from the fluidization of ejecta material during an impact into a water or ice-rich regolith (Carr et al., 1977; Johansen, 1978; Mouginis-Mark, 1979).

Based on the above assumption, consider the result of a major impact in the equatorial region of Mars. Thermal models of the Martian crust indicate that the potential thickness of equatorial ground ice is of the order of 1 km (e.g., see Fanale 1976, Rossbacher and Judson 1981). As first noted by Allen (1979a), the production of a crater many tens of kilometers in diameter should result in the excavation of any ground ice which existed in the region interior to the crater walls prior to the impact (Figure 3.2). While backfilling and melting of nearby ground ice may partially replenish some of the lost H_2O near the crater periphery, it appears unlikely that its lifetime would be very long given the high temperatures and porosity of the post-impact

Figure 3.1. A classic example of a Martian rampart crater is the crater Yuty (~ 20 km diameter, located at 22° N, 34° W). Rampart craters are found at all latitudes on Mars and in terrains which date from the oldest to the most recent. If the distinctive morphology of this type of crater does indeed originate from an impact into a water or ice-rich regolith, then rampart craters represent the single most abundant piece of morphologic evidence for the global distribution of ground ice on Mars.



Figure 3.1

Figure 3.2. The eventual ground ice distribution which may result from a major equatorial impact (Clifford and Johansen, 1982).

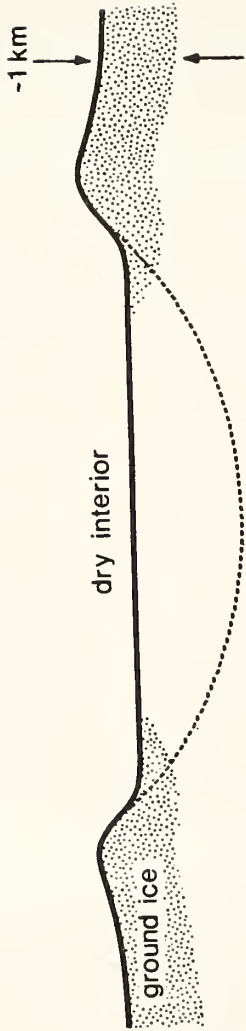


Figure 3.2

environment.

Therefore, it is interesting to note that within a number of large impact craters in the equatorial region of Mars there exist clearly defined rampart craters (Allen, 1979a). If one accepts the interpretation that the morphology of this type of crater owes its origin to an impact into a water or ice-rich regolith, then the existence of rampart craters within the interiors of numerous older and larger craters in the equatorial region of Mars presents a problem; for it is difficult to conceive of a scenario by which any ground ice that existed prior to the original cratering event could have managed to survive to produce the well defined fluidized ejecta pattern often seen as the result of a second and sometimes third (Figure 3.3) consecutive and concentric impact.

Other puzzling geomorphic examples also exist. As first noted during the Mariner 9 mission (Mutch et al., 1976), the southern two-thirds of Mars is dominated by ancient cratered highlands, while the northern third is covered by a younger smooth plains unit that averages some two kilometers lower in elevation. The border between these two provinces is approximated by a great circle which is inclined about 35 degrees to the planet's equator (Mutch et al., 1976). It has been proposed that the primary origin of this dichotomy was due to subcrustal erosion by a large convective cell within the mantle (Wise et al., 1979), but there is evidence which suggests that, near the present boundary between these two regions, the topographically lower northern plains may have developed through the surficial destruction of

Figure 3.3. A rampart crater within two earlier and concentric impact features (20° S, 203° W) (Clifford and Johansen, 1982). The oldest crater in the sequence (Hadley) is approximately 110 km in diameter, while the innermost crater (arrow) has a diameter of roughly 13 km.



Figure 3.3

the older cratered highlands (Soderblom and Wenner, 1978; Rossbacher, 1983). Soderblom and Wenner (1978) and Rossbacher (1983) have argued that this peripheral erosion of the cratered uplands was due to the loss of ground ice within the uppermost one or two kilometers of the regolith. Yet, as seen in Figure 3.4, this proposal is difficult to reconcile with the occurrence of clearly defined rampart craters within this eroded region.

There are at least two possible explanations that may account for these observations. First, contrary to popular belief, rampart craters may not be specific indicators of the presence of regolith H_2O . Schultz and Gault (1979) have shown that atmospheric braking may have a considerable effect on ejecta blanket morphology. Indeed, under the right pressure conditions, atmospheric braking is capable of producing many of the features generally associated with rampart craters. However, the principal shortcoming of this and other alternative explanations for the origin of Martian rampart craters is that, by themselves, they appear unable to account for the reported latitudinal dependence of rampart crater ejecta morphologies. These morphologies vary from an apparent low-mobility/high-viscosity ejecta pattern at colder latitudes to a highly fluidized multilobate-style near the equator (Johansen, 1978; Saunders and Johansen, 1980; Blasius *et al.*, 1981a,b). Advocates of the ground ice hypothesis suggest that this observed latitudinal dependence is consistent with thermal models of the regolith, which predict that the depth of frozen ground on Mars thins appreciably as one moves equatorward from the poles.

Figure 3.4. A possible example of thermokarst on Mars (23° N, 30° W). The plateau region, visible in the lower half of this photograph, is bordered by a highly eroded scarp. The apparent retreat of the scarp and the occurrence of irregular depressions within the plateau is thought to result from the local depletion of interstitial ice whose removal may have precipitated the subsidence of the overlying terrain. Note the occurrence of a rampart crater (~ 6 km in diameter) within the theoretically ice-free lower plains.

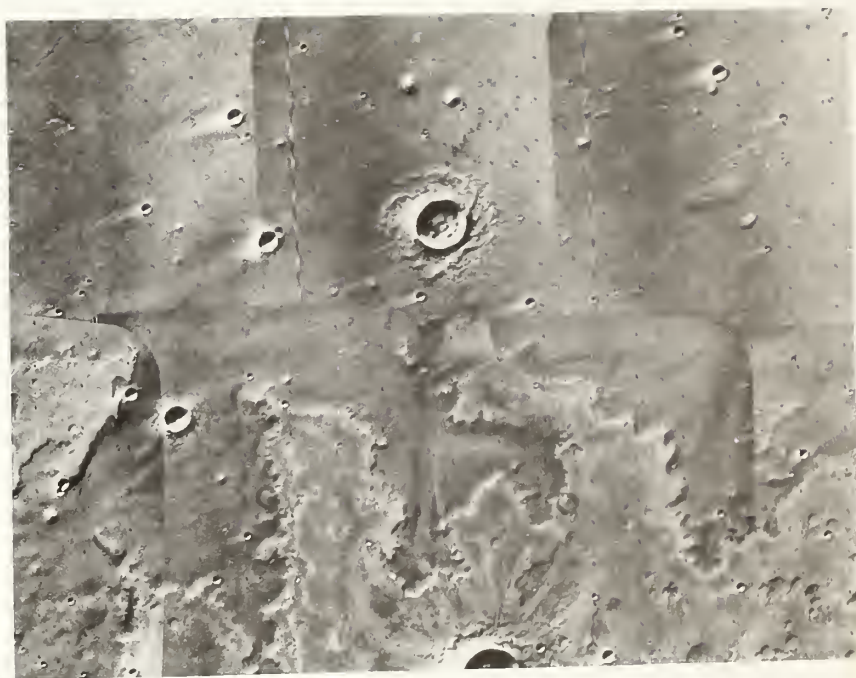


Figure 3.4

It appears that the most reasonable explanation for the occurrence of rampart craters in terrains which are theoretically ice-free is that at some time following the original loss of ground ice, it was replenished by some non-atmospheric means. This conclusion is consistent with our present understanding of both the geology and past climate of Mars.

For any subsurface source to be able to replenish near-surface ground ice, some process for the vertical transport of H_2O between the source region and the base of the ground ice layer is required. In the next section, three possible processes for this transport will be discussed.

C. Processes of Replenishment

Current estimates of the inventory of H_2O on Mars, which range from a globally averaged layer some $10^2 - 10^3$ meters deep (Pollack and Black, 1979; J. S. Lewis, personal communication, 1980), are sufficiently large that a significant fraction of this water may be stored within an extensive network of subpermafrost aquifers similar to those found in Siberia, the Antarctic, and other cold regions on Earth. Such aquifers may be of regional and possibly even global extent (Carr 1979; Clifford and Huguenin 1980; Clifford, 1980d). Alternatively, the occurrence of large quantities of subsurface water may be restricted solely to regions of past major volcanic activity, such as Tharsis and Elysium, where juvenile water has preferentially been injected into the

crust (Carr 1979; Fanale, personal communication, 1983). In either case, the vertical transport of H_2O from such subsurface reservoirs appears to be a viable mechanism for the replenishment of equatorial ground ice.

1. Hydrothermal convection. In light of the photogeologic evidence for the widespread occurrence of volcanism on Mars (Greeley and Spudis, 1981), the most obvious mechanism for the vertical transport of H_2O is hydrothermal convection. There exist a number of features whose origin might be explained by this process. For instance, Morris (1980) has suggested that dark surface stains that parallel a major fault-line just west of Olympus Mons may have resulted from the hydrothermal circulation of mineral-laden groundwater (Figure 3.5a). Hydrothermal circulation has also been suggested as a possible explanation for the origin of the numerous small channels commonly observed to emanate from the outside rims of craters in the heavily cratered terrain of Mars (Figure 3.5b) (Pieri, 1979; Schultz and Glicken, 1979; Clifford, 1980d).

2. Shock-induced transport. Shock waves generated by earthquakes, impacts, and explosive volcanic eruptions can produce a transient compaction of water-bearing sediments that may force water to the surface through fractures and pores in the Martian crust. During the great Alaskan earthquake of 1964, this process resulted in water and sediment ejection from the ground as far as 400 km from the

Figure 3.5a. Twelve aligned dark patches are evident in red-filter imagery of this region just west of Olympus Mons (17° N, 142° W). Morris (1980) suggests that these patches may have formed as mineral-laden groundwater discharged along a subsurface fissure paralleling the major fault line observed to the north. (Figure courtesy of E. C. Morris.)

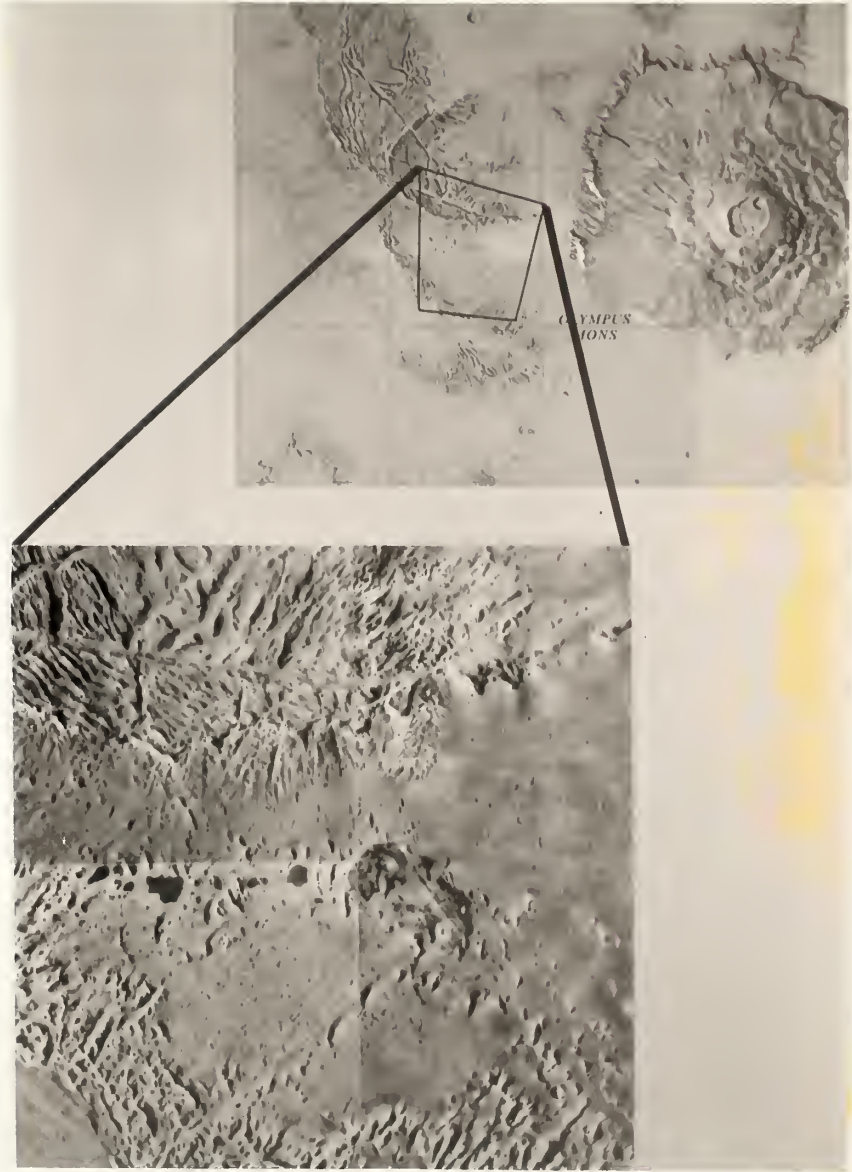


Figure 3.5a

Figure 3.5b. Small channels within the heavily cratered terrain of Mars (25° S, 10° W). The preferential origin of many of the Martian valley networks within both the ejecta blankets and along the outside rims of craters suggests a possible genetic relationship. One explanation for this association is that the heat generated by the impact process led to the local melting of ground ice and subsequent hydrothermal circulation of this H_2O to the surface (Clifford, 1980d).



Figure 3.5b

earthquake's epicenter (Figure 3.6) (Waller, 1968). The energy released by this earthquake was approximately 2×10^{16} J (Stacey, 1977) - or roughly equivalent to that of a 5-megaton nuclear explosion. While the historical frequency of earthquakes of this magnitude on Mars may have been low, the Martian cratering record provides abundant evidence that the planet has witnessed numerous events of a similar, and often much greater, magnitude. Indeed, the impacts that produced the larger basins, such as Hellas and Argyre, may alone have generated enough seismic energy to have replenished Martian ground ice on a global scale. Even without these larger impacts, however, the density of craters found over much of the surface suggests that shock-induced transport resulting from smaller impacts may have been sufficient to replenish near surface ground ice over much of the planet.

While both shock-induced transport and hydrothermal convection are likely mechanisms for the vertical transport of H_2O in the Martian crust, their active operation has been spatially localized and discontinuous in time. So too, the magnitude of transport that has occurred by these processes is difficult to quantify. Fortunately, neither of these objections apply to the third and final process we shall consider.

3. Thermal moisture movement. Although far less dramatic and energetic than either of the two processes discussed above, perhaps the most important mechanism for the vertical transport of H_2O on Mars has been the process of thermal moisture movement (Clifford, 1980d; 1982a).

Figure 3.6. Water and sediment ejection along ground fissures during the great Alaskan earthquake of 1964 (Waller, 1968).



Figure 3.6

The presence of a geothermal gradient in the Martian crust will give rise to a corresponding vapor pressure gradient. As a result of this pressure difference, any water vapor present in the crust will diffuse from the higher temperature (high vapor pressure) depths to the colder (lower vapor pressure) near-surface regolith.

It has been known for almost 70 years that H_2O transport in excess of that predicted by Fick's law will occur in a porous medium under the influence of a temperature gradient, the direction of transfer being from warm to cold (Bouyoucos, 1915). At the present time two different but widely accepted models for calculating the magnitude of this type of thermally driven moisture transfer have been proposed in the soils literature (Philip and deVries, 1957; Cary, 1963). The Philip and deVries (1957) approach is based on a mechanistic description of the transport process. They suggest that the exchange of water vapor in an unsaturated soil occurs between numerous small "islands" of liquid which exist at the contact points of neighboring soil particles. The existence of a temperature gradient in the soil causes water from the warmer liquid islands to evaporate, diffuse across the intervening pore space, and condense on the cooler liquid islands at the opposite ends of the pore. In this fashion both moisture and latent heat are transferred through the soil (Figure 3.7).

It should be noted that the microscopic temperature gradient across an individual pore is not the same as the measured macroscopic temperature gradient. The macroscopic gradient is an average of the individual gradients which exist across the volumes of air, water, and

Figure 3.7. The process of thermal moisture transfer proposed by Philip and de Vries (1957) (Clifford, 1980).

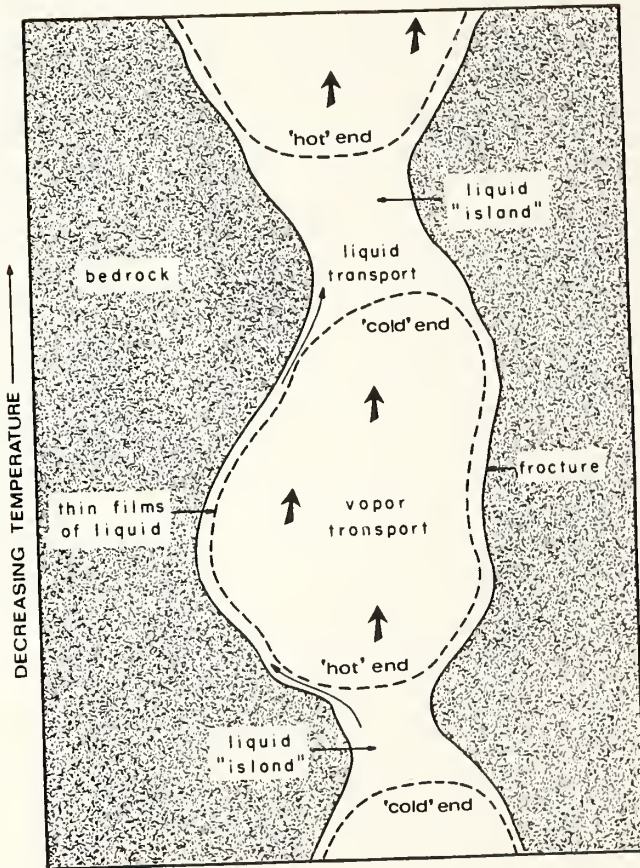


Figure 3.7

solids, present in the soil. Of these gradients, the gradient through the air in the pores will be the largest. Since it is the air temperature gradient which governs the magnitude of vapor diffusion, the total amount of H_2O transport through the soil can be several times greater than that predicted on the basis of the macroscopic temperature gradient alone (Philip and deVries, 1957).

The Cary (1963) model of H_2O transport differs from the Philip and deVries approach in that it makes no assumptions regarding the actual mechanism of vapor transport but merely attempts to provide a phenomenological description of the process based on the thermodynamics of irreversible process (Cary, 1963). Despite the differences in approach, it has been shown that the final form of the flux equations for both models are identical (Taylor and Cary, 1964, Jury and Letey, 1979). After Cary (1966), we can describe the thermally driven vapor flux by the equation

$$J_V = - \frac{\beta D_{AB} P_s H}{R T^3} \frac{dT}{dz} \quad (\text{III.1})$$

where D_{AB} is the binary diffusion coefficient of H_2O in CO_2 , P_s is the saturated vapor pressure of H_2O at a temperature T , H is latent heat of vaporization, R is the universal gas constant, and β is a dimensionless factor whose value (typically around 1.83 (Jury and Letey, 1979)) depends on regolith temperature, porosity, and water content. Making use of this equation, we find that for a Martian geothermal gradient of 25 K/km, the calculated flux of H_2O to the

freezing front at the base of the ground ice layer is approximately 4×10^{-5} g/cm² per Martian year. Over the course of Martian geologic history this will supply enough H₂O from a subpermafrost groundwater system to replenish a layer of ground ice over 1 km thick. It should be noted that this transport will occur on a continuous and global basis for as long as there exists a geothermal gradient and subsurface reservoir of H₂O.

Inspection of Equation (III.1) reveals that the flux of H₂O leaving the groundwater surface greatly exceeds that which finally reaches the freezing front at the base of the ground ice layer. This difference is due to the decrease in saturated vapor pressure which occurs with decreasing temperature. As shown by Jackson *et al.* (1965), once a closed system has been established (*i.e.*, the ground ice capacity of the near-surface regolith has been saturated under conditions where the ice exists in stable equilibrium with the atmosphere), a dynamic balance of opposing fluxes is achieved. As water vapor rises from the warmer depths to the colder regolith above, it will condense, creating a circulation system of rising vapor and descending liquid condensate (Figure 3.8).

While the process of thermal vapor transport may, by itself, resolve the problem of ground ice replenishment, it is important to note that thermally driven liquid transport can also occur if the water content of the regolith is high enough to provide thin film continuity (Figure 3.7) (Philip and deVries, 1957). The thermal liquid flux originates from the temperature dependence of the surface tension.

Figure 3.8. The presence of a geothermal gradient in the Martian crust may give rise to a convective cycling of H_2O between a subsurface reservoir of groundwater and near-surface ground ice.

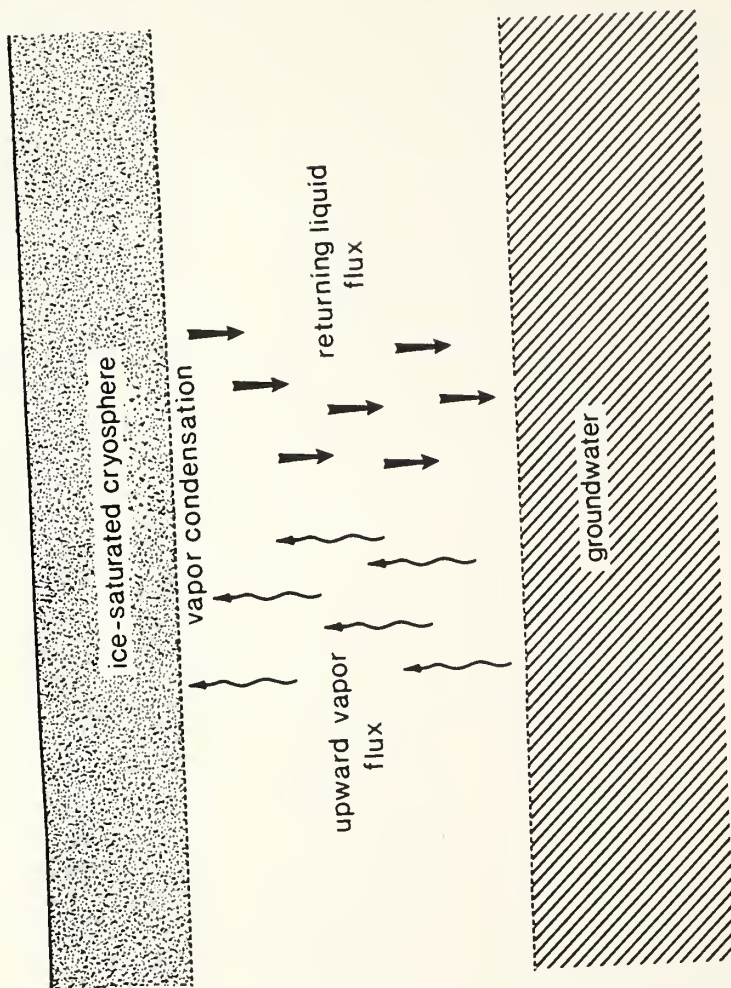


Figure 3.8

Thus a temperature gradient can induce a surface tension gradient which can draw liquid water and its associated solutes into the colder regions of the crust.

By such processes of thermal vapor and liquid transport the interiors of equatorial craters, and the eroded terrains surrounding the southern hemisphere's ancient cratered highlands, may have been recharged with ground ice from sources of H_2O deep within the Martian crust (Figure 3.9).

E. Conclusion

If H_2O exists in sufficient quantities for subpermafrost aquifers to exist on Mars, or if juvenile water is currently being released by the planet's interior, then several processes for the vertical transport of H_2O from these sources appear viable; they are: hydrothermal convection, shock-induced transport, and thermal moisture movement. While all three of these processes may have led to the transport of significant quantities of H_2O to the near-surface regolith, calculations indicate that over the course of Martian geologic history thermal vapor transport alone may have been sufficient to account for the emplacement and subsurface replenishment of equatorial ground ice. This process will occur on a global scale, given the existence of a geothermal gradient and the continuity of pore space between the source region and the near-surface regolith.

Figure 3.9. The vertical transport of H₂O in response to the Martian geothermal gradient may be the mechanism whereby the interiors of equatorial craters are recharged with ground ice (Clifford and Johansen, 1982).

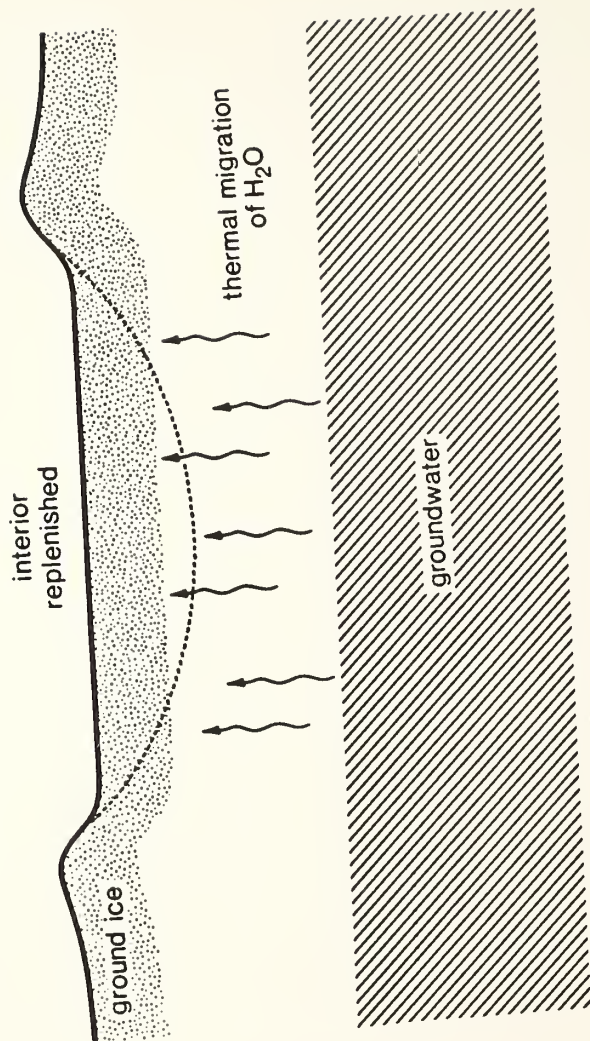


Figure 3.9

CHAPTER IV
POLAR BASAL MELTING ON MARS

A. Introduction

The Martian cryosphere has been defined as that region of the Martian crust where temperatures remain continuously below the freezing point of water (Fanale, 1976, Rossbacher and Judson, 1981). Its extent is determined by the latitudinal variation of mean annual surface temperatures, the thermal conductivity of the regolith, and by the value of the Martian geothermal heat flux. Based on reasonable estimates of these variables, present thermal models suggest that the depth to the 273 K isotherm varies from approximately 1 km at the equator to slightly in excess of 3 km at the Martian poles (Figure 4.1) (Fanale, 1976; Rossbacher and Judson, 1980).

Recent estimates of the total inventory of H₂O on Mars (McElroy et al., 1977; Pollack and Black, 1979; Lewis, personal communication, 1980) are sufficiently large ($\geq 10^7$ km³) that the pore volume of the Martian cryosphere may very well be saturated with ice, at least near the poles. Therefore, the deposition of any additional material in the Martian polar regions will result in a situation where the equilibrium depth to the melting isotherm has been exceeded; thus, basal melting will begin, and continue, until the equilibrium depth to the melting isotherm is once again established.

The water which results from basal melting will fill the available

Figure 4.1. A pole-to-pole cross section of the Martian crust illustrating the theoretical latitudinal variation in depth to the 273 K isotherm (after Fanale (1976) and Rossbacher and Judson (1981)).

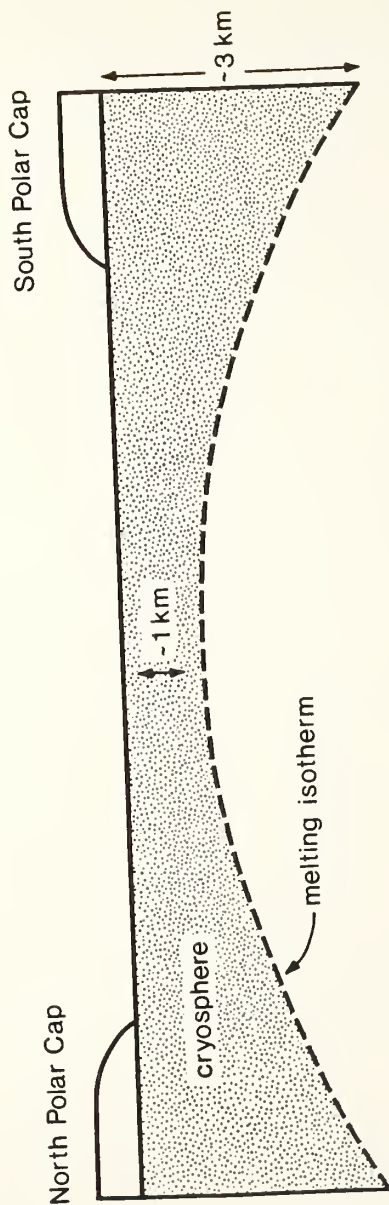


Figure 4.1

pore space that exists beneath the Martian cryosphere. Calculations indicate that the total pore volume of the Martian crust is substantial, and may be sufficient to store a quantity of H_2O equivalent to a globally averaged layer approximately 1 km in depth (Chapter V). Some possible consequences of this large storage potential will be presented later in this chapter.

Polar basal melting on Mars has previously been cited as a potentially important process in understanding the climatic history of H_2O on Mars and the evolution of the Martian polar terrains (Clifford and Huguenin, 1980; Clifford, 1980a,b,c; Howard, 1981). In this chapter the thermal requirements and implications of this process will be discussed in greater detail.

B. A Geologic Summary of the Martian Polar Terrains

1. Composition. During their respective hemispheric winters, seasonal polar caps are observed to grow on Mars until they completely cover the regions poleward of $\pm 40^\circ$ (Thomas, 1981). In the spring, these seasonal caps shrink to perennial remnants that are but a few percent of their maximum seasonal extent. Early thermal modeling by Leighton and Murray (1966) and Leovy (1966) showed that the temporal behavior of the seasonal polar caps could most easily be explained if they were composed of CO_2 ice. This prediction was later confirmed by thermal and spectroscopic observations made during the flyby of the Mariner 7 spacecraft (Neugebauer et al., 1971).

While the Mariner 7 results ended the debate over the composition of the seasonal polar caps, questions still remained regarding the composition of the much smaller remnant caps which were observed to persist at both poles throughout their respective summers. These questions went unresolved until the arrival of the Viking mission to Mars in 1976.

Viking observations of the perennial north polar ice deposits revealed summertime brightness temperatures as high as 205 K, well in excess of the 148 K sublimation temperature of CO_2 at the present 6.1 millibar mean atmospheric surface pressure of Mars (Kieffer et al., 1976). In addition, concurrent measurements of the water vapor column abundance above the polar ice indicated that the atmosphere was saturated with respect to a surface reservoir of H_2O at 205 K (Farmer et al., 1976). These observations demonstrated conclusively that the composition of the volatile component of the remnant northern cap was water ice.

While the observed high summer brightness temperature of the north pole eliminated any possibility of a CO_2 or CO_2 -clathrate component in the polar ice, it also provided strong evidence that the polar deposits consisted of something other than simply H_2O alone. Based on the assumption that the polar deposits were in radiative equilibrium with incoming solar radiation at the time of the summertime temperature measurements, it was determined that the polar ice cap had a maximum bolometric albedo of 0.45 (Kieffer et al., 1976); this figure differs substantially from the known albedo of pure ice of 0.7. In light of

this observation, and the established observational record of frequent planetary-scale dust storms on Mars, Kieffer et al. (1976) concluded that the most reasonable explanation for the origin of the low albedo of the north polar ice was by the deposition and subsequent entrainment of atmospheric dust. This conclusion was supported by high resolution imagery of the polar cap which showed that interbedded with the polar ice were numerous horizontal layers of a dark material, presumably dust (Cutts et al., 1976).

With the identification of H₂O ice in the north, it was generally expected that the composition of the south perennial ice cap would also prove to be H₂O. The basis for this expectation was that southern summer on Mars occurs very near perihelion; therefore, it was anticipated that southern summer polar temperatures would be higher than those measured in the north. During the southern summer, however, Viking Orbiter thermal observations failed to indicate polar ice surface temperatures much above the 148 K sublimation temperature of CO₂ (Kieffer, 1979). Water vapor measurements made over the south pole at this time were also substantially below those which had been observed earlier over the north (Davies and Wiano, 1981; Jakosky and Farmer, 1982).

These observations led Kieffer (1979) to conclude that the southern perennial cap had remained covered with CO₂ ice throughout the Martian year. However, Jakosky and Farmer (1982) have pointed out that, in light of the persistently low temperatures measured over the south polar cap, it must have acted as a cold trap for atmospheric

H₂O; therefore, it seems reasonable to assume that the cap is at least partially composed of water ice. Jakosky and Farmer (1982) further suggest that the low south polar surface temperatures and water vapor abundances measured during the Viking mission were a consequence of the high atmospheric opacity which resulted from the extensive dust-storm activity observed earlier that year. In support of this hypothesis they cite the previous Earth-based observations of Barker et al. (1970), who measured high water vapor abundances over the south polar region during southern summers of little or no dust storm activity.

2. Geology. As revealed in high-resolution Mariner 9 and Viking imagery, the north and south polar terrains represent both the youngest and most complex surfaces to be found on Mars. The four principal geologic units common to both Martian poles are: (1) the remnant ice cap, (2) polar layered deposits, (3) etched and pitted terrain, and (4) the debris mantle (Murray et al., 1972; Soderblom et al., 1973a,b). In the north, these polar terrains overlie the moderately cratered plains, while in the south they blanket the ancient (~4 billion year old) heavily cratered highlands (Murray et al., 1972; Soderblom et al., 1973a).

The extreme youth of both the polar icecaps and layered deposits is supported by Viking high-resolution photographs of the north polar region. These images reveal that, within the 8×10^5 km² covered by the northern layered deposits, there are no craters with diameters

greater than 300 meters. As noted by Cutts et al. (1976), this observation argues for an age of the exposed surface which is less than 10^6 years.

The northern layered deposits occupy the region poleward of 80°N ; the remnant ice cap, which has a diameter of roughly 1000 km (Carr, 1981), both overlies and appears to be genetically related to these layered deposits. Both units are characterized by numerous laterally extensive horizontal layers that have individual thicknesses of 14-46 meters (Blasius et al., 1982). Within the area occupied by the perennial cap, the deposits appear to be composed predominantly of water ice, with a small and stratigraphically variable component of entrained dust (Toon et al., 1980). Near the edge of the layered deposits, photographic evidence suggests that the volumetric mixing ratio of ice to dust is significantly reduced; therefore, in this region, the successive layers that comprise the deposits may consist primarily of dust which has been cemented and stabilized by the presence of pore ice (Cutts et al., 1979). On the basis of Mariner 9 radio occultation data, Dzurisin and Blasius (1975) have estimated that these layered polar units reach a maximum thickness of 4-6 km near the center of the perennial cap.

As seen in Figure 4.2, the most distinctive characteristic of the northern cap is the pattern of dark parallel linear troughs which swirl out in a counterclockwise direction from the pole (Soderblom et al., 1973a; Cutts et al., 1976; Howard et al., 1982). Individual troughs are typically several hundred kilometers long, 5-15 km wide, and reach

Figure 4.2. The Martian north polar cap as seen by Viking [811A01, 811A02]. The large channel-like feature seen near the center of the photograph is Chasma Boreale, while the dark polar troughs can be seen spiralling outward from the center of the cap.

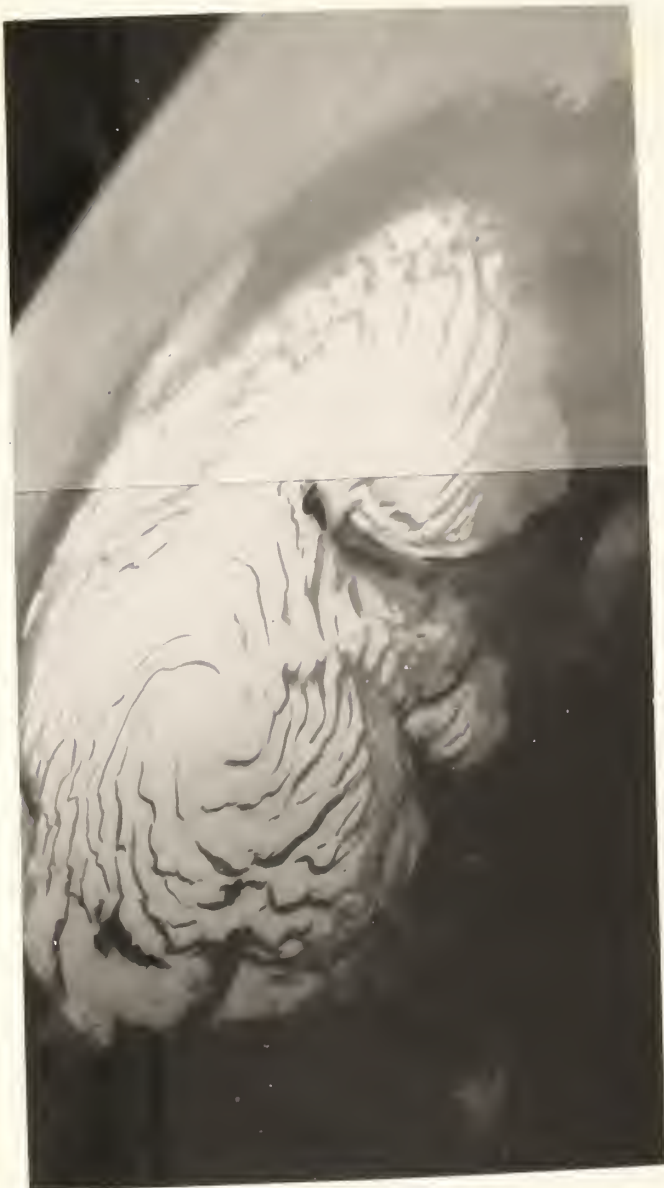


Figure 4.2

depths of 0.1-1 km; while the surface slopes, exhibited by their bordering scarps, may be as steep as 8° (Howard et al., 1982). Also visible in Figure 4.2 are several major erosional reentrants. The largest of these, Chasma Boreale (85°N , 0°W), originates from deep within the interior of the cap and extends radially to its edge over a distance of approximately 500 km.

In the south, the position of the small remnant polar cap (~ 350 km diameter) is centered at 86°S , 30°W (Carr, 1981). This off-axis location is attributed to the presence of a large impact basin centered at 83°S , 266°W (Wilhelms, 1973), whose interior slopes have changed the point of minimum annual insolation away from the geometric pole (Dzurisin and Blasius, 1975; Carr, 1981).

Similar to its northern counterpart, the notable features of the southern cap are the complex of parallel troughs that spiral clockwise and outward from the pole, as well as several large erosional reentrants located within the more extensive defrosted layered deposits. The largest of the erosional reentrants, Chasma Australe (88°S , 270°W), has roughly the same general scale, shape, and orientation, as Chasma Boreale in the north.

The south polar layered deposits cover a region some 1,500 to 2,000 km in diameter, an area roughly twice as large as covered by the equivalent unit in the north. As in the north, the southern deposits appear to be composed of 40 or more individual layers of material, each layer averaging some 30 m in thickness. However, radio occultation data (Dzurisin and Blasius, 1975) suggest that the total thickness of

these deposits is significantly less than in the north, reaching a maximum of only 1 to 2 km in the vicinity of 87°S , 0°W .

By far the most extensive polar unit in both the northern and southern hemispheres is the debris mantle. In a study of Mariner 9 orbital imagery, Soderblom et al. (1973b) noted that the terrains poleward of $\pm 35^{\circ}$ appear to be covered by a blanket of debris that thickens towards the poles and ultimately merges with the polar layered deposits. This unit appears to consist of an extensive blanket of eolian sediment, which in many areas near the poles appears to have undergone significant modification by the Martian winds. In the north, this modification has led to the formation of a broad circumpolar dune field near the latitude of 80°N (Cutts et al., 1976; Breed et al., 1979; Thomas, 1982), while in the south, it has resulted in extensive erosion, with exposures of the underlying heavily cratered basement in the region poleward of 70°S . The resulting topography of scoured depressions and free-standing mesas has been described as etched and pitted terrain (Murray et al., 1972; Sharp, 1973c).

3. Origin and evolution. Since Mariner 9 obtained the first clear photographs of the Martian polar terrains in 1971, various theories have been proposed to explain their origin and evolution. The resulting debate has produced what appears to be a general consensus regarding the active constructional and erosional processes responsible for the polar features we observe today (Howard et al., 1982).

One of the essential elements of this consensus model is the

belief that the polar deposits have originated from the preferential atmospheric deposition of dust and H_2O ice in the regions occupied by the seasonal CO_2 polar caps (Cutts, 1973a; Pollack et al., 1979). According to this model, dust which is raised into the atmosphere during the Martian global dust storms acts as nucleation centers for H_2O ice condensation. As either hemisphere enters the fall season, these suspended dust particles receive an additional coating of CO_2 ice that makes them heavy enough to precipitate from the atmosphere. In this fashion, atmospheric deposition contributes to the formation of the seasonal polar caps at temperate and polar latitudes.

Observational support for this model has come from photographs taken by Viking Lander 2 ($48^{\circ}N$, $225.6^{\circ}W$). During the two consecutive Martian years of observation, the lander photographs revealed the sudden appearance of a reddish-tinted "snow" in early fall (Jones et al., 1979; Wall, 1981). This thin snow cover persisted throughout the northern winter and became patchy by early spring. It was not until many weeks after surface temperatures had risen above the CO_2 frost point, however, that all the condensate finally disappeared, leaving in its place a thin veneer of dust; this observation appears to confirm the existence of a significant H_2O ice component within the seasonal deposit (Jones et al., 1979; Wall, 1981).

The ultimate fate of the dust and H_2O which precipitates from the atmosphere during the formation of the seasonal cap is a function of the latitude at which the deposition occurs. At the very highest and coldest latitudes, where H_2O ice is in equilibrium with the water

vapor content of the Martian atmosphere, the ice-rich depositional layer persists throughout the year, thus adding to the perennial cap. On the other hand, at those latitudes where temperatures sometime during the Martian year rise above the frost point, any surface H_2O is eventually lost by sublimation. Therefore, within the area that extends equatorward from the periphery of the layered terrain to the latitudes of about $\pm 40^\circ$, dust is the only visible contribution to the polar deposits. Of course, at depth, the temperature within the accumulating dust mantle may remain well below the frost point. If so, H_2O ice will be retained within the dust pores, significantly enhancing the stability of the dust against further erosion.

The banded nature of the polar layered terrains suggests that, over the course of Martian geologic history, the depositional and erosional balance at the poles has been modulated by periodic variations in insolation resulting from cyclical changes in the planet's obliquity and orbital elements (Murray et al., 1973; Ward, 1974; Toon et al., 1980; Cutts and Lewis, 1982). For example, the obliquity of Mars oscillates about its present value of 25.2° with a period of 1.2×10^5 years (Ward, 1974; Toon et al., 1980). The amplitude of this oscillation also varies, and reaches a maximum value of 13° every 1.3×10^6 years. At low obliquity, seasonal temperature fluctuations and mean annual polar temperatures are both at a minimum. This situation is dramatically reversed during times of high obliquity, when summers of continuous illumination alternate between winters of total darkness, producing both extreme seasonal variations and higher

mean temperatures at the poles.

Superimposed on the obliquity variation are such additional factors as the 5.1×10^4 year precessional cycle and two superposed periods of change in orbital eccentricity (a 1.8×10^6 year cycle with an amplitude of 0.1, and a 2.3×10^6 year cycle with an amplitude of 0.04). These combine to produce eccentricities that range from a minimum of 0 to a maximum of 0.14 (Ward, 1974; Toon et al., 1980). While changes in precession and eccentricity will affect both the duration and peak value of solar insolation during polar summers, obliquity variations are the only changes that actually affect the mean annual insolation at a given latitude.

The mean annual insolation at the poles is given by:

$$\langle I \rangle_{\text{pole}} = S_0 \sin(i) / \pi(1-e^2)^{1/2} \quad (\text{IV.1})$$

where S_0 is the solar constant at the distance of Mars, i is the obliquity, and e is the orbital eccentricity (Hoffert et al., 1981). On the basis of Equation (IV.1) and the assumption that the polar surface is in radiative equilibrium on a mean annual basis, it follows that:

$$\epsilon \sigma T_S^4 = \langle I \rangle_{\text{pole}} (1 - A_p) \quad (\text{IV.2})$$

where T_S is the mean annual surface temperature, A_p is the polar cap albedo, ϵ is the emissivity, and σ is the Stefan-Boltzman constant.

Therefore, the mean annual polar surface temperature as a function of obliquity and eccentricity is given by:

$$T_s = [\langle I \rangle_{\text{pole}} (1 - A_p) / \epsilon \sigma]^{1/4} \quad (\text{IV.3})$$

In Figure 4.3 mean polar surface temperatures are plotted as a function of the present range of obliquity. At the low end, an obliquity of 13° corresponds to a mean annual polar surface temperature of 143 K; at the high end, an obliquity of 38° corresponds to a temperature of 184 K. Substitution of the minimum or maximum values of orbital eccentricity will affect these results by only a few tenths of a degree.

The long-term variation of mean polar temperatures may have affected the evolution of the polar terrains in several ways. For example, at low obliquity, colder polar temperatures will result in a shift of the surface frost point latitude of H_2O to a position several degrees closer to the equator than it is at present, thus permitting the equatorward advance of the boundaries of the various polar terrains by a similar degree. By the same token, the warmer temperatures associated with higher obliquities will shift these boundaries closer to the pole. This suggests that the current boundary between the various polar terrains is only a surface manifestation of the present insolation balance; therefore, at depth, these units may be interbedded over considerable distances (Squyres, 1979).

In addition to modulating the areal extent of the polar deposits,

Figure 4.3. Mean annual polar surface temperatures as a function of obliquity (calculated from Equation (IV.3)).

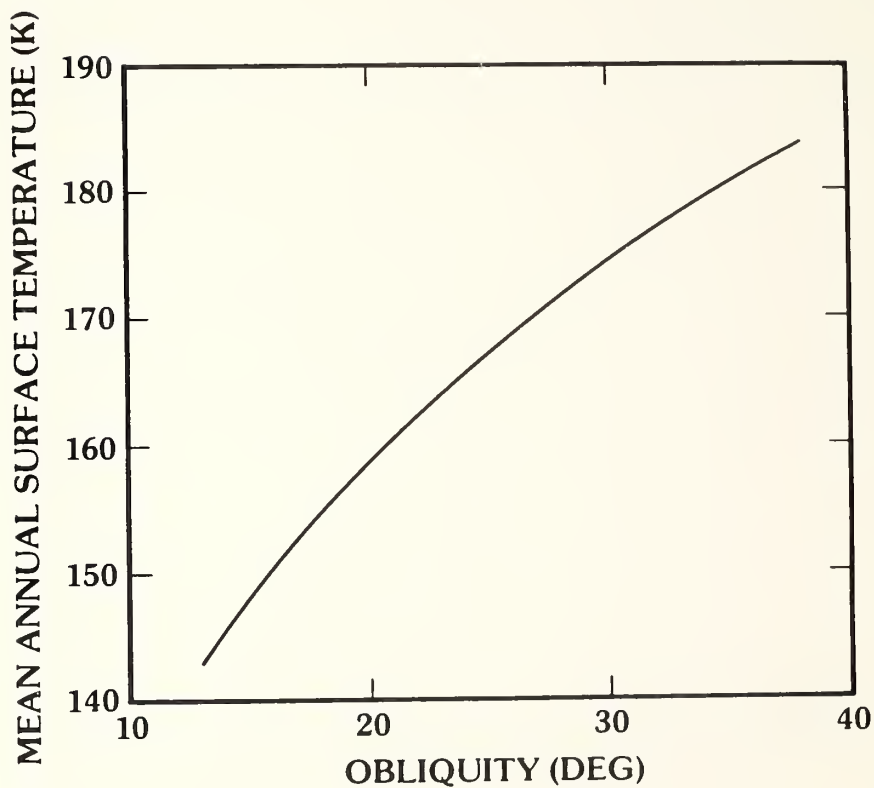


Figure 4.3

climatic variations may also directly influence the quantity of material that is actually deposited and retained by the cap. For example, at low obliquity, when the Martian polar caps are at their coldest, the present winter cover of CO_2 ice may persist throughout the year. If so, atmospheric pressures on Mars might be lowered to the point where summer winds would be unable to elevate dust from the planet's surface; as a result, deposition at the poles would cease altogether. Alternatively, at times of high obliquity, sublimation due to high polar temperatures could substantially reduce or eliminate the H_2O ice component in the annual depositional layer. This suggests the possibility that significant amounts of polar accumulation may occur only under climatic conditions similar to those we observe at present (Toon et al., 1980; Cutts and Lewis, 1982).

C. Basal Melting

On Earth, the term "basal melting" is usually applied only when melting occurs at the interface between an ice sheet and the bed on which it rests. That is, when an ice sheet is thick enough for the combination of the Earth's geothermal heat flux and any frictional heat produced by glacial sliding to raise the temperature at its base to the melting point, then basal melting is said to occur. However, as illustrated by Figure 4.4, it may be appropriate to broaden this definition with regard to Mars.

Figure 4.4a is an idealized cross-section of the Martian polar

Figure 4.4. An idealized cross section of the Martian polar crust illustrating the possible time evolution of basal melting.

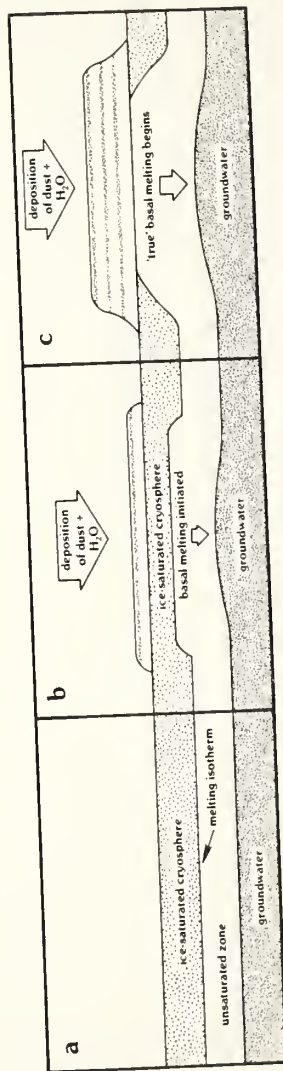


Figure 4.4

regolith as it might have appeared prior to the deposition of any dust or ice. As noted in the introduction, thermal models suggest that the depth to the 273 K isotherm in this region is approximately 3 km (Fanale, 1976; Rossbacher and Judson, 1981). Because the cold polar regolith has been the dominant thermodynamic sink for H_2O on Mars, it seems reasonable to expect that, if the ground ice capacity of the regolith has been saturated anywhere on the planet, it has most likely been here.

Given the above assumption, the deposition of any additional dust and H_2O at the Martian surface will result in a situation in which the equilibrium depth to the melting isotherm has been exceeded (Figure 4.4b). In response to this added layer of insulation, the melting isotherm will rise higher in the regolith until the equilibrium depth is once again established. It is important to note that while melting may not technically occur at the actual base of the polar deposits, melting at the base of the cryosphere will result from any increase in polar deposit thickness. Should the deposition of dust and H_2O continue, then the polar deposits may finally reach the required thickness for "true" basal melting to occur (Figure 4.4c).

Of course, the actual depth to the melting isotherm will exhibit a large degree of climatic variability. This variability results from two effects: (1) the climatic oscillation of mean annual surface temperatures, and (2) climatic changes in annual mass balance. Clearly, any change in mean annual surface temperature will have a direct bearing on the depth to the melting isotherm, the depth

decreasing for warmer temperatures and increasing for colder. A less obvious effect results from changes in annual mass balance. If the rate of polar deposition increases faster than the rate at which the caps can thermally reequilibrate, then the thickness required for basal melting will necessarily increase. By the same argument, significant periods of ablation will cause a reduction in this thickness (Weertman, 1961a). The combination of changes in both mean annual surface temperature and annual mass balance may result in situations where the melting isotherm periodically intrudes into the base of the polar deposits, while at other times it may lie well below this interface.

In light of the above, and to avoid any potential semantic complications, the use of the term "basal melting" will be broadened in this discussion to include any situation where pore or glacial ice is melted as the result of a rise in the position of the melting isotherm, regardless of whether this melting occurs at the actual base of the polar deposits or within the underlying regolith.

1. Thermal calculations. The thickness of the Martian polar deposits required for basal melting can be calculated by solving the one-dimensional steady-state heat conduction equation. Following Weertman (1961a), this thickness is given by:

$$H = k_{\text{eff}} (T_{\text{mp}} - T_{\text{s}}) / (Q_{\text{g}} + Q_{\text{f}}) \quad (\text{IV.4})$$

where k_{eff} is the effective thermal conductivity of the polar

deposits, T_{mp} is the melting point temperature of the ice (which may be depressed below 273 K due to pressure and solute effects), T_s is the mean annual surface temperature, Q_g is the geothermal heat flux, and Q_f is the frictional heat due to glacial sliding.

The effective thermal conductivity of the polar deposits is dependent on the quantity of dust entrained in the ice. After de Vries (1963, 1975) the effective conductivity, k_{eff} , of this dust/ice mixture can be calculated from the relation:

$$k_{eff} = (f_i k_i + F f_d k_d) / (f_i + F f_d) \quad (IV.5)$$

where k_i and k_d are the thermal conductivities of the ice and dust, f_i and f_d are their respective volume fractions ($f_i + f_d = 1$), and where F has been described as a weighting factor that represents the ratio of the average temperature gradient through the dust grains versus the average temperature gradient through the ice.

According to this model, the value of F is dependent on both the shape and orientation of the dust grains (de Vries, 1975). For an assumed random particle orientation, F is given by:

$$F = \frac{1}{3} \sum_{x=1}^3 \left[1 + g_x \left(\frac{k_d}{k_i} - 1 \right) \right]^{-1} \quad (IV.6)$$

where the dust particle shape is assumed to be ellipsoidal, having principal axial lengths g_1 , g_2 , and g_3 , such that:

$$\sum_{x=1}^3 g_x = 1 \quad (\text{IV.7})$$

(de Vries, 1963, 1975; McGaw, 1969).

Laboratory measurements of the thermal conductivity of water/soil mixtures have shown good agreement with values calculated from Equations (IV.5-IV.7) if the soil particle shapes are modeled as ellipsoids with a major axis six times the length of the two minor axes (de Vries, 1963; McGaw, 1969). As noted by McGaw (1969), however, few soils are actually composed of particles that can be characterized by this particular geometry. Therefore, while Equations (IV.6-IV.7) may yield values for a (1:1:6) axial ratio which are empirically correct, the theoretical basis for this success is unclear. If we accept the de Vries model for calculating the thermal conductivity of the Martian polar deposits then, based on estimated thermal conductivities for ice and dust of 8.6×10^{-3} cal/cm-s-K and 1×10^{-4} cal/cm-s-K respectively (Davies et al., 1977), Equation (IV.6) yields a value of F of approximately 2.05.

Calculated values of H for various mean annual surface temperatures, dust contents, and melting temperatures, are presented in Table 4.1 and Figure 4.5. In these calculations, the value of the geothermal heat flux was taken to be $22 \text{ cal/cm}^2\text{-yr}$, based on the theoretical calculations of Fanale (1976). In light of the observational evidence against significant basal sliding (i.e., no terminal moraines) presented by Howard et al. (1982), the value of Q_f was taken as zero. As a point of reference, the present mean annual

Table 4.1. Basal melting thicknesses (km), $T_s = 165$ K.

Dust Content (%)	Melting Temperatures		
	220 K	250 K	273 K
20	4.57	7.02	8.90
40	2.95	4.53	5.74
60	1.75	2.68	3.40
80	0.82	1.26	1.59

Figure 4.5. Required depths for basal melting given various basal melting temperatures, dust contents, and mean annual surface temperatures.

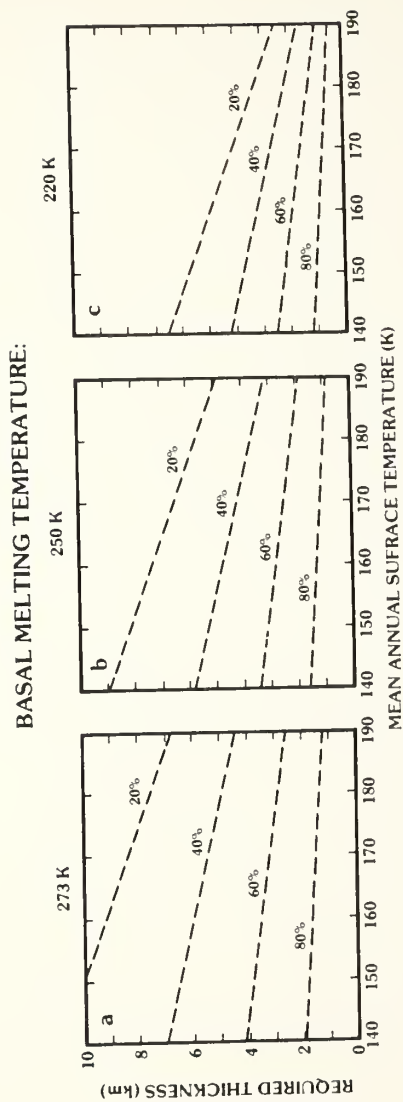


Figure 4.5

temperature of the north polar cap is approximately 165 K.

For the calculations summarized in Table 4.1 and Figure 4.5, melting point temperatures of 220 K and 250 K were included to allow for the possibility that salts contained in the dust, specifically CaCl_2 and NaCl , might significantly lower the temperature required for basal melting. As indicated by the results of the Viking inorganic chemical analysis experiments, these salts may be present in significant quantities in the Martian regolith (Clark, 1978).

The presence of even a small quantity of salt may be important, for it opens the possibility that melting may occur, not at a discrete depth defined by a particular isotherm, but over a broad range of temperatures representing an equally broad range of depths within the polar deposits (Ricc-de Bouard, 1977). For example, in studies of terrestrial temperate glaciers, water is typically found in microscopic veins, some tens of microns in diameter, along the three-grain intersections of ice crystals and as small lenses along grain boundaries (Nye and Mae, 1972; Raymond and Harrison, 1975). Nye and Frank (1973) suggest that these veins may form a three dimensional internal drainage network within the ice that may result in the transport of heat (by advection), as well as dissolved gasses and solutes (Raymond and Harrison, 1975). By such an internal drainage system, water which is produced by the presence of solutes and by heat arising from the internal deformation of the ice sheet may drain to the base.

The thicknesses for basal melting calculated on the above assump-

tions (Table 4.1) suggest that it is by no means certain that the present Martian polar caps are cold-based. Even if "true" basal melting does not presently occur at the poles, these results suggest that melting at the base of the cryosphere (Figure 4.4b) is entirely reasonable. During times of higher obliquity, and thus higher mean annual surface temperatures, the projected depths of basal melting presented in Figure 4.5 suggest that true basal melting might well be inevitable, at least in the north. If so, then the geothermal heat flux of $22 \text{ cal/cm}^2\text{-yr}$ estimated by Fanale (1976) has the potential for melting as much as a 0.5 cm layer of ice from beneath the polar caps each Martian year. Of course, should basal sliding occur on Mars, the frictional heat input could substantially exceed the geothermal contribution. As seen in Figure 4.6, a sliding velocity of 10 m/yr under an applied basal shear stress of 1 bar would be sufficient to halve the thicknesses for basal melting presented in Figure 4.5.

2. Flow calculations. One of the primary arguments against the possibility of flow and basal sliding in the polar regions of Mars has been the assertion that current temperatures at the poles are too cold to permit flow (Sharp, 1974; Howard et al., 1982). It is important to note, however, that both theoretical studies and field observations of terrestrial glacial flow indicate that virtually all of the deformation within an ice sheet occurs at its base, where the temperature and shear stress are greatest (Paterson, 1981). This fact and the results of the thermal calculations presented in the previous section suggest that,

Figure 4.6. Frictional heat produced by basal sliding under an applied shear stress of 0.5 and 1 bar (Weertman, 1961a).

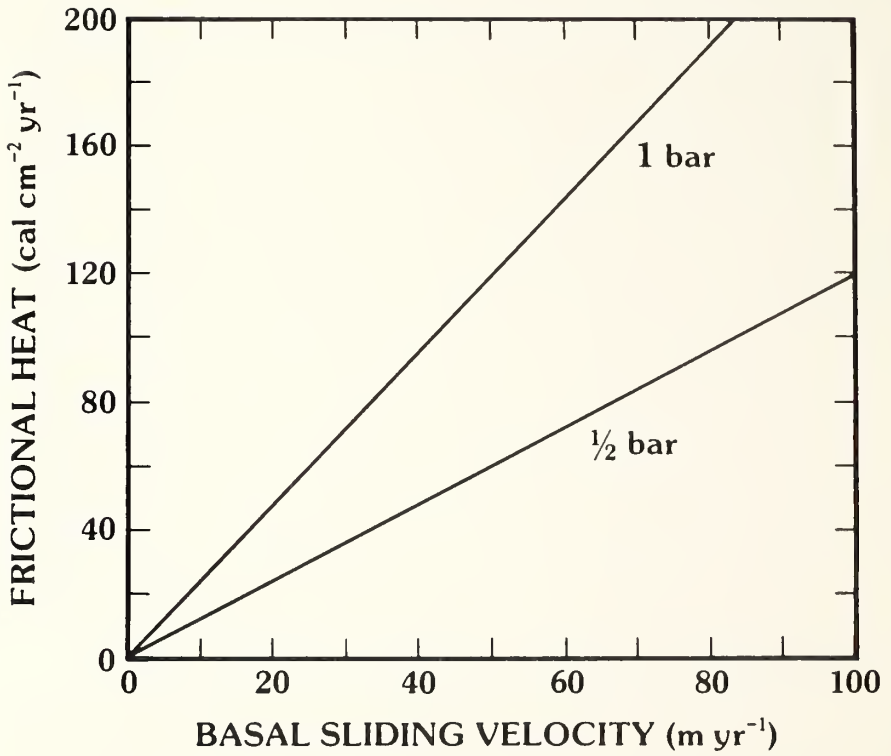


Figure 4.6

contrary to earlier beliefs, polar glacial flow on Mars cannot be ruled out simply on the basis of low polar surface temperatures.

An important observational check that may help to resolve this uncertainty is a comparison between both the theoretical equilibrium and observed polar cap profiles (Orowan, 1949; Nye, 1959; Weertman, 1961b). (In this section, all references made to polar cap thickness and basal temperature are made with regard to the interface between the polar deposits and the bed on which they rest).

The strain rate of glacial ice, $\dot{\epsilon}$, is related to the shear stress, τ , by Glen's law:

$$\dot{\epsilon} = A \tau^n \quad (\text{IV.6})$$

where n is a constant which has been determined to have a mean value of 3 based on the results of various glacial studies (Weertman, 1973), and where A is the flow law constant which is a function of temperature, crystal size and orientation, and impurity content (Paterson, 1981). The temperature dependence of A is given by the Arrhenius equation:

$$A = A_0 \exp(-Q/RT) \quad (\text{IV.7})$$

where A_0 is constant ($\sim 8.1 \times 10^{-9} \text{ s}^{-1} \text{ bar}^{-3}$) with respect to temperature (but still remains a function of crystal size, orientation, and impurity content), Q is the activation energy for creep (which has a value of 139 kJ/mol for $263 \text{ K} < T < 273 \text{ K}$, and a value of 60 kJ/mol

for $T < 263$ K), R is the gas constant, and T is the temperature (Weertman, 1973; Paterson, 1981).

In Figure 4.7, A has been plotted as a function of temperature over the range which is likely to characterize Martian polar ice temperatures at depth. The resulting variation in A covers nine orders of magnitude. This means that at a temperature even slightly below 273 K, the effective shear stress which must be exerted to obtain a given strain rate increases dramatically. This is clearly evident in Figure 4.8, where the effective strain rate of ice has been plotted as a function of shear stress for both 273 K and 263 K. The implications of this result on the theoretical profile of a Martian ice cap are significant.

First let us consider the simple model of an equilibrium ice sheet profile discussed by Orowan (1949), which is based on the assumption of perfect plasticity. The thickness, h , of the ice sheet at a distance, x , from its center is given by:

$$h = [(2 \tau_b / \rho_i g)(L - x)]^{1/2} \quad (\text{IV.8})$$

where ρ_i is the density of ice, g is the gravitational acceleration at the Martian surface, L is the half-width of the polar cap ($\sim 5 \times 10^5$ m and $\sim 1.75 \times 10^5$ m for the north and south polar caps respectively; Carr, 1981), and τ_b is the basal shear stress, which is assumed to have a perfectly plastic value of 1 bar at 273 K. The resulting profiles for both the north and south remnant Martian polar caps are seen in

Figure 4.7. Variation of flow law constant with temperature.

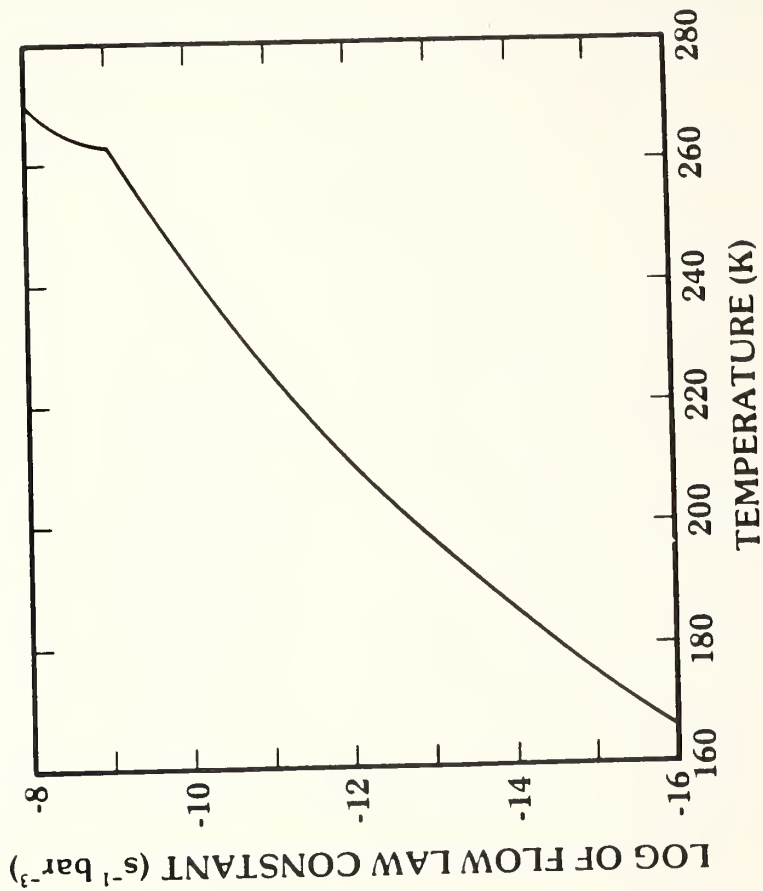


Figure 4.7

Figure 4.8. The deformation of temperate (273 K) ice is often approximated by the assumption of a perfectly plastic yield stress of 1 bar. For comparison the stress-strain relation for ice at 263 K is also shown. The equivalent perfectly plastic yield stress for this colder temperature is 3.19 bars.

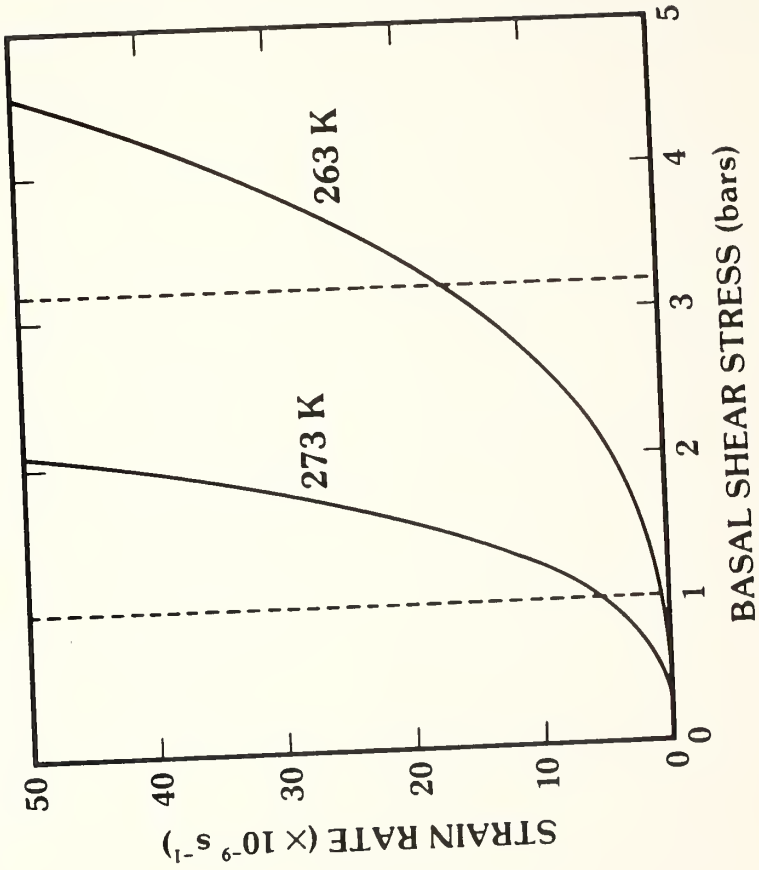


Figure 4.8

Figure 4.9. The profile for the northern cap, which has a maximum predicted height of 5.5 km, is consistent with the estimated 4-6 km thickness inferred by Dzurisin and Blasius (1975). On the other hand, the predicted profile of the south polar cap appears to overestimate its actual height by as much as a factor of 2.

Of course a perfectly plastic yield stress of 1 bar is an approximation that is only valid when considering pure ice at a temperature of 273 K. As seen in Figures 4.7 and 4.8, a lower ice temperature will require a higher shear stress. For example, in Figure 4.10 the profile of the north polar cap has been plotted for a yield stress of 3.19 bars. This yield stress is equivalent to the perfectly plastic case for ice at a temperature of 263 K. Figure 4.10 illustrates that even for a slight reduction in basal temperature the resulting theoretical profile of the north polar cap substantially exceeds its inferred thickness of 4 to 6 km (Dzurisin and Blasius, 1975).

Several general observations can be made in comparing the actual Martian polar ice thicknesses with those predicted by Orowan's theoretical model. First, had the observed height of either Martian polar cap substantially exceeded the theoretical heights calculated from Equation (IV.8), we could have concluded with reasonable confidence that the temperature of the basal ice was below 273 K. However, the close agreement between the inferred and calculated thicknesses limits consideration to just two possibilities: (1) the basal temperature is presently at the melting point, or (2) the cap is

Figure 4.9. Theoretical profiles of the Martian north and south polar caps calculated on the basis of Orowan's (1949) model of perfect plasticity (Equation (IV.8)).

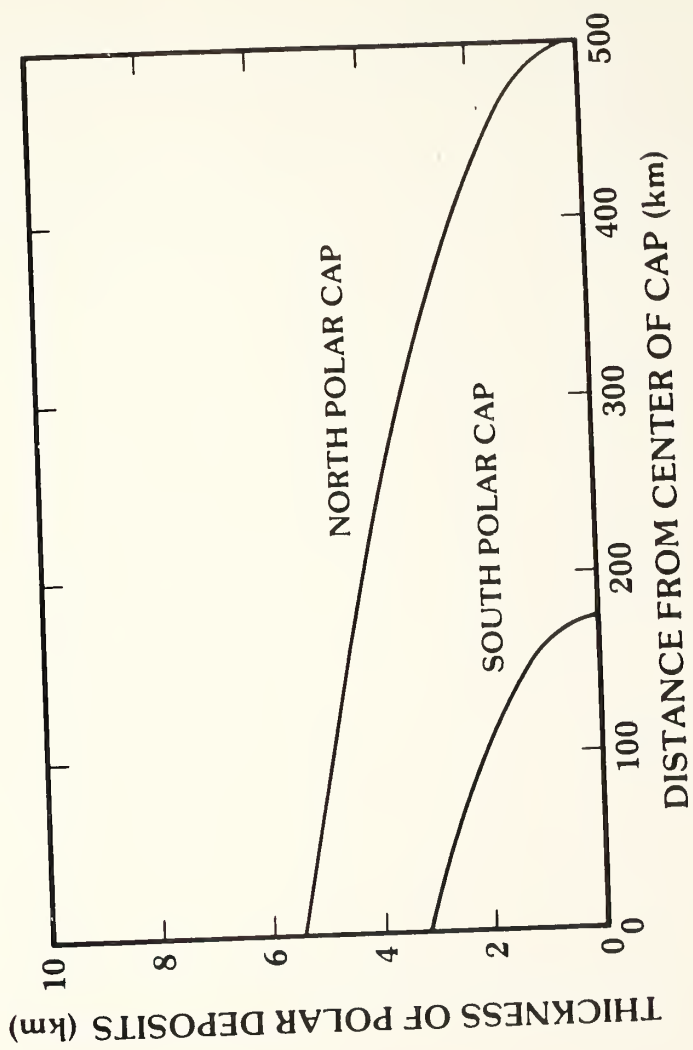


Figure 4.9

Figure 4.10. A comparison of polar cap profiles illustrating the effect of basal temperature.

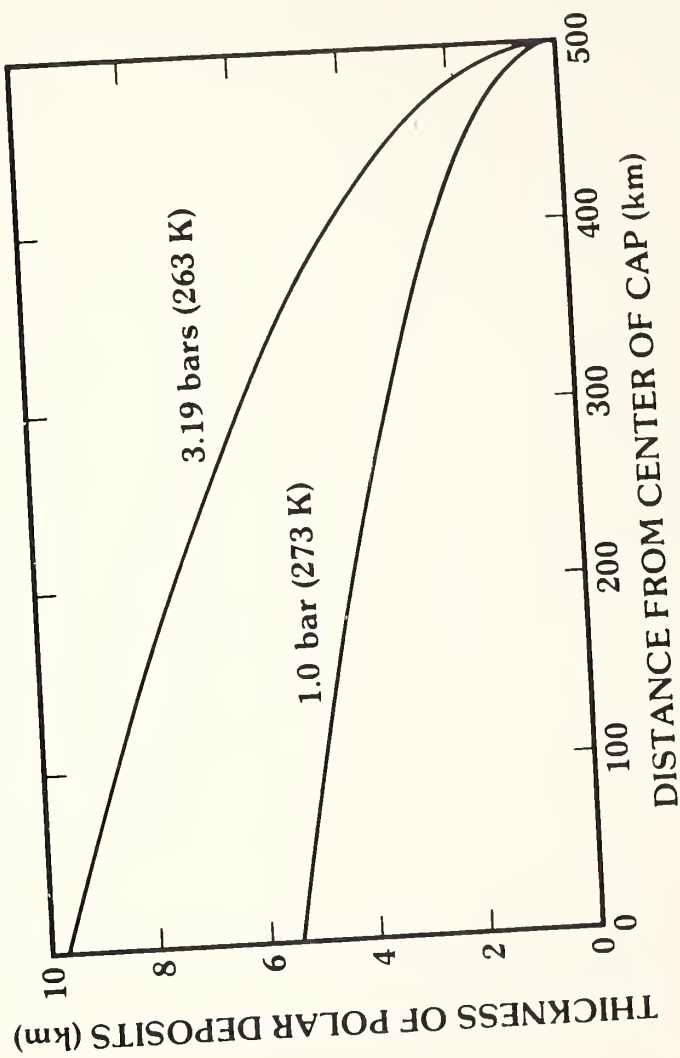


Figure 4.10

cold-based and has simply not yet achieved the required height necessary for the basal ice to undergo significant plastic deformation. This latter explanation appears to be particularly applicable to the south polar cap, where the inferred thickness of 1-2 km is approximately 40-70% smaller than the equilibrium profile predicted by Orowan's model.

Of course, the foregoing analysis assumes that the mechanical properties of the Martian polar deposits are essentially those of pure H₂O ice and that the flow of this ice can reasonably be approximated by a perfectly plastic yield stress of one bar. As a test of these assumptions we can consider the more sophisticated theoretical models of Nye (1959) and Weertman (1961b), where equilibrium ice sheet profiles are calculated, not on the assumption of perfect plasticity, but on the basis of a more realistic flow law, similar to that given by Equation (IV.6). The resulting expression for the height of the profile is:

$$h^{2+1/m} = (2m+1)(a/B)^{1/m} (L^{1+1/m} - x^{1+1/m}) / [(m+1)(\rho_i g)] \quad (\text{IV.9})$$

where 'a' is the accumulation rate, $m = (n+1)/2$, and B is a constant (with the units of velocity) defined as:

$$B = 25 a L^3 / (4 H^5 \rho_i^2 g^2) \quad (\text{IV.10})$$

where H is the maximum observed thickness of the polar cap (Weertman,

1961b). Substituting the appropriate Martian values in Equation (IV.10), we find that B is approximately 0.021 m/yr, as compared to a typical terrestrial value of 81.2 m/yr for the Greenland ice cap (Weertman, 1961b). The primary reason for the difference between these two figures is the three order of magnitude smaller accumulation rate ($\sim 1 \times 10^{-4}$ m/yr) inferred for Mars.

In Figure 4.11 the north and south polar cap profiles have been recalculated based on Equation (IV.9). In both instances the agreement with observation is quite good, illustrating the merit of the more detailed theoretical treatments of both Nye (1959) and Weertman (1961b), and the assumption that the mechanical properties of the Martian polar ice caps are similar to those of terrestrial ice sheets. In light of the evidence for the presence of significant quantities of dust within the deposits, the validity of this last observation may be fortuitous. One possible explanation for this similarity may be that any increase in the shear strength resulting from the entrainment of dust has effectively been counterbalanced by the presence of other weakening impurities such as salts or gas bubbles (Weeks and Asur, 1967).

It is important to emphasize that the theoretical ice cap profiles calculated here are equilibrium profiles; that is, they are contingent on the assumption that any mass a polar cap gains by accumulation on its surface it subsequently loses by flow and ablation at its perimeter. Given this constraint we can easily calculate the amount of radial flow required to maintain the Martian polar caps at their

Figure 4.11. Theoretical profiles of the Martian north and south polar caps based on the more realistic flow models of Nye (1959) and Weertman (1961b).

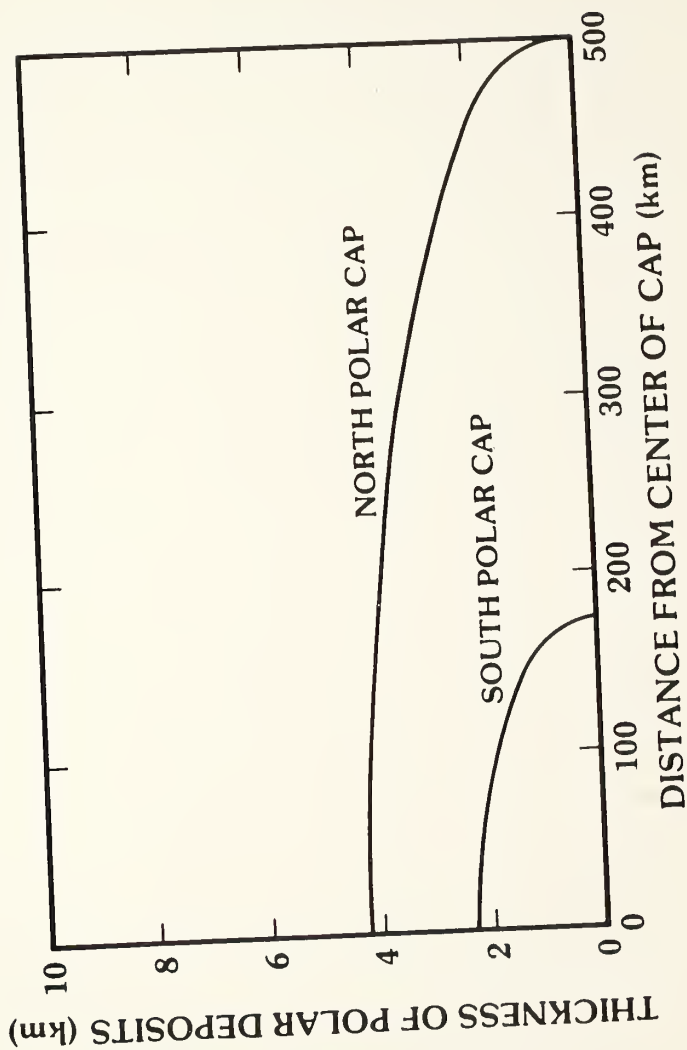


Figure 4.11

present size. For an accumulation rate of $\sim 10^{-4}$ m/yr, averaged over the area of the cap, the necessary outward flow at the perimeter is approximately 10^{-2} m/yr. Evidence for such a small flow rate may be difficult to identify from Viking orbital imagery. For instance, concurrent ablation and erosion by strong seasonal polar winds might easily inhibit the formation of a discernable moraine at the edge of the cap.

In summary, the calculations presented in this section suggest that both flow and basal melting may currently be active processes in the polar regions of Mars. This is especially true in the north, where the total thickness of polar ice is sufficiently large that relatively small quantities of dust and/or salt are required for melting and deformation to occur at the cap's (true) base.

D. Discussion

The process of basal melting may be a key factor in understanding the climatic cycling of H_2O on Mars and the evolution of the Martian polar terrains. Six examples of the potential importance of this process are presented in the following discussion.

1. Storage of a primitive Martian ice sheet. In the Martian northern plains and near the south polar cap, examination of high resolution Viking Orbiter imagery has revealed a number of features which bear a strong resemblance to Iceland's table mountains (Allen, 1979b; Hodges

and Moore, 1979). Because table mountains on Earth are formed by subglacial volcanic eruptions, the discovery of possible analogs on Mars has led to speculation that an extensive ice sheet may once have covered sizeable areas of both the northern and southern hemispheres. From an examination of the height of these landforms Allen (1979b) has determined that the thickness of this unit may have ranged from 100 to 1200 m. Such estimates have prompted Arvidson et al. (1980) to argue that, in the absence of any obvious volatile sinks of sufficient size, the difficulties involved in the removal and storage of such a large volume of ice make it difficult to support a subglacial origin for the Martian 'table mountains'.

First, consider the problem of storage. As noted by Fanale (1976), Carr (1979) and others, repeated impacts have significantly modified the structure of the outer layer of the Martian crust over the course of geologic history. On the Moon, which has experienced a similar cratering history, studies of the seismic propagation characteristics of the outer layer of the lunar crust suggest that it is brecciated to a depth of roughly 20 km (Carr, 1979). Gravitationally scaling these lunar results to Mars indicates that the regolith may remain porous down to a depth of approximately 10 km, and that it may have sufficient pore volume to store a quantity of H_2O equal to a 600 m layer averaged over the planet's surface (Clifford, 1981b). Should these calculations be correct, then the potential storage capacity of the Martian crust would clearly be sufficient to accommodate the volume of H_2O contained in a sizeable primitive

Martian ice sheet. The major problem, therefore, is how to take advantage of this potential storage capacity.

Ice will remain stable on the Martian surface only at those latitudes where the temperature remains continuously below the frost point. If Mars once possessed extensive polar ice sheets, then this fact may help to account for their subsequent disappearance. Consider, for example, a situation in which the Martian climate warmed after the ice sheets had reached their maximum areal extent. As mean annual temperatures increased in the equatorial and temperate zones, the position of the frost-point latitude migrated towards the poles. When this latitude passed the outer perimeter of the ice sheet, the ice would have begun to ablate and redistribute itself poleward via cold-trapping. As a consequence, what the ice sheet lost in areal extent it gained in thickness at the poles. With this added thickness, the melting isotherm readjusted to maintain its equilibrium depth from the surface, resulting in the onset of basal melting (Figure 4.12).

If the area involved in basal melting was equal to the present extent of the north and south polar deposits, and if the geothermal heat flux had a value of approximately $22 \text{ cal/cm}^2\text{-yr}$ (Fanale, 1976), then a 500 m thick ice sheet that once covered 40% of the planet's surface could be introduced into the Martian crust as groundwater in as little as a few million years.

2. Origin of Chasma Boreale. As discussed earlier, Chasma Boreale (85°N , 0°W) is a wide channel-like feature in the Martian north

Figure 4.12. A possible mechanism for the removal and storage of a primitive Martian ice sheet (after Clifford (1980c)). Following a climatic period of extensive glaciation, mean annual temperatures may have begun to rise at equatorial and temperate latitudes. As the frost point latitude receded, the ice sheet may have begun to ablate and redistribute itself poleward. Eventually the required thickness for basal melting may have been achieved, permitting the storage of the bulk of the ice sheet as groundwater.

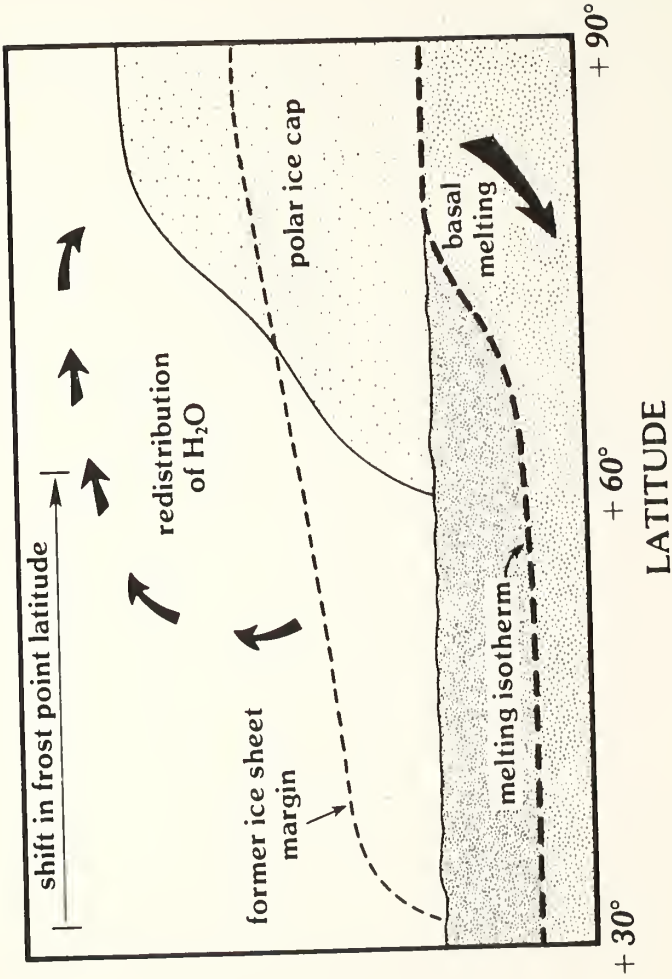


Figure 4.12

polar deposits that begins abruptly with a large triangular head near the center of the cap and extends equatorward for some 500 km, terminating in a broad erosional fan at the edge of the residual cap (Figure 4.2). Similar features, of smaller scale, are found elsewhere in the north at 84° N, 127° W and 84° N, 242° W; while in the south, several older and more highly eroded reentrants exist. The largest of these is Chasma Australe (87° S, 0° W), which resembles Chasma Boreale in both morphology and scale.

In a review of the various insolation-dependent models that have been proposed for the origin of the north and south polar terrains, Blasius et al. (1982) have remarked on the inability of these models to account for the broad linear depressions, like Chasma Boreale, that are radially oriented and cross-cut the outward spiralling polar troughs. One possibility, suggested by Clifford (1980a,b; 1982b), is that these features were formed by the Martian equivalent of a terrestrial jokulhaup — the catastrophic discharge of a large subsurface reservoir of glacial meltwater.

Should basal temperatures within the central regions of the Martian polar caps reach the melting point, then the geothermal heat flux estimate of Fanale (1976) suggests that as much as 0.5 cm of ice could melt from the base of the caps each Martian year. In reference to terrestrial ice sheets, Weertman (1961a, 1966, 1972) has shown that in regions where the ice sheet is underlain by low-permeability bedrock, basal meltwater will flow in a thin layer from the central part of the cap to its periphery. This flow is driven by the

differential in hydrostatic head which results from the radial decrease in lithostatic pressure exerted by the overburden cap.

As the baseflow moves radially outward from the region of active basal melting, it enters a surrounding zone where the polar cap thickness is too thin for the contributions of geothermal and any sliding heat to maintain the base at the melting temperature; consequently, some of the baseflow is refrozen to the base of the ice, releasing sufficient latent heat to compensate for the geothermal and sliding heat deficit (Weertman, 1961a).

On Mars, the water that is not refrozen to the bottom of the ice sheet may ultimately be driven into a region where the bed on which the ice sheet rests is sufficiently permeable to allow its introduction into a subpolar aquifer system (Clifford and Huguenin, 1980; Clifford 1980a) or, alternatively, it may build up at the frozen edge of the cap until the hydrostatic pressure of the basal reservoir finally affects the stability of the overlying cap. In this last case, the sudden flotation of ice at the edge of the polar cap could lead to the catastrophic release of the accumulated reservoir of basal meltwater. Such a scenario may account for the preferential occurrence of most reentrants along the periphery of the polar caps.

While the model described above may successfully account for the origin of the reentrants found near the edge of the Martian polar deposits, it fails to account for the larger features such as Chasma Boreale and Chasma Australe, which originate much closer to the central portion of their respective caps. One possible explanation for the

origin of these features is suggested by the results of recent radio-echo soundings of the interior of the Earth's Antarctic ice sheet. These soundings have revealed the presence of numerous basal lakes beneath the 3-4 km thickness of the polar ice (Oswald and Robin, 1973; Robin et al., 1977).

The discovery of basal lakes came as a surprise. While previous studies had suggested that large areas of the Antarctic ice sheet had reached the melting point at its base, calculations by Weertman (1961a, 1966, 1972) suggested that any meltwater so derived would flow towards the cap's edge as a thin (millimeters thick) sheet. However, Oswald and Robin (1973) showed that within the interior of the ice sheet, where surface slopes are small, the gradient in hydrostatic head imposed by the the cap should be low enough for depressions within the underlying bedrock to accumulate substantial (>1 meter) thicknesses of basal meltwater. They determined that the necessary requirement for such accumulation is that the slope of the walls of the basal depression must be at least ten times greater than the local surface slope of the overlying ice sheet.

With regard to Mars, one might reasonably expect that the surface underlying the polar layered deposits was extensively cratered early in the planet's history. Therefore, near the center of the cap, where the likelihood is greatest that the base of the deposits has at one time reached the melting point, there may exist numerous areas that satisfy the minimum basin wall slope criterion outlined by Oswald and Robin (1973). Therefore, should the basal melting rate in the Martian polar

terrains exceed the infiltration capacity of the underlying bed, a growing reservoir of meltwater might well accumulate within the confines of an ancient crater or impact basin. The continuation of this process could ultimately lead to a situation where the capacity of this reservoir was exceeded, leading to the breaching and possible catastrophic drainage of the subglacial lake.

The sudden release of meltwater from a basal lake could induce additional melting via the heat generated by viscous dissipation within the flow and by friction between the water and overlying ice (Shreve, 1972; Rothlisberger, 1972; Weertman, 1972), producing a positive feedback effect that could significantly increase the magnitude of the catastrophic flood. Therefore, as the baseflow gains in volume, it may result in the rapid enlargement of the original subglacial passage as water is forced down the hydrostatic pressure gradient towards the edge of the cap. In this way, the flood could grow to the point of breakout at the Martian surface, resulting in the formation of such features as Chasma Boreale and Chasma Australe (Clifford, 1980a,b).

A potential problem for this scenario is that, once breached, would a crater or basin wall erode rapidly enough to result in the catastrophic drainage of an interior lake? This problem would be simplified if the ice surrounding the basal lake were frozen to its bed. Given such an initial condition, the upper surface of the basal lake could grow to an elevation substantially above the height of the surrounding basal topography. When the volume of the lake finally became large enough to cause flotation of the cap, catastrophic

drainage would then be assured. This scenario is similar to the model proposed by Nye (1976) to explain the origin of the subglacial outbursts (jokulhlaups) associated with the catastrophic drainage of Grimsvotn, a subglacial lake in the center of the Vatnajokull ice cap in Iceland.

Of course, variations on this proposal are also possible. As in the case of Grimsvotn, it is possible for a basal lake on Mars to result from the presence of a local geothermal "hot spot" or subglacial volcanic eruption. Even though the existence of such thermally active regions on Mars is entirely reasonable, reliance on this same (essentially ad hoc) explanation for the origins of both Chasma Boreale in the north and Chasma Australe in the south may stretch credibility to the breaking point.

In partial support of a fluvial origin for the major polar reentrants are the morphologic similarities between Chasma Boreale and features, found elsewhere on the planet, whose origin is popularly attributed to a catastrophic release of groundwater. Of particular interest are the similarities between Chasma Boreale (Figure 4.13a) and Riva Vallis (2°S , 43°W) (Figure 4.13b).

The morphologic differences that exist between Chasma Boreale and Riva Vallis can reasonably be attributed to their differing geologic environments. For example, the large blocks of disrupted crustal material that are visible on the floor of Riva Vallis would not be expected in Chasma Boreale. The stability of the polar deposits is, to a large degree, due to both the comparatively high albedo of the



Figure 4.13a. Chasma Boreale (85°N, 0°W).



Figure 4.13b. Riva Vallis (2°S, 43°W).

ice-covered surface and the large incidence angle of incoming sunlight (Howard, 1978; Blasius et al., 1982). The disruption of these deposits by the catastrophic release of a subglacial lake would alter the sensitive insolation balance that had previously protected the polar ice from sublimation. As a consequence of the large-scale exposure of low albedo dust, and the change in sun angles, the ice matrix should rapidly sublime from the polar debris. The removal of this binding agent would then allow strong polar winds, confined by the channel, to erode and transport the resulting sediment down the length of the channel floor (Cutts, 1973b).

It should be noted that a fluvial origin of Chasma Boreale was first advocated by Wallace and Sagan (1979), who suggested that the direct absorption of sunlight within the Martian polar ice may have led to significant near-surface melting, creating extensive polar lakes beneath a thin (~7 m) cover of ice. Early shaded relief maps of the Martian north polar region, which were based on poor and incomplete Mariner 9 photographic coverage, indicated the presence of a large crater (labeled "Zw") at the head of Chasma Boreale. Wallace and Sagan (1979) suggested that this association was probably not coincidental, and that the impact that created Zw may have ruptured a near-surface lake whose outflow then carved Chasma Boreale. However, subsequent Viking high-resolution coverage of this region revealed that the crater Zw was an artifact created by viewing the head of Chasma Boreale at large incidence angles and under poor seeing conditions. One might also question the likelihood of near-surface polar lakes. In their

calculations Wallace and Sagan (1979) argued that there would be little, if any, significant attenuation of incident solar radiation through the top 7 m of polar ice. Yet, the evidence for a substantial dust component in the Martian ice would seem to contradict this assumption. Even if one assumed a bulk extinction coefficient as low as 0.01 cm^{-1} , a value typical of relatively clean glacial ice on Earth (Grenfell and Maykut, 1977), less than 5% of the incoming solar radiation would penetrate below a depth of 3 m, thus making the existence of any stable near-surface reservoir of liquid water extremely unlikely.

While a fluvial origin for Chasma Boreale and the other major polar reentrants is clearly not the only possible explanation for the origin of these features, it appears to be a likely consequence of what one might expect if polar basal melting has in fact occurred on Mars.

3. Polar basal lakes as possible isolated habitats of primitive Martian life. As noted previously, radio-echo sounding investigations of the Earth's Antarctic ice sheet have revealed the existence of numerous basal lakes at depths as great as 4 km below the ice sheet's surface (Oswald and Robin, 1973; Robin et al., 1977). These lakes, which are believed to have formed by geothermal melting, appear to be a minimum of several meters deep and cover individual areas as large as 180 km x 45 km (Robin et al., 1977).

It has been suggested that spore-forming microorganisms originally deposited at the surface of the Antarctic ice cap might be transported

through the entire thickness of the ice sheet via the continued deposition of snow at the ice sheet's surface and geothermal melting at the ice sheet's base (Oswald and Robin, 1973). Because a basal lake may be an environment which is stable on a time scale of millions of years, Oswald and Robin (1973) have suggested that microorganisms introduced into such a basal lake may find conditions that are suitable for survival, adaptation, and growth.

If similar lakes exist on Mars, they may provide isolated environments for the continued survival of ancient Martian life-forms (Lederberg and Sagan, 1962; Wallace and Sagan, 1979). Because a significant amount of dust is elevated planet-wide and transported to the poles each year during the formation of the seasonal polar caps, Martian global dust storms may act as efficient biological 'samplers' of much of the planet's surface. Current climatic models suggest that this process of polar deposition has been in operation over much of Martian geologic history (Toon et al., 1980; Fanale et al., 1982); thus, if primitive Martian lifeforms have existed anywhere on the planet during this time period, a sample of this life may be preserved within the polar ice.

If the Martian poles evolve by basal melting, then the eventual introduction of these organisms into basal lakes may result in the formation of isolated habitats many kilometers below the Martian polar landscape. Abundant liquid water at a constant temperature between 220-273 K (depending on both the type and quantity of dissolved salts), as well as the absence of destructive atmospheric oxidants and intense

UV radiation, would provide an environment in marked contrast to that which is present at the Martian surface.

Yet, life within polar basal lakes faces its own significant environmental problems. For instance, the absence of both sunlight and free oxygen places a severe constraint on the possible range of metabolic processes capable of sustaining any remnant of early Martian life. So too, the possible combination of high salinity and low temperature (220-273 K) in basal lakes may create an environment which is too hostile for even the hardiest of microorganisms to survive (Miller, 1983).

A search for polar basal lakes on Mars based solely on the weight of their potential biological importance appears unwarranted; however, a broader investigation of the Martian polar terrains using high-powered radar altimeters would do much to improve our understanding of the caps' internal structure and evolution. A direct consequence of such an investigation would be the identification of any basal lakes which might exist in these terrains.

4. Basal melting at temperate latitudes. The discussion of basal melting presented so far in this chapter has been limited to its potential occurrence in the polar regions of Mars; however, it is important to note that the process of basal melting is not necessarily restricted to the region occupied by the visible polar caps. Indeed, wherever the ground ice capacity of the Martian cryosphere has been saturated, the deposition and retention of any additional material at

the regolith's surface will eventually lead to basal melting.

As noted by Soderblom et al. (1973b), the terrains poleward of $\pm 35^\circ$ appear to be covered by a mantle of what is inferred to be eolian debris. This discovery is consistent with both theoretical arguments and Viking Lander 2 photographs, which suggest that the dust raised during the major perihelion dust storms is preferentially deposited at these latitudes during the formation of the seasonal polar caps (Pollack et al., 1979; Wall, 1981).

The accumulation of eolian mantles at temperate latitudes on Mars may have significant implications for the long-term cycling of H_2O . For example, Farmer and Doms (1979) have proposed that the seasonal storage of atmospheric water vapor may occur in the Martian regolith at depths where, sometime during the year, the regolith temperature falls below the frost point of H_2O . The importance of this seasonally occurring ground ice, which has been dubbed "tempofrost" by Farmer (1976), may extend well beyond its temporary storage potential.

The interface between the occurrence of tempofrost and perennial ground ice is determined by the depth to which the annual thermal wave elevates the temperature of the regolith above the frost point (Figure 4.14). The deposition of a layer of dust over the original surface will result in a corresponding upward displacement of this interface within the regolith. Thus, a small portion of the tempofrost which was present prior to the dust layer deposition will be retained as perennial ground ice. Eventually, the melting isotherm at the base of the cryosphere will see the added insulation provided by the deposited

Figure 4.14. Basal melting at temperate latitudes as the result of eolian deposition.

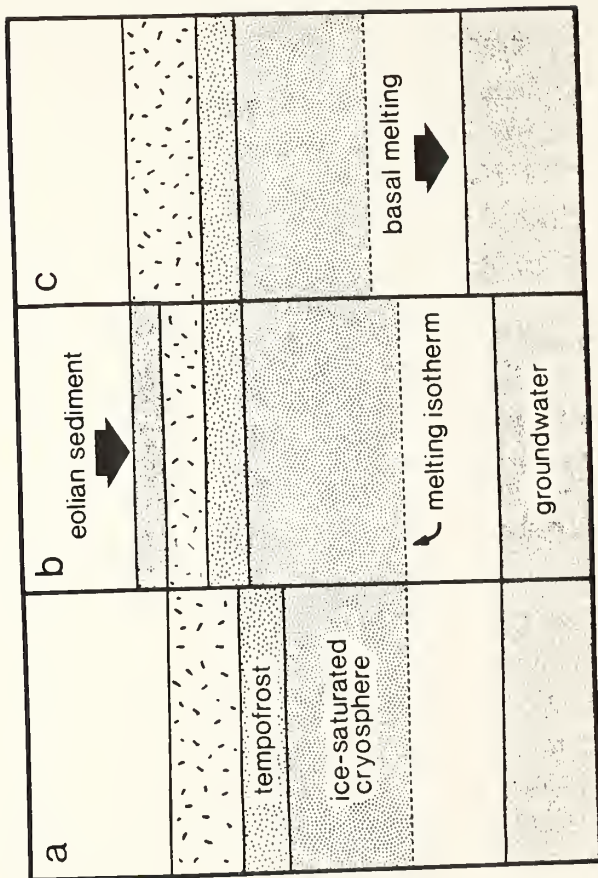


Figure 4.14

layer of dust and will, in response, rise within the regolith, resulting in basal melting.

A simple calculation can provide a rough estimate of the potential quantity of water cycled annually by these processes. If we consider only that region for which there is observational evidence of deposition (poleward of the Viking Lander 2 site at 48° N) then, following the reasoning of Pollack et al. (1979), we calculate a dust sedimentation rate of $\sim 8 \times 10^{-3}$ g/cm² per Martian year. Assuming a regolith bulk density of 1.5 g/cm³ and a porosity of 50% (Moore et al., 1979), we find that the deposition of dust at temperate latitudes may lead to the annual retention of as much as 0.5 km³ of tempofrost as perennial ground ice. If the thermal properties and porosity of the dust layer are similar to that of the regolith at depth, then the subsequent rise of the melting isotherm should release an equivalent amount of perennial ground ice as meltwater (Figure 4.14). If deposition is also presently occurring at temperate and polar latitudes in the south then this annual figure may actually be doubled.

Of course, the tempofrost and basal melting processes can also operate in reverse. In those regions where the regolith is undergoing preferential erosion, the annual thermal wave can penetrate deeper into the regolith; thus, where H₂O once existed as perennial ground ice it may now occur only as tempofrost. At depth, in response to the net reduction in overlying insulation caused by surface erosion, the melting isotherm will readjust by retreating downward into the crust. This displacement will create a cold-trap at the base of the cryosphere

that will act as a sink for any subpermafrost H_2O until such time as the available pore space between the old and new position of the melting isotherm is saturated with ice (Clifford, 1980d, 1982a).

This discussion suggests that the erosional and depositional evolution of the Martian surface may be intimately tied with long term sources and sinks of atmospheric H_2O . It also suggests the possibility that the annual behavior of atmospheric water vapor may be far more dynamic than currently believed.

5. The mass balance of the polar terrains. It is generally accepted that the polar layered terrains owe their origin and apparent youthfulness to the annual deposition of dust and H_2O , and that the magnitude of this deposition has been modulated throughout Martian geologic history by periodic variations in polar insolation due to changes in the planet's orbital elements and obliquity (Cutts et al., 1977; Pollack et al., 1979; Toon et al., 1980). Based on their evident thickness, and the absence of any craters larger than 300 meters in diameter, it is estimated that the present polar deposits accumulated on a time scale of $\lesssim 10^7$ years. But there exists a serious problem inherent in this depositional model (Clifford and Huguenin, 1980); recent studies suggest that the climatic conditions conducive to polar deposition on Mars are not unique to the present epoch but have apparently existed throughout most of the planet's geologic history (e.g., see Fanale et al., 1982). Given such conditions, how does one account for the absence of this older material at the Martian poles?

In response to this question Carr (1981) has suggested that periods of intense polar erosion may alternate with climatic periods of polar accumulation. Such erosion must be extremely efficient in redistributing the resulting debris if it is to eliminate any previous record of polar construction. However, no major variable in the Martian climate has yet been identified with a period greater than the $\sim 10^6$ year variation in orbital eccentricity (Toon et al., 1980; Fanale et al., 1982). Further, the change in polar insolation which results from this 10^6 year cycle appears to fall well short of that required to counter the net long-term deposition of ice and dust within the polar terrains (Toon et al., 1980; Fanale et al., 1982). This conclusion is supported by both the inferred 10^7 year age of the polar deposits and by the lack of observational evidence indicative of any widespread erosion of the polar laminae (Howard et al., 1982).

Another possible solution to the mass balance problem has been proposed by Toon et al. (1980), who have suggested that new polar laminae may simply be created at the expense of the old. This possibility is suggested by current models of the evolution of the polar troughs (Howard, 1978; Howard et al., 1982). These features, which form the conspicuous spiral patterns seen in the remnant polar caps (Figure 4.2), are thought to originate near the edge of the deposits and migrate towards the pole. Such a migration is thought to be driven by the preferential sublimation of ice from the equatorward-facing slopes of the troughs. Dust, liberated from the polar ice, may then be scavenged by polar winds and redistributed over temperate and

polar latitudes, while the sublimed ice may simply be recycled by cold-trapping on the poleward-facing slopes and on the flats which separate the polar troughs. In this fashion Toon et al. (1980) suggest that the polar deposits have essentially reached a state of equilibrium whereby ancient ($\geq 10^9$ year old) polar material is continually reworked, maintaining a comparatively youthful surficial appearance in spite of its great age.

However, based on a detailed study of Martian polar stratigraphy made from high-resolution Viking Orbiter photographs, Howard et al. (1982) have argued that a simple local recycling of polar laminae is untenable. They support this conclusion by citing observational evidence that the erosion of equatorward-facing scarps has not kept pace with layer deposition near the poles, requiring a net long-term accumulation of material within the polar terrains (Howard et al., 1982).

To summarize, it appears that any solution to the mass balance problem must: (1) be consistent with theoretical models of the Martian climate, which suggest that a net depositional environment has existed at the poles throughout most of Martian geologic history, (2) be able to account for the observational evidence that the evolution of the near-polar terrains has indeed been dominated by depositional processes, (3) be able to accommodate a rate of deposition, implied by the lack of craters within the deposits, of $\sim 10^{-4}$ - 10^{-3} m/yr (Cutts et al., 1976), and (4) it must satisfy all of the previous conditions within the constraint imposed by the implied deficit of material

currently observed at the poles.

There are two explanations that appear to meet these requirements. The first is based on the geologic evidence for polar wandering presented by Schultz and Lutz-Garihan (1981a,b; 1982). The evidence consists of two types: (1) the identification of a number of extensive antipodal layered deposits in the equatorial region that bear certain similarities to the present polar layered terrains, and (2) the preferential occurrence of elongated craters along great circles, which Schultz and Lutz-Garihan (1982) have attributed to grazing impacts caused by former satellites whose orbits tidally decayed with time. If this last interpretation is correct, then the pole positions implied by these great circles should indicate former orientations of the planet's crust with respect to its spin axis. Interestingly, there appears to be a fair amount of agreement between the polar locations indicated by the distribution of grazing impacts and the observed positions of the near-equatorial layered deposits.

To account for these observations Schultz and Lutz-Garihan (1981a,b) proposed that a major reorientation of the Martian crust in relation to its spin axis resulted from a change in the planet's moment of inertia caused by the formation of the Tharsis volcanic province. Although the actual details of the dynamics of this process are presently unclear, the slow migration of the geographic location of the Martian poles does provide a possible solution to the mass balance problem, given that the occurrence of this process has spanned Martian geologic time and that the age of the present polar locations is $\lesssim 10^7$

years.

However, if significant polar wandering has not occurred or if it was restricted to a period very early in Martian geologic history, then an alternative solution to the mass balance problem must be found. The process of basal melting may provide this solution (Clifford and Huguenin, 1980). Once the polar deposits have reached the required thickness for basal melting, they will have achieved a condition of relative equilibrium between the accumulation of H_2O at the polar surface and its melting at the base of the cap. Indeed, with an estimated geothermal heat flux of $\sim 22 \text{ cal/cm}^2\text{-yr}$ (Fanale, 1976; Toksoz and Hsui, 1978), it appears that basal melting could easily keep pace with the inferred polar deposition rate of a 1 km thick layer of H_2O ice every 10^6 years (Cutts et al., 1976). Thus, the occurrence of basal melting is consistent with theoretical models and with the observational evidence that argues for the long-term net deposition of H_2O at the Martian poles (Fanale et al., 1982; Howard et al., 1982).

Of course, while the occurrence of basal melting may resolve the eventual fate of polar ice, there still remains the problem of the polar dust. Fortunately, the dust mass balance problem is significantly more tractable, in that the nonvolatile nature of the polar dust allows it to be physically removed from the polar troughs by surficial processes of erosion and redistributed to nonpolar latitudes. Another alternative suggested by the possibility of basal melting is that the slow flow of polar ice may eventually transport any basal debris to the polar cap periphery where it may be scoured away by the

Martian winds.

It should be cautioned that the apparent success of basal melting in resolving the Martian polar mass balance problem may be more perceived than real. While basal melting makes available a potential pore volume storage capacity as large as $\sim 10^8 \text{ km}^3$ within the Martian crust, this capacity would be filled rather quickly given a polar deposition and basal melting rate of the order of $0.1\text{-}1 \text{ km}^3$ of H_2O per Martian year. One solution which has been proposed to resolve this dilemma is discussed below.

6. A model for the climatic behavior of H_2O . Recent calculations on the stability of ground ice in the equatorial region of Mars suggest that any ground ice emplaced earlier than 3.5 billion years ago may have long since been lost by sublimation to the atmosphere (Clifford and Hillel, 1983). Yet various lines of morphologic evidence suggest that substantial quantities of ground ice have been present in virtually all equatorial terrains, from the oldest to the most recent (Johansen, 1978; Allen, 1979b; Rossbacher and Judson, 1981). In an attempt to address this apparent conflict, a model for the climatic behavior of H_2O on Mars has been proposed (Clifford and Huguenin, 1980; Clifford, 1981b). This model is based on the assumption that the planetary inventory of H_2O is sufficient to create an interconnected supermafrost groundwater system of global extent.

As equatorial ground ice is depleted it may be replenished by the thermal migration of H_2O from the proposed groundwater system below

(cf. Chapter III). The groundwater system is in turn replenished when H_2O , sublimated from equatorial ground ice, is cold-trapped into the polar regions where, as before, the added layer of insulation results in basal melting. The deep percolation of water beneath the polar caps will result in the rise of the local water table in the form of a groundwater mound (Figure 4.4). The gradient in hydraulic head created by the presence of the groundwater mound will then drive the flow of groundwater to the equator. This model is illustrated in Figure 4.15.

The principal asset of this model is that it represents an essentially steady-state hydrologic cycle that does not require any significant periods of climatic change to account for the global redistribution of H_2O . Its major shortcoming is the present uncertainty as to whether the inventory of H_2O on Mars is large enough to have saturated the ground ice capacity of the regolith and support the required planet-wide groundwater system. If the required quantity of H_2O does presently exist on Mars, then the model discussed here should naturally evolve. A more detailed discussion of this model is presented in Chapter V.

E. Conclusions

Given that the ground ice capacity of the Martian cryosphere is likely to be saturated near the poles, any deposition that occurs at the polar surface will result in the melting of pore ice at the base of the cryosphere. Should the deposition of dust and H_2O in this region

Figure 4.15. A model for the climatic behavior of water on Mars.

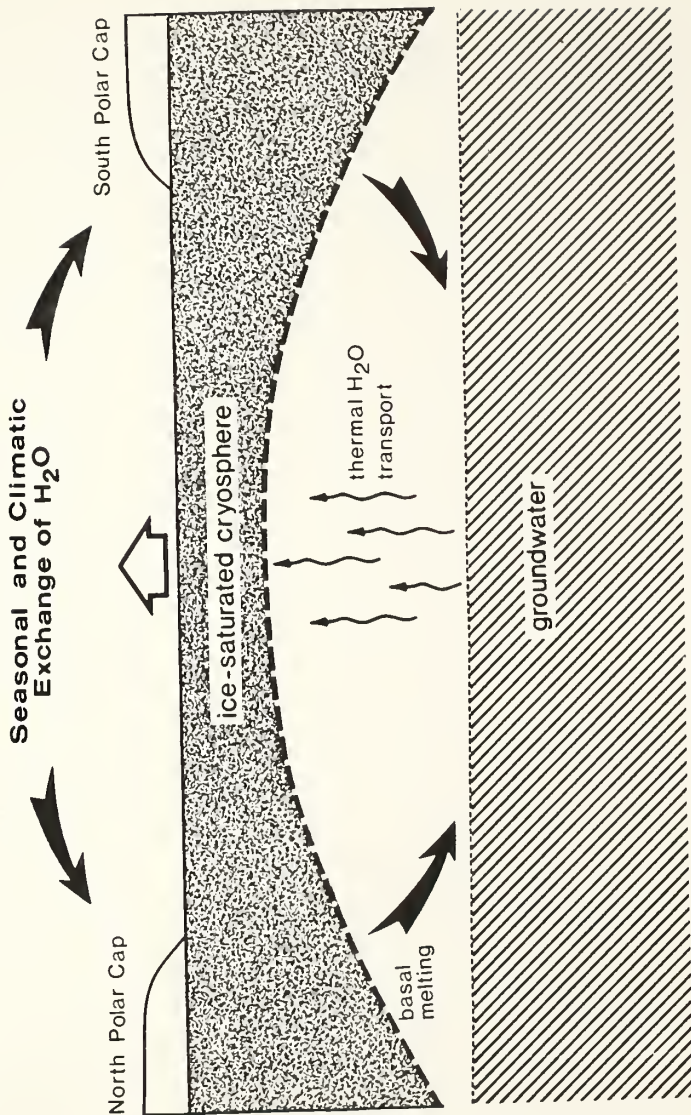


Figure 4.15

continue long enough, the polar deposits will eventually reach a thickness sufficient for melting to occur at their physical base. The occurrence of such melting may have had a profound effect on both the evolution of the Martian polar terrains and the long-term climatic cycling of H_2O .

F. Notation

- a polar accumulation rate, cm s^{-1} .
- A flow law constant, $\text{s}^{-1} \text{bar}^{-3}$.
- A_b mean bolometric albedo of north polar cap, .45.
- A_o temperature invariant flow law constant,
 $8.1 \times 10^{-9} \text{s}^{-1} \text{bar}^{-3}$.
- e orbital eccentricity.
- f_d volume fraction of dust in polar deposits.
- f_i volume fraction of ice in polar deposits.
- F thermal weighting factor.
- g acceleration of gravity, 371cm s^{-2} .
- g_x principal axial length of particle ellipsoid.
- h height of ice sheet profile, cm.
- H thickness required for basal melting, cm.
- H_m maximum observed thickness of polar cap, cm.
- i obliquity, deg.
- $\langle I \rangle$ pole mean polar insolation, $\text{cal cm}^{-2} \text{s}^{-1}$.
- k_d thermal conductivity of dust, $8.6 \times 10^{-3} \text{cal cm}^{-1} \text{s}^{-1} \text{K}^{-1}$.
- k_{eff} effective thermal conductivity of polar deposits,
 $\text{cal cm}^{-1} \text{s}^{-1} \text{K}^{-1}$.
- k_i thermal conductivity of ice, $1 \times 10^{-4} \text{cal cm}^{-1} \text{s}^{-1} \text{K}^{-1}$.
- L half-width of polar cap, cm.
- m $=(n+1)/2$.
- n shear stress exponent in flow law, 3.

- Q activation energy for creep, 139 kJ/mol (263 K < T < 273 K),
 60 kJ/mol (T < 263K).
- Q_f frictional heat due to glacial sliding, cal cm⁻² s⁻¹.
- Q_g geothermal heat flux, $\sim 7 \times 10^{-7}$ cal cm⁻² s⁻¹.
- R universal gas constant, 8.314 J mol⁻¹ K⁻¹.
- S_o Martian solar constant, 4.18×10^{-3} cal cm⁻² s⁻¹.
- T temperature, K.
- T_{mp} melting point temperature of ice, K.
- T_s mean annual polar surface temperature, K.
- x distance from center of cap, cm.
- ϵ emissivity.
- $\dot{\epsilon}$ strain rate, s⁻¹.
- ρ_i density of polar ice, g cm⁻³.
- σ Stefan-Boltzman constant, 1.36×10^{-12} cal cm⁻² K⁻⁴ s⁻¹.
- τ shear stress, bar.
- τ_b basal shear stress, bar.

CHAPTER V
A MODEL FOR THE CLIMATIC BEHAVIOR
OF WATER ON MARS.

A. Introduction

Theoretical estimates of the amount of water Mars has outgassed over its geologic history, expressed in terms of a uniform layer of liquid averaged over the planet's surface, range from a layer as shallow as 10 meters (Anders and Owen, 1977), to one as much as a kilometer or more in depth (J. Lewis, personal communication, 1980). Currently, the most widely accepted estimate is equivalent to a layer some 100 - 250 meters deep (McElroy et al., 1977; Pollack and Black, 1979). However, the quantity of water which is actually present in observable reservoirs on Mars, such as its permanent polar caps and atmosphere, represents only a small fraction of the theoretical total. This deficit suggests that substantial quantities of H₂O may be stored as ground ice, and possibly as groundwater, within the Martian crust.

Three models which have been proposed to account for the latitudinal distribution and climatic behavior of water on Mars; they are: 1) the atmospheric equilibrium model, 2) the fossil ground ice model, and 3) the subpermafrost groundwater model. A principal difference between these models is the relative extent to which their assumed H₂O inventories saturate the available pore space in the

Martian cryosphere (that region of the crust where temperatures have remained continuously below the freezing point). Based on reasonable estimates of the latitudinal variation of mean annual surface temperatures, the thermal conductivity of the regolith, and the value of the Martian geothermal heat flux, present thermal models suggest that the depth to the 273 K isotherm varies from approximately 1 km at the equator to slightly in excess of 3 km at the poles (Fanale, 1976; Rossbacher and Judson, 1980).

Both the atmospheric equilibrium model and the fossil ground ice model are based on the supposition that the total inventory of water on Mars is less than that required to saturate the available pore space within the Martian cryosphere; while the subpermafrost groundwater model is based on a planetary inventory of H_2O which exceeds this potential ground ice capacity. In the following discussion the principal characteristics and possible ramifications of each of these three models will be briefly reviewed.

1. The atmospheric equilibrium model. Probably the simplest model for the climatic behavior of water on Mars is based on the assumption that the regolith is in complete diffusive equilibrium with the Martian atmosphere. Observations made by the Viking Orbiter Mars atmospheric water detectors (MAWD) indicate a global frost-point temperature of approximately 198 K (Farmer and Doms, 1979). Thus, given the present range of mean annual surface temperatures on Mars, the occurrence of ground ice in equilibrium with the water vapor content of the

atmosphere is restricted to the colder latitudes poleward of $\pm 40^\circ$ (Figure 5.1a) (Leighton and Murray, 1966; Fanale, 1976; Farmer and Doms, 1979).

The fact that mean annual equatorial temperatures have associated equilibrium vapor pressures that greatly exceed the partial pressure of H_2O in the atmosphere has important implications for the long-term behavior of H_2O on Mars. For example, should the release of juvenile water by local volcanic activity result in the emplacement of ground ice within the equatorial regolith, the low relative humidity of the atmosphere will ensure its rapid sublimation. Because the cold polar regions are the dominant thermodynamic sink for any H_2O released to the atmosphere, there is a preferential transfer of this H_2O from the "hot" equatorial latitudes to the colder poles (Flasar and Goody, 1976).

It is important to note that the loss of H_2O from the equatorial regolith is irreversible under the present conditions of surface temperature and atmospheric pressure on Mars; therefore, once ground ice has been removed from the equatorial regolith, it can not be replenished by any atmospheric means. Although changes in surface insolation, brought on by periodic variations in the planet's obliquity and orbital elements, may lead to significant H_2O exchange between the two polar reservoirs, they will result in only a small displacement of the frost-point latitude about its current location (Toon et al., 1980).

The major test of the atmospheric equilibrium model is that it

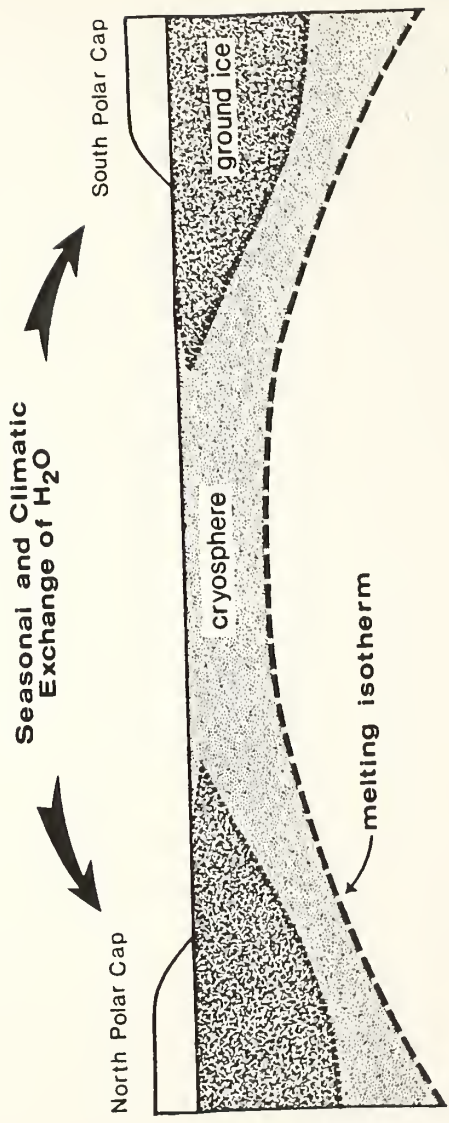


Figure 5.1a. The atmospheric equilibrium model.

predicts an essentially dry equatorial regolith. Yet, photographs taken during the Mariner and Viking missions to Mars have provided considerable geomorphologic evidence that the distribution of ground ice on Mars may be global, and not simply restricted to the two polar reservoirs illustrated in Figure 5.1a (Johansen, 1978; Mouginiis-Mark, 1979; Allen, 1979a; Blasius and Cutts, 1981; Rossbacher and Judson, 1981). If the interpretation of these various morphologies is correct, then their presence in virtually every terrain, from the oldest to most recent, suggests that substantial quantities of H_2O may have been present within the equatorial regolith throughout much of Martian geologic history. Because this conclusion is irreconcilable with a model for the distribution of ground ice based on complete diffusive equilibrium with the Martian atmosphere, it is generally acknowledged that an alternative model for the long-term behavior and distribution of H_2O on Mars must now be considered.

2. The fossil ground ice model. One explanation which has been proposed to account for the presence of ground ice in the equatorial regolith, is that it may be a relic of a substantially different climate that existed very early in Martian geologic history. The subsequent depletion of this fossil layer of ground ice might then have been retarded by the diffusion-limiting properties of a fine-grained regolith. This explanation is based on an extrapolation of the work of Smoluchowski (1968), who showed that under certain limited conditions of porosity, pore size, temperature, and depth of burial, a 10 m thick

layer of ground ice might survive in disequilibrium with the Martian atmosphere for as long as a billion years.

The fossil ground ice model appears to provide a credible explanation for the apparent global distribution of ground ice on Mars; however, in all other respects, the predicted behavior of H_2O based on this model closely resembles that predicted by its predecessor (Figure 5.1b). For instance, while the presence of a fine-grained regolith may greatly retard the evaporative loss of ground ice within the latitude band of $\pm 40^\circ$, it cannot eliminate this loss entirely. Consequently, the equatorial regolith will act as a net annual source of atmospheric water vapor as the inventory of equatorial ground ice is slowly depleted. As before, the ultimate fate of this excess atmospheric H_2O is that it will be cold-trapped at higher latitudes, where it will become part of the seasonal and climatic exchange that occurs in response to periodic variations in surface insolation.

In light of its apparent ability to account for the global distribution of regolith H_2O , the fossil ground ice model has gained popular acceptance. Of course, given few constraints, one could easily create a model of the Martian regolith with physical properties sufficient to preserve a buried layer of ground ice for an indefinite period of time; however, while such a model may be physically possible, it may also bear very little resemblance to reality. Indeed, a recent study, based on data obtained during the Viking mission to Mars, suggests that the actual physical properties of the Martian regolith

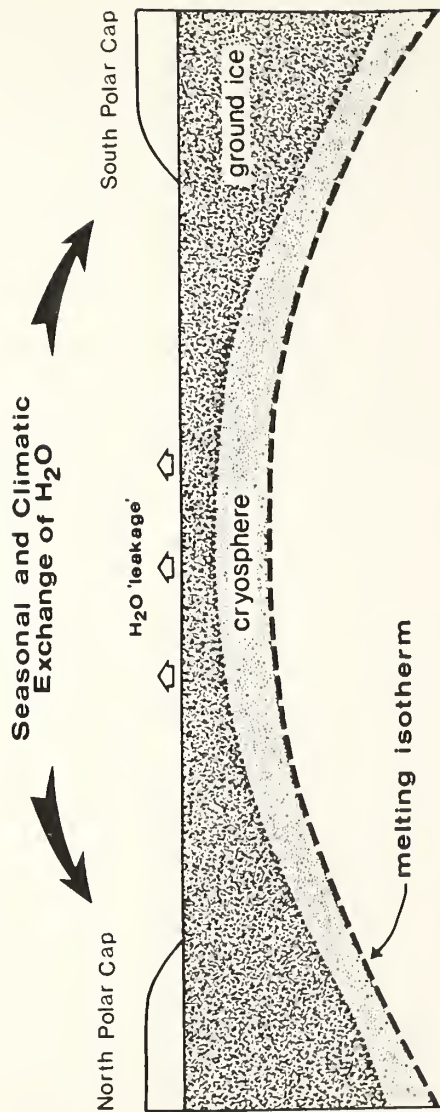


Figure 5.1b. The fossil ground ice model.

may fall short of those necessary to preserve equatorial ground ice throughout the course of Martian geologic history (Clifford and Hillel, 1983). If this analysis is correct, it again raises the question of how to account for the seemingly abundant morphologic evidence that ground ice may have survived within the equatorial regolith for billions of years.

Perhaps the simplest explanation for the long-term survival of equatorial ground ice is that it has undergone a process of continuous or episodic replenishment (Clifford, 1980d; 1982a). However, as noted earlier, under present climatic conditions the atmospheric depletion of equatorial ground ice appears irreversible. Therefore, if replenishment has occurred, it suggests that the processes involved in the distribution and climatic behavior of water on Mars may actually be more complex than those that are characteristicly attributed to the fossil ground ice model.

3. The subpermafrost groundwater model. If the inventory of H_2O on Mars exceeds the ground ice capacity of the regolith, then the excess H_2O will be stored as groundwater beneath the cryosphere (Figure 5.1c). As discussed by Clifford and Huguenin (1980) and Clifford (1980d; 1981a), the existence of such a planetary scale subpermafrost groundwater system on Mars may have a significant impact on the climatic cycling of H_2O .

The principal difference between the subpermafrost groundwater model and earlier climatic models is the possibility that subsurface

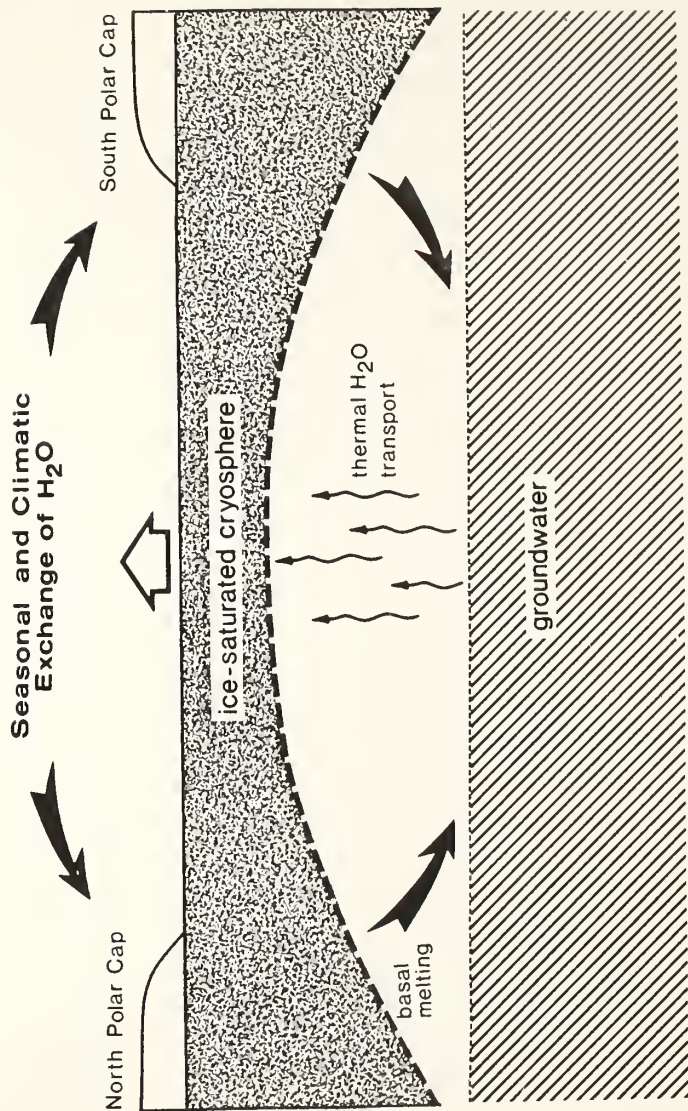


Figure 5.1c. The subpermafrost groundwater model.

H_2O transport might complement long-term atmospheric exchange. Given an inventory of H_2O that exceeds the ground ice capacity of the Martian regolith, the annual deposition of dust and H_2O at the poles will result in a situation where the equilibrium depth to the melting isotherm has been exceeded. Thus, in response to this added layer of insulation, the melting isotherm will rise higher in the regolith until such time as the equilibrium depth is once again established. This will result in the melting of any pore ice present at the base of the cryosphere. The deep percolation of this meltwater beneath the polar caps will result in the rise of the local water table in the form of a groundwater mound. Given a regolith of sufficient permeability, the gradient in hydraulic head created by the presence of the groundwater mound will then drive the flow of groundwater to the equator. At equatorial latitudes, the presence of a geothermal gradient within the Martian crust will result in a net discharge of the groundwater system as water vapor is thermally pumped from the higher temperature (higher vapor pressure) depths to the colder (lower vapor pressure) near-surface regolith. In this fashion equatorial ground ice may ultimately be replenished, thus completing the proposed cycle.

Various aspects of the subpermafrost groundwater model, including the inherent instability of equatorial ground ice, the thermal transport of H_2O , and basal melting, have been discussed at length in earlier chapters of this dissertation. Therefore, the following discussion will focus on the geologic requirements and actual mechanics of subsurface flow.

B. The Martian Megaregolith

The existence of a global groundwater system on Mars is necessarily subject to certain geologic constraints; the most obvious of which is that there must exist a suitably porous and permeable layer in which the groundwater can reside. In this section we will summarize the evidence supporting the existence of such a layer on Mars and attempt to quantify some of its more important physical parameters, such as its porosity, total pore volume, and depth to self compaction.

1. Origin and structure. At the present time, the only means of determining the porosity of the Martian crust, and its variation with depth, is by analogy with either the Earth or Moon. Whereas comparisons of the Earth and Mars may often be justified, it is unlikely that many of the processes that have contributed to the widespread occurrence of thick and highly porous geologic units on the Earth (e.g., extensive fluvial erosion and marine sedimentation) can also be invoked for Mars. Any structural comparison is further complicated by the great disparity in mean crustal ages between the two planets. On Mars much of the surface is covered by a heavily cratered highlands unit which is thought to date back almost 4 billion years ago to the tail-end of the heavy bombardment period (Neukum and Wise, 1976). However, on Earth, recent studies indicate that the mean age of the continental crust lies between 1.5-1.8 billion years (Jacobsen and Wasserburg, 1979a), while the oceanic crust is even younger (less than .18 billion years)

(Jacobsen and Wasserburg, 1979b). Thus, the extensive reworking of the Earth's crust by the processes of erosion and plate tectonics has virtually eliminated any remnant of its early structure.

Differences between the Moon and Mars are somewhat less severe. Both bodies appear to have comparable crustal ages (Neukum and Wise, 1976) and their surfaces clearly reveal the similar extent to which impact and volcanic processes have played a role in the structural modification of their crusts. In light of the above, it would seem more appropriate to develop a structural model of the Martian crust based on a lunar analog (with due consideration given to the potential effects of an atmosphere and subsurface water) than to attempt such a model based on the far more complex constructional and erosional history of the Earth.

Field studies of terrestrial impact craters (Dence et al., 1977; Pohl et al., 1977) and theoretical models of the cratering process (Melosh, 1980; O'Keefe and Ahrens, 1981) have established that impacts alter the structure of a planetary crust in two important ways: (1) by the production and dispersal of large quantities of ejecta, and (2) through the intense fracturing of the surrounding and underlying basement. By these processes, repeated impacts have led to the production of a lunar "megaregolith" (Hartmann, 1973). This view is supported by an analysis of the seismic propagation characteristics of the outer layer of the lunar crust, which suggests that it is brecciated to considerable depth (Toksoz, 1979). For the near-surface of the Moon, P-wave velocities are observed to increase with depth

until they reach a local maximum at about 20 km (Toksoz, 1979; Binder, 1980; Binder and Lange, 1980). This behavior has been attributed to a reduction of pore volume within the crust as lithostatic pressure increases with depth. The transition between fractured and coherent lunar basement is believed to coincide with the beginning of the constant velocity zone observed at a depth of 20 km, where lithostatic pressure is thought to be sufficient (> 1 kbar) to completely close all fractures and intergranular pore spaces (Toksoz, 1979; Binder, 1980; Binder and Lange, 1980).

As discussed by Fanale (1976), Carr (1979), and others, Mars is thought to have experienced a similar cratering history. Fanale (1976) has calculated that the total volume of Martian crater ejecta was probably sufficient to produce a global blanket of unconsolidated material as much as 2 kilometers thick. As noted by Carr (1979), it is likely that volcanic flows, weathering products, and various forms of sedimentary deposits, are interbedded with this crater ejecta; while extensive fracturing of the underlying basement, from impact generated shock waves and tectonic activity, is likely to have occurred to great depths (Figure 5.2).

2. Porosity profile and total pore volume. To account for the seismic properties of the near-surface layer of the Moon, Binder (1980) and Binder and Lange (1980) have presented a model of the lunar crust in which the porosity declines exponentially with depth, falling to less than 1 percent at a depth of 20 km. Based on such a model, the

Figure 5.2. An idealized stratigraphic column of the Martian crust based on the discussions of Fanale (1976) and Carr (1979).

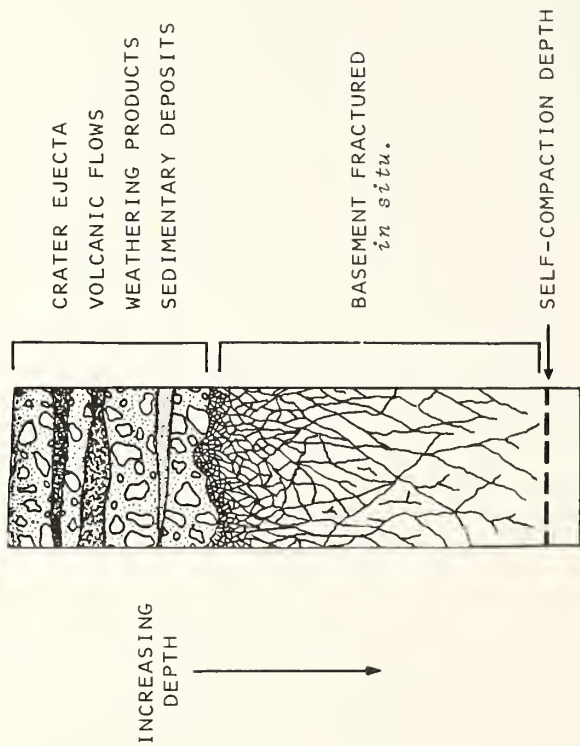


Figure 5.2

porosity at any depth 'z' is given by:

$$\phi(z) = \phi(0) \exp(-z/K) \quad (V.1)$$

where $\phi(0)$ is the porosity at the lunar surface and where K, the porosity decay constant, is assumed to have a lunar value of 6.5 km.

Given that the density of the Martian crust is comparable to its lunar counterpart, then by a simple gravitational scaling of the decay constant in Equation (V.1) we can obtain a similar expression to calculate the porosity and depth to self-compaction of the Martian megaregolith. Thus, for Mars we have:

$$\begin{aligned} K_{\text{Mars}} &= 6.5 \text{ km} (1.61 \text{ m s}^{-2}/3.71 \text{ m s}^{-2}) \\ &= 2.82 \text{ km.} \end{aligned} \quad (V.2)$$

In Figure 5.3, two hypothetical porosity profiles of the Martian crust are presented. The first is based on a surface porosity of 20%, as assumed in the case of the Moon by Binder and Lange (1980). This model yields a self-compaction depth for the Martian regolith of approximately 8.5 km. By integrating the regolith porosity down to this depth, we find that the total pore volume of the Martian crust is roughly $7.8 \times 10^7 \text{ km}^3$; enough to store a volume of H_2O equivalent to a layer of water approximately .54 km deep averaged over the planet's surface.

In the second model a surface porosity of 50 percent has been

Figure 5.3. Theoretical porosity profiles of the Martian crust based on the lunar model of Binder (1979). The curve calculated on the basis of a surface porosity of 20% is simply the lunar model of Binder (1979) gravitationally scaled to Mars. The curve corresponding to a surface porosity of 50% is included to account for the possibility that various processes of physical and chemical weathering may have substantially increased the available pore space in the outer crust. In reality, the actual porosity of the Martian crust is likely to fall between these extremes. Near the surface, where weathering processes have been most active, the porosity profile is likely to be similar to the 50% curve; while at depth the gravitationally scaled lunar curve may be more appropriate.

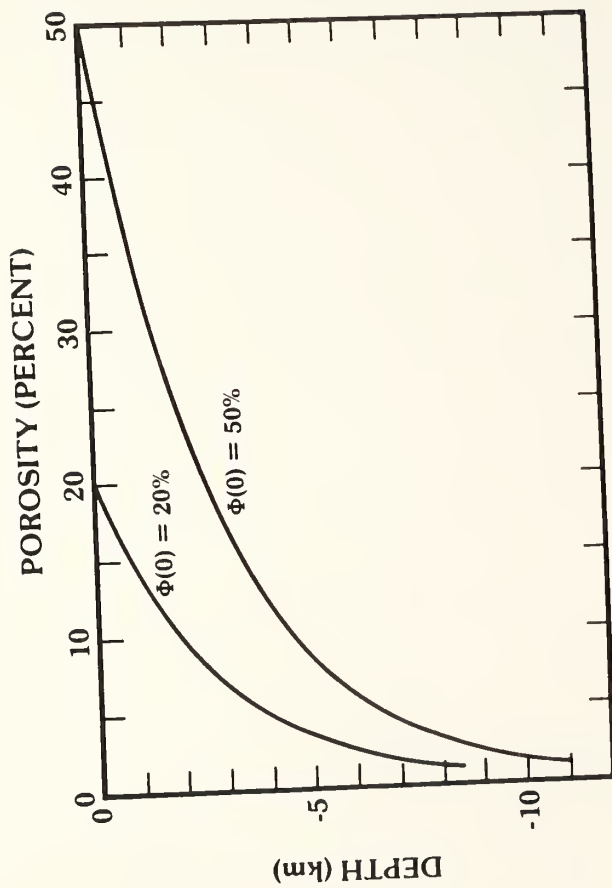


Figure 5.3

assumed; this value is in accord with estimates inferred from Viking Lander data and is consistent with what one might expect based on the wide variety of weathering processes that may occur on Mars (e.g., Malin, 1974; Huguenin, 1976; Gooding, 1978). The self-compaction depth predicted by this model is of the order of 11 km; while the total pore volume is approximately 2×10^8 km, corresponding to a global layer of water some 1.4 km deep.

The presence of substantial quantities of groundwater in the Martian crust could significantly affect these porosity estimates. As discussed by Hubert and Rubey (1959) and others (Serafim, 1969; Byerlee and Brace, 1972), the hydrostatic pressure of water within a pore can reduce the net lithostatic pressure acting to close it. Thus for a "wet" Mars, significant porosity may occur at depths below those calculated for the "dry" models in Figure 5.3. It should be noted, however, that the presence of groundwater may also act to reduce overall porosity by solution, compaction, and cementation (Maxwell, 1964; Rittenhouse, 1971). Such processes are of greatest significance under conditions of high temperature and pressure (Maxwell, 1964; Pettijohn, 1975). Because these conditions are generally expected to occur only at great depth on Mars, where calculated porosities are low to begin with, their impact on the overall porosity of the megaregolith should not be large.

Finally, one qualification to the applicability of this lunar porosity model to Mars must be noted. As discussed by Neukum and Wise (1976), the lunar highlands are generally believed to have reached

saturation for crater diameters <50 km, while the heavily cratered terrain of Mars is evidently undersaturated at all crater diameters. The extent to which this difference in crater densities may have reduced the overall porosity and depth of the Martian megaregolith is not readily apparent.

C. Regolith H₂O on Mars

Given the structural description of the Martian crust presented in the previous section, a number of questions arise regarding both the origin and distribution of H₂O within the regolith. Specifically: How was the regolith initially charged with H₂O? What role have the thermodynamic, chemical, and structural properties of the regolith played in determining the distribution of ground ice and groundwater within the crust? Finally, just how large a planetary inventory of H₂O is actually required to create a planetary-scale subpermafrost groundwater system? The answers to these questions will have a direct bearing on our understanding of the long-term behavior of H₂O on Mars.

1. The emplacement of regolith H₂O. The morphologic evidence for the widespread occurrence of ground ice on Mars, and the difficulty involved in accounting for this distribution given the present Martian climate, has led a number of investigators to conclude that Mars may have possessed a substantially different climate very early in its

geologic history (Mutch et al., 1976; Masursky et al., 1977; Carr, 1979; Toon et al., 1980; Luchitta, 1981; Rossbacher and Judson, 1981). Evidence in support of this conclusion comes from models of the outgassing history of Mars, which suggest that the planet may have originally possessed a substantially denser atmosphere (McElroy et al., 1977; Pollack and Black, 1979). Indeed, extensive erosion resulting from a dense early atmosphere is considered a likely cause of the early episode of crater obliteration inferred from crater diameter-frequency plots of the ancient cratered highlands (Mutch et al., 1976; Arvidson et al., 1980; Carr, 1981). Often cited as additional evidence for a more clement period in the early Martian climate are the Martian valley networks, features which bear a close resemblance to terrestrial runoff channels and which are found almost exclusively in the ancient (~4 billion year old), heavily cratered terrain of Mars (Pieri, 1979, 1980; Carr and Clow, 1981).

Based on the above evidence, one scenario that has evolved for the global emplacement of regolith H_2O on Mars is that early climatic conditions were conducive to the widespread precipitation of H_2O as rain (Mutch et al., 1976; Masursky et al., 1977; Pieri, 1979, 1980; Carr and Clow, 1981). Indeed, Masursky et al. (1977) argue that the morphology of the Martian valley networks can reasonably be attributed to the occurrence of rainfall and surface runoff early in the planet's geologic history. However, Pieri (1979, 1980) finds no compelling evidence that the Martian valley networks were eroded as the result of atmospheric precipitation. Instead, Pieri (1979, 1980) attributes the

morphology of the valley networks to groundwater-driven basal sapping. He further suggests that the groundwater responsible for this action was emplaced during a period of precipitation which occurred so early in Martian geologic history that no physical record from this period remains.

While it is possible that evidence of an ancient period of global precipitation may have been lost due to repeated impacts and eolian erosion, it seems equally reasonable to take this lack of evidence at face value and consider the possibility that global precipitation may never actually have occurred. In this regard, Soderblom and Wenner (1978) suggest that the emplacement of regolith H_2O on a global scale was the result of the direct injection and migration of juvenile water derived from the planet's interior. As shown by Clifford (1980d, 1982a) such subsurface emplacement is possible even under climatic conditions that closely approximate those we observe today.

Given either mode of emplacement, as the interior of the planet gradually cooled, regolith H_2O may have become segregated into a slowly thickening zone of near-surface ground ice and a deeper region of subpermafrost groundwater (Carr, 1979). If the planetary inventory of H_2O was less than the available pore volume of the cryosphere, then all of the H_2O may have ultimately been taken up as ground ice (Soderblom and Wenner, 1978). Alternatively, an inventory of H_2O which exceeded the pore volume of the cryosphere would have resulted in the formation of permanent and extensive bodies of subpermafrost groundwater (Clifford and Huguenin, 1980).

2. Extent of the cryosphere. The Martian cryosphere is defined as that region within the crust where the temperature of the regolith has remained continuously below the freezing point of water (Rossbacher and Judson, 1981). If we assume that water in the regolith has a solute-free freezing point of 273 K, then the necessary temperature condition which defines the upper boundary of the cryosphere is satisfied at every latitude, below a depth of several centimeters. Unfortunately, because of the number of variables involved, determining the the depth to the lower boundary of the Martian cryosphere is considerably more difficult.

As on the Earth, the magnitude of the Martian geothermal gradient will depend on both the value of the geothermal heat flux and the volume-averaged thermal conductivity of the planet's crust. Given a near constant gradient, the latitudinal variation in Martian mean annual surface temperatures will translate into a corresponding latitudinal variation in the depth at which the temperature of the regolith is elevated above the freezing point of water. The depth 'd' to the melting isotherm can be calculated from the steady-state one-dimensional heat conduction equation:

$$d = k (T_{mp} - T_{ms})/Q_g \quad (V.3)$$

where k is the thermal conductivity of the regolith, T_{ms} is the mean annual surface temperature, T_{mp} is the melting point temperature, and Q_g is the value of the geothermal heat flux. Based on a melting

point temperature of 273 K, and reasonable estimates of the thermal conductivity of the regolith ($8 \times 10^4 \text{ erg cm}^{-1} \text{ s}^{-1}$) and the value of the Martian geothermal heat flux ($30 \text{ erg cm}^{-2} \text{ s}^{-1}$), we find that the depth to the melting isotherm varies from approximately 1 km at the equator to slightly in excess of 3 km at the poles (Table 5.1) (Fanale, 1976; Rossbacher and Judson, 1981).

However, given the considerable evidence for the presence of various salts within the regolith, the possibility exists that the freezing point of any H_2O in the regolith will be depressed well below 273 K (Clark, 1978; Brass, 1980; Clark and Van Hart, 1981). For example, saturated solutions of NaCl and CaCl_2 have associated freezing points of 252 K and 218 K respectively (Clark and Van Hart, 1981); whereas multi-component salt solutions may have eutectic temperatures which are as low as 210 K (Brass, 1980). As seen in Tables 5.1 and 5.2, the presence of such potent freezing point depressors within the regolith would significantly reduce the size of the Martian cryosphere. If the porosity vs. depth relationship of the Martian crust is accurately described by the model presented in Equation (V.2), then a rough estimate of the total pore volume of the cryosphere can be obtained by integrating Equation (V.2) down to the depths presented in Table 5.1. For the given combinations of regolith porosities and melting point temperatures, the total pore volume of the Martian cryosphere is found to lie within the range of $1.0 \times 10^7 - 9.6 \times 10^7 \text{ km}^3$. The quantity of H_2O required to saturate this pore volume is equivalent to a layer of water approximately 70 - 670 meters

Table 5.1. Latitudinal variation of cryosphere thickness.*

Latitude	Mean annual surface temperature (K)	Cryosphere depths (km)		
		$T_{mp} = 273$ K	252 K	218 K
0°	225	1.28	0.72	0.0
10°N/S	222	1.36	0.80	0.0
20°N/S	218	1.47	0.91	0.0
30°N/S	215	1.55	0.97	0.08
40°N/S	205	1.81	1.25	0.35
50°N/S	185	2.35	1.79	0.88
60°N	170	2.75	2.19	1.28
60°S	173	2.67	2.11	1.2
70°N	155	3.15	2.59	1.68
70°S	170	2.75	2.19	1.28
80°N	146	3.39	2.83	1.92
80°S	163	2.93	2.37	1.47
90°N	142	3.49	2.93	2.03
90°S	160	3.01	2.45	1.55

*After Fanale (1976) and Rossbacher and Judson (1981).

Table 5.2. Pore volumes of cryosphere for various surface porosities and melting isotherm temperatures.

Melting Isotherm (K)	Pore volume ($\times 10^7 \text{ km}^3$)		Equivalent layer of H_2O (m)	
	$\phi(0)=20\%$	$\phi(0)=50\%$	$\phi(0)=20\%$	$\phi(0)=50\%$
218	1.01	2.53	70	175
252	2.90	7.26	200	500
273	3.86	9.64	270	670

deep averaged over the Martian surface (Table 5.2).

Studies of Martian rampart craters, whose distinctive morphologies have been attributed to impacts into a water- or ice-rich regolith (Carr et al., 1977; Johansen, 1978; Mouginiis-Mark, 1979), may provide observational support for the predicted latitudinal variation of cryosphere thicknesses. The results of several of these studies indicate that rampart crater ejecta morphologies undergo a transition from a crater population dominated by an apparent low-mobility/high-viscosity ejecta pattern near the poles, to a highly fluidized/low-viscosity style near the equator (Johansen, 1978; Saunders and Johansen, 1980; Blasius et al., 1981). Advocates of the H₂O/rampart crater hypothesis suggest that this observed latitudinal dependence is consistent with thermal models of the regolith which predict that the depth of frozen ground on Mars decreases appreciably from the poles to the equator. The explanation offered for this behavior is that impacts near the pole will frequently result in the excavation of ground ice alone, whereas impacts near the equator penetrate the thinner ground ice layer and excavate considerable volumes of water-saturated crust.

Of course, the values of heat flux and thermal conductivity on which the results in Tables 5.1 and 5.2 are based represent only globally averaged values; the actual Martian crust is likely to display considerable heterogeneity in these properties over its surface and at depth, resulting in sizable local departures from the expected depth of the Martian cryosphere calculated on the assumption of a homogeneous crust.

3. Saturated thickness of groundwater. Given a quantity of H_2O sufficient to fill the available pore volume of the Martian cryosphere, how much additional H_2O is required to produce a groundwater system of global proportions? Since any groundwater present in the regolith will drain to saturate the region of lowest gravitational potential, we can obtain a rough idea of the volume of water required to produce a global aquifer of any given thickness by once again referring to the theoretical porosity profile described by Equation (V.1).

As a first approximation, Mars can be considered as a perfect sphere that exhibits no topographic relief, has a surface porosity of 50%, and a near-surface porosity profile described by Equation (V.1). By integrating the pore volume of the region between the self-compaction depth and any lesser depth within the regolith, the equivalent volume of water required to produce an aquifer of any given thickness is obtained. For example, in Figure 5.4, we see that a quantity of water equivalent to a layer 10 meters deep averaged over the Martian surface is sufficient to saturate the lowermost .85 kilometers of our model regolith; while a quantity of water equal to a 100 meter uniform layer would create an aquifer nearly 4.3 km deep. Reducing the surface porosity in Equation (V.1) from 50% to 20% will not alter these calculated thicknesses; it will, however, reduce the depth to the lower boundary of the system (the self-compaction depth) from roughly 11 km to approximately 8.5 km.

Of course, Mars is not a perfect sphere; its outer crust has been affected by a variety of geologic processes that have created a surface

Figure 5.4. Resulting aquifer thicknesses for groundwater inventories equivalent to a globally averaged layer 10 and 100 meters deep. The porosity profile of the crust is taken from Figure 5.3.

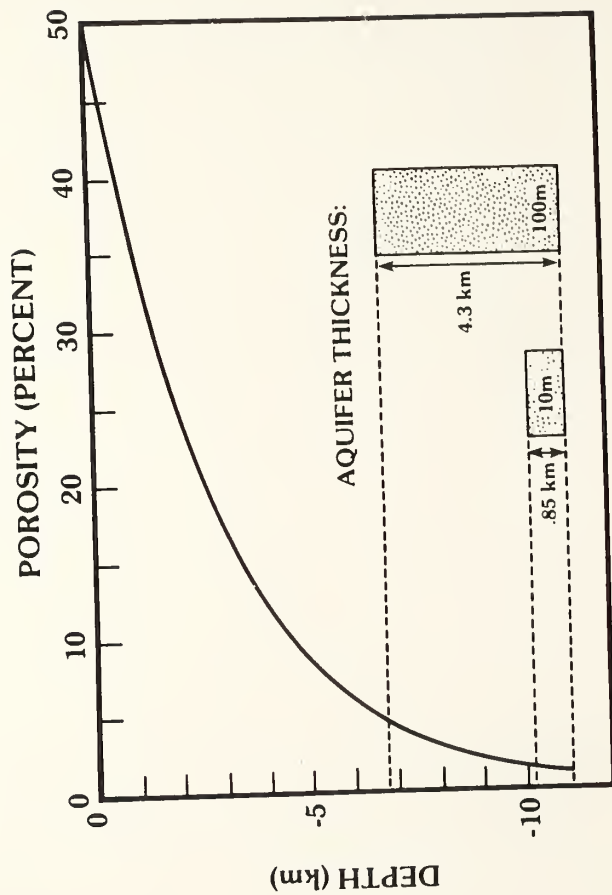


Figure 5.4

of considerable heterogeneity and topographic relief. This diversity is undoubtedly also reflected in the variability of such characteristics as the local porosity profile of the crust and the depth to self-compaction. An example of how these factors might affect the distribution and saturated thickness of groundwater on Mars is presented in Figures 5.5 and 5.6.

Figure 5.5 is a pole-to-pole cross section of the Martian crust where, after Mutch et al. (1976), the surface elevations are averaged as a function of latitude. The cross section illustrates the potential relationship between surface topography, permafrost, and the proposed groundwater system. Clearly, the lower boundary of the groundwater system is determined by the local depth to self-compaction, while the upper boundary is defined on a global basis by a surface of constant geopotential; the local variation in the vertical distance separating these two boundaries produces a corresponding variation in the saturated thickness of groundwater.

If the depth to self-compaction mirrors the gross variation of surface topography, as assumed in this illustration, then the saturated thickness of groundwater is likely to reach its greatest depths beneath topographic lows, such as the region encompassed by the northern third of the planet and by major impact basins such as Hellas and Argyre. Likewise, below major topographic highs, such as Tharsis and Elysium, the absolute elevation of the self-compaction depth may rise above the absolute elevation of the global groundwater table; should this occur, groundwater will be absent beneath these regions.

Figure 5.5. A pole-to-pole cross section of the Martian crust illustrating the relationship between topography, ground ice, and the proposed groundwater system. Surface elevations are averaged as a function of latitude after Mutch et al. (1976). Ground ice thicknesses are taken from Fanale (1976). The self-compaction depth is assumed to be a uniform 10 km.

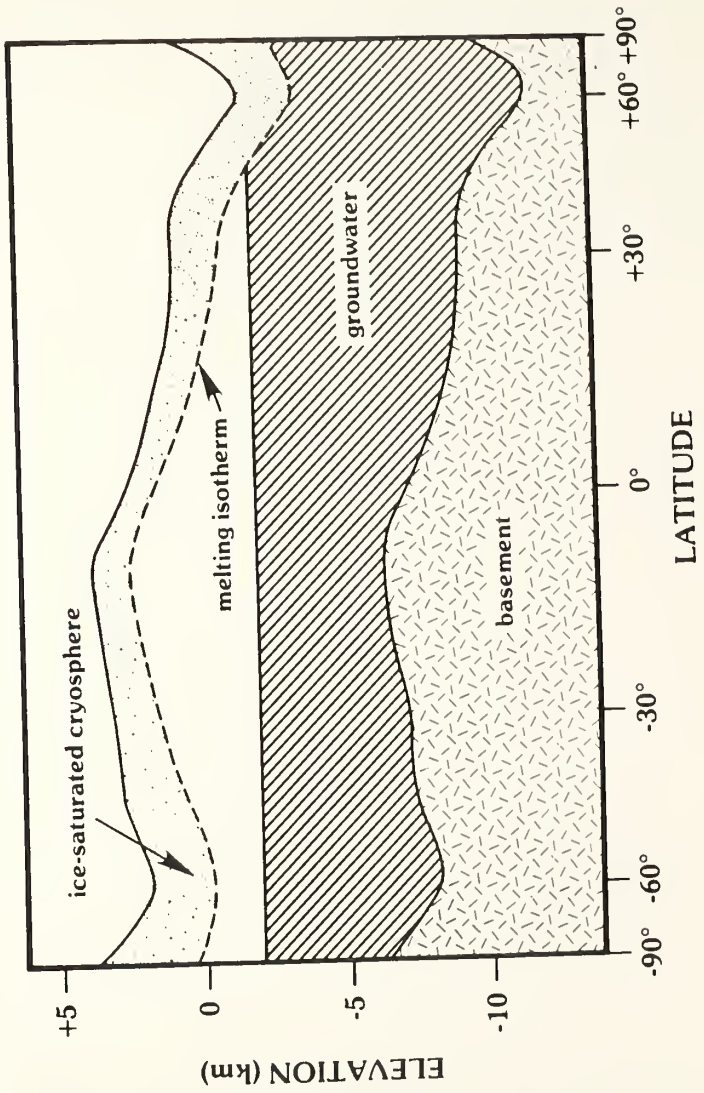


Figure 5.5

Figure 5.6. A highly schematic depiction of the possible areal distribution that a global subpermafrost groundwater system might have on Mars.



Impermeable
Basement



Aquifer

Figure 5.6

While the position of the groundwater table in the Martian crust will be determined by a surface of constant geopotential, ground ice will follow the gross variation of surface topography. This distribution results from the fact that the position of a particular isotherm within the crust is determined by the geothermal gradient. Therefore, given similar conditions of surface temperature, heat flow, and regolith thermal conductivity, the depth from the Martian surface to the melting isotherm will be the same on top of a mountain as it is on the floor of an impact basin. As can be seen in Figure 5.5, this may have significant implications for the vertical stratification of H_2O in the crust.

As noted earlier, in regions occupied by topographic highs, the self-compaction depth may rise to a higher absolute elevation than the global water table; as a result, only near-surface ground ice may be present in a vertical section of the local crust. Within regions of slightly lower elevation, both ground ice and groundwater may be present; however, the vertical distances separating these zones may be substantial, leaving an intervening unsaturated zone which could be many kilometers in thickness. In the lowest topographic regions, the available pore space throughout the entire crustal column may be saturated with both ground ice and groundwater. Indeed, the surface elevations of some of the very lowest regions, such as the interior of Hellas basin, may actually lie below the level of the global water table. In such instances the kilometer or more thickness of near-surface ground ice will be under a substantial hydraulic head;

therefore, a rupture of this barrier could lead to a significant release of subpermafrost groundwater (Carr, 1979). However, such a rupture is eventually self-sealing, because as the water erupts onto the surface it will lower the local piezometric surface until such time as the hydraulic head falls below the elevation of the basin floor. At this point the water-saturated regolith will refreeze at the site of breakout and, as time progresses, the original ground ice thickness will eventually be reestablished.

One consequence of the fact that groundwater will seek out and saturate the lowermost porous regions of the crust is that the areal distribution of a groundwater system on Mars is likely to be substantially less than 100% (Figure 5.6); therefore, for a given quantity of water, the resulting aquifer thickness will be greater than that calculated on the basis of global coverage. Based on this study, we see that, once the pore volume of the cryosphere has been saturated with ice, very little additional water is required to produce a planetary-scale groundwater system of substantial thickness.

D. The Occurrence of Groundwater and the Permeability of the Earth's Crust.

While the calculations presented in the previous section indicate that a planetary-scale groundwater system on Mars is physically possible, we must also consider whether it is geologically reasonable. Unfortunately, a clear answer to this question is clouded by the fact

that subsurface hydrology remains an inexact science even here on Earth.

Deep well observations indicate that groundwater is present at depth virtually everywhere within the Earth's continental crust (Waltz, 1969; de Marsily et al., 1977; Fetter, 1980). According to Brace (1971), the zone of saturation generally continues to depths that are at least 4-5 km below the regional water table; however, there is a growing body of evidence suggesting that groundwater may be present at even greater depths. Much of this evidence comes from studies of the electrical conductivity of the upper 20 km of the Earth's crust. These measurements reveal that the conductivity of the crust is at least several orders of magnitude higher than that of dry laboratory rock samples studied under similar conditions of temperature and pressure (Hyndman and Hyndman, 1968; Brace, 1971; Nekut et al., 1977; Thompson et al., 1983; Shankland and Ander, 1983). Although a wide variety of explanations have been proposed to account for these observations, laboratory studies and theoretical arguments both strongly suggest that the high conductivity of the crust owes its origin to the existence of water-saturated permeable rock at depth (Hyndman and Hyndman, 1968; Brace, 1971; Shankland and Ander, 1983).

As discussed by Legrand (1979), Brace (1980), Seeburger and Zoback (1982), and others, the Earth's crust is largely composed of fractured rock. While early data suggested that the density of fractures in rock declines appreciably with depth (Snow, 1968), more recent investigations indicate that this correlation is limited to the weathered near-

surface layer. Indeed, in a study of ten deep test wells, drilled to depths of 200-1000 meters in various regions of North America, numerous fractures were discovered down to the limit of exploration (Seeburger and Zoback (1982). Based on these observations, Seeburger and Zoback (1982) conclude that fractures in the Earth's crust probably persist to depths far in excess of 1 km. Similar results were obtained in an investigation of two 1.6 km boreholes drilled into the Precambrian basement of northern Illinois (Haimson and Doe, 1983). As in the study by Seeburger and Zoback (1982), Haimson and Doe (1983) found no evidence for a significant decline in fracture density with depth.

The pervasive nature of crustal fractures means that few, if any, geologic formations can be considered absolutely impermeable (de Marsily et al., 1977; Fetter 1980; Brace, 1980); therefore, crustal fractures provide the hydraulic links by which groundwater systems on Earth are interconnected. The extent of this interconnection has become increasingly apparent from the results of various hydrogeologic studies which have been conducted to investigate the possible contamination of groundwater supplies by the careless disposal of radioactive and toxic chemical wastes. Some of the first evidence for the existence of interbasin groundwater flow came from Death Valley, California, where it was observed that the discharge of certain springs was much larger than could be accounted for based on the available local recharge (Hunt and Robinson, 1960). This suggested the possibility that water derived from the higher intermountain basins to the east may have been transported to Death Valley through an extensive

network of hydraulically connected fractures within the intervening rock. Convincing support for this hypothesis came from the near identical chemical composition of spring water in Death Valley and water found to the east in the intermountaine valley of Ash Meadows, Nevada.

The discovery of interbasin flow between Ash Meadows and Death Valley raised concern about the potential for contamination from underground nuclear tests at the nearby Nevada Test Site (Winograd, 1962). Extensive drilling revealed that, although the three large intermontaine basins encompassed by the Test Site were topographically isolated, the water levels within the various test wells were nearly identical, a result which argued strongly for hydraulic interconnection. To the east of the Nevada Test Site, yet another regional groundwater flow system was discovered. In this instance the evidence linked 13 intermountaine valleys into a regional flow system measuring roughly 240 by 70 miles (Eakin, 1966). Indeed, as investigations continue, it is now believed that most of eastern Nevada and western Utah may be underlain by deep regional flow systems (Mifflin and Hess, 1979).

The importance of fractured rock in providing an interconnected hydraulic network is not relegated to studies of groundwater alone. For instance, the geochemical similarity of oil in central and eastern Wyoming and the carbonaceous material found in the black shales of the Phosphoria Formation in northern Utah, eastern Idaho, and southwestern Wyoming has been cited as evidence for the long-distance migration of

petroleum (Sheldon, 1967; Claypool et al., 1978). This proposal is supported by satellite imagery, which reveals that the region is pervaded by an extensive network of fractures which may have provided hydraulic continuity over a distance of some 400 km (Wise and Allison, in preparation, 1984).

Despite the low porosity of fractured crystalline rock (~1 percent), the ability to readily transmit groundwater or substances as viscous as petroleum suggests that its permeability can often be quite high (Legrand, 1979; Brace, 1980; Fetter, 1980). This is because the pore geometry of a fracture is inherently more efficient at conducting a fluid per unit porosity than the geometry of an intergranular pore network; thus a rock with a fracture porosity of only .011% can have the same permeability as a silt with a porosity of 50% (Snow, 1968).

The critical factor in any study of the permeability of fractured rock is the size scale of the rock sample under consideration. For example, laboratory measurements of coherent samples that measure several centimeters in size will generally provide an indication of only the minimum permeability of a rock-mass (Brace, 1980). However, at the size scale of interest for most hydrogeologic studies (generally tens of meters to kilometers), virtually all igneous, metamorphic, and consolidated sedimentary rocks on Earth appear to have undergone a considerable degree of fracturing, dramatically increasing their effective permeabilities (Streltsova, 1976; Legrand, 1979; Brace, 1980; Seeburger and Zoback, 1982). Unfortunately, the heterogeneous nature of fractured rock makes any rigorous analysis of this permeability

extremely difficult. Therefore, the failure of broad aerial surveys or isolated test wells to locate these important hydraulic conduits often leads to the false assumption that an apparently coherent rock-mass is impermeable. In no case has this point been made more clearly than in studies undertaken to locate hydraulically isolated geologic formations as safe repositories for the disposal of radioactive waste.

An example of such a study is the Lac du Bonnet batholith (96x25 km) located in southeastern Manitoba. Satellite imagery, aerial photographs, and extensive field studies failed to reveal any major surface fractures in the pluton; indeed, these observations indicated that the batholith had undergone the least deformation of any geologic formation in the region. However, subsequent high resolution seismic reflection profiles revealed that the pluton was far from homogeneous, and contained numerous horizontal fractures and fracture zones of potentially high permeability (Mair and Green, 1981).

The spatial variability of such fractures in deep test wells has also been clearly established. Indeed, for wells separated by only a few kilometers, fracture density and orientation often vary significantly, with some wells exhibiting a fairly uniform distribution of fractures with depth, while others may display concentrations of fractures in densely fractured intervals (Seeburger and Zoback, 1982); Haimson and Doe, 1983). As a result, within a given test area, different drill holes will typically show as much as a four-order-of-magnitude difference in permeability for the same depth interval (Brace, 1980).

Brace (1980) has summarized the results of in situ borehole permeability measurements in crystalline and argillaceous rocks, and has found little evidence for any measurable decline in permeability with depth, especially below 500 m. Indeed, various mine and borehole studies show that there typically exist zones of permeability in the 1-100 md range within the parent rock, even at depths as great as 3.3 km. Based on the results of such studies, and permeabilities inferred from large-scale geologic phenomena (such as earthquakes triggered by fluid injection from nearby wells), Brace (1980) has concluded that at a size scale of kilometers, the average permeability of the top 10 km of the Earth's crust is roughly 10 md.

Given this background, we can now evaluate the requirements and likelihood of pole-to-equator groundwater flow on Mars.

E. The Physical Requirements for Global Groundwater Flow on Mars.

As discussed in the introduction, once the pore volume of the Martian cryosphere has been saturated with ice, the deposition of dust and H₂O in the polar regions will create a situation where the equilibrium depth to the melting isotherm has been exceeded, thus basal melting will begin and continue until such time as the equilibrium depth is once again established. The subsequent deep percolation of meltwater will result in the rise of the local water table in the form of a groundwater mound (Figure 5.7). The gradient in hydraulic head

Figure 5.7. Given a planetary inventory of H_2O which exceeds the pore volume of the Martian cryosphere, the onset of basal melting at polar and temperate latitudes will lead to the rise of the subpolar water table in the form of a groundwater mound. The gradient in hydraulic head created by the presence of the mound will then drive the pole-to-equator flow of groundwater.

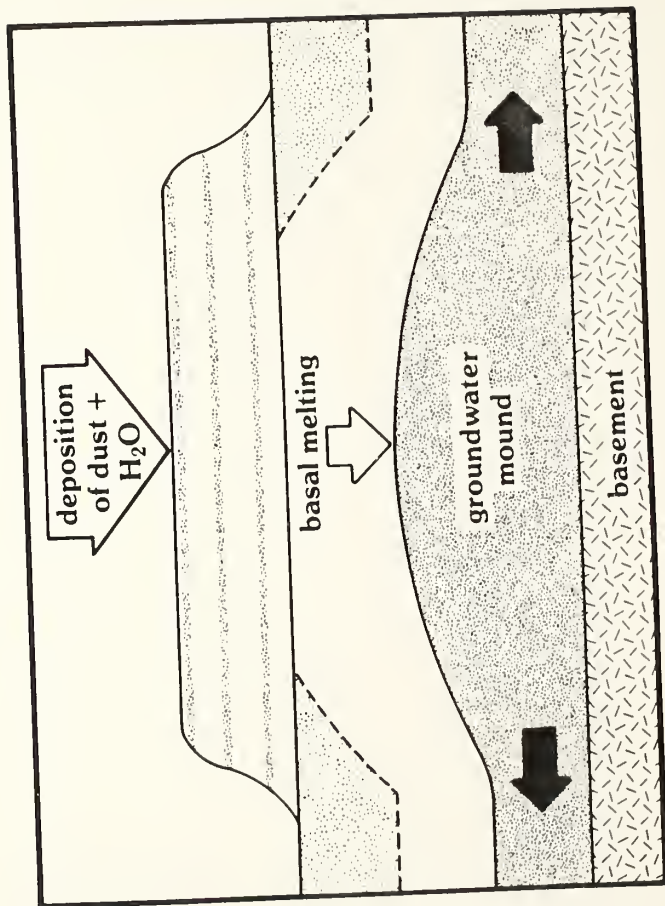


Figure 5.7

created by the presence of the mound will then drive the flow of groundwater from the poles towards the equator, where the system will experience a net discharge as the Martian geothermal gradient pumps H_2O vapor from the warmer depths to the colder near-surface regolith (Figure 5.1c) (Clifford, 1980d, 1982a).

The two primary factors determining the magnitude of subsurface transport are the size of the groundwater mound and the effective permeability of the Martian crust. In the following discussion both the growth of the groundwater mound and the permeability requirements for global groundwater flow will be analysed based on well established terrestrial hydrogeologic models.

1. The growth of the groundwater mound. The problem of groundwater flow on Mars induced by basal melting is analogous to one that has frequently been addressed on Earth: the artificial recharge of an aquifer beneath a circular spreading basin (Hantush, 1967). To obtain an analytical expression for the growth of a groundwater mound beneath a recharging source it is necessary to make a number of simplifying assumptions: (1) the aquifer is homogeneous, isotropic, infinite in areal extent, and rests upon a horizontal and impermeable base; (2) the hydraulic properties of the aquifer are invariant in both space and time; and (3) the downward percolation of water proceeds at a constant rate which is sufficiently small compared to the aquifer permeability that the influx is almost completely refracted in the direction of the local slope of the water table when it reaches the groundwater mound

(Hantush, 1967; Marino, 1975; Schmidtke et al., 1982).

After Hantush (1967), the flow of groundwater in an unconfined aquifer beneath a circular recharging area is described by:

$$\frac{\partial^2 Z}{\partial r^2} + \frac{1}{r} \frac{\partial Z}{\partial r} + \frac{2wv}{kg} = \frac{\epsilon v}{\bar{h}kg} \frac{\partial Z}{\partial t} \quad (\text{V.4})$$

where $Z = h^2 - h_1^2$, r is the radial distance from the center of the mound, h is the height of the water table above the base of the aquifer after an elapsed time t , h_1 is the initial saturated thickness of the aquifer, w is the rate of recharge, k is the aquifer permeability, g is the acceleration of gravity, v is the viscosity of the groundwater, ϵ is the effective porosity, and \bar{h} is a constant of linearization which represents the weighted mean depth of saturation (approximated by $\bar{h} = .5(h_m + h_1)$ (Hantush, 1964)). The boundary and initial conditions that apply to Equation (V.4) are:

$$Z(r, 0) = 0$$

$$\partial Z(0, t) / \partial r = 0$$

$$Z(\infty, t) = 0$$

$$w = w \quad 0 < r < a$$

$$= 0 \quad r > a$$

These conditions correspond to four basic assumptions: (1) that the water table is initially horizontal, (2) the groundwater mound is symmetric about its vertical axis, (3) the effect of recharge on the

shape of the water table is negligible at large radial distances, and (4) the recharge is limited to a circular region of radius a (Hantush, 1967; Marino, 1975; Schmidtke et al., 1982).

Hantush (1967) solved Equation (V.4) using Laplace and zero-ordered Hankel transformations, and found that at a time t the maximum height h_m of the water table (evaluated at $r=0$) could be found from:

$$h_m^2 - h_i^2 = \frac{Qv}{2\pi kg} \left[W(u_o) + (1 - e^{-u_o})/u_o \right] \quad (V.5)$$

where $Q = w \pi a^2$, $u_o = a^2 v \epsilon / 4kght$, and where $W(u_o)$ is the well function for a nonleaky aquifer given by:

$$W(u_o) = \int_{u_o}^{\infty} \frac{e^{-u}}{u} du \quad (V.6)$$

In Table 5.3 groundwater mound heights are presented after as a function of time based on aquifer hydraulic properties which might reasonably characterize the Martian crust. In these calculations the aquifer was assumed to have an initial thickness of 1 km, an effective porosity of .1, and a permeability of 10 md. The size of the recharge area was modeled after the size of the Martian permanent north polar cap ($a = 500$ km); while the assumed recharge volume (Q) of $10^{-1} \text{ km}^3 \text{ H}_2\text{O}/\text{yr}$ is consistent with a basal melting rate of $\sim 10^{-2} \text{ cm}/\text{yr}$. Given these conditions, we find that the resulting groundwater mound could grow to a height of 1 km in $\sim 10^7$ years.

Of course, when the radial discharge of groundwater within the

Table 5.3. Groundwater Mound Heights as a Function of Time.*

Time (yrs)	u_o	$W(u_o)$	Mound Height (m) ($h_m - h_i$)
1×10^6	5.212	9.43×10^{-4}	899
5×10^6	7.369	3.48×10^{-1}	2920
2.5×10^7	8.688	1.95	5370
1.25×10^8	1.159	3.93	7250

*Assumed values: porosity = 10%, permeability = 10^{-2} darcies, basal melting rate = $.1 \text{ km}^3/\text{yr}$, basal melting radius = 500 km, initial aquifer thickness = 1 km.

aquifer finally balances the vertical recharge, a steady-state condition is reached. The permeability requirements necessary to support such steady-state flow can be examined using established models of unconfined and confined steady-state well flow. In this analysis the radius of the well 'a' is analogous to the radius of the recharge (basal melting) area discussed in the previous problem; while, as before, the groundwater mound height is taken to be the difference between the maximum and minimum hydraulic heads. The distance 'R' to the region of lowest hydraulic head represents the separation between the regions of net vertical recharge and discharge, and is taken here to be of the same scale as the planetary radius of Mars. These relationships are illustrated in Figures 5.8 and 5.9.

The appropriate governing equation and boundary conditions for steady unconfined well flow are (Todd, 1959):

$$\frac{\partial}{\partial r} \left[r \frac{\partial (h^2)}{\partial r} \right] = 0 \quad (\text{V.7})$$

$$h^2 = h_i^2 \quad (r=R)$$

$$Q = 2\pi rhv \quad (\text{conservation of mass})$$

where v is the specific discharge (the discharge per unit area) given by Darcy's law:

$$v = - \frac{kg}{\nu} \frac{\partial h}{\partial r} \quad (\text{V.8})$$

Figure 5.8. A schematic diagram of unconfined steady-state well flow.

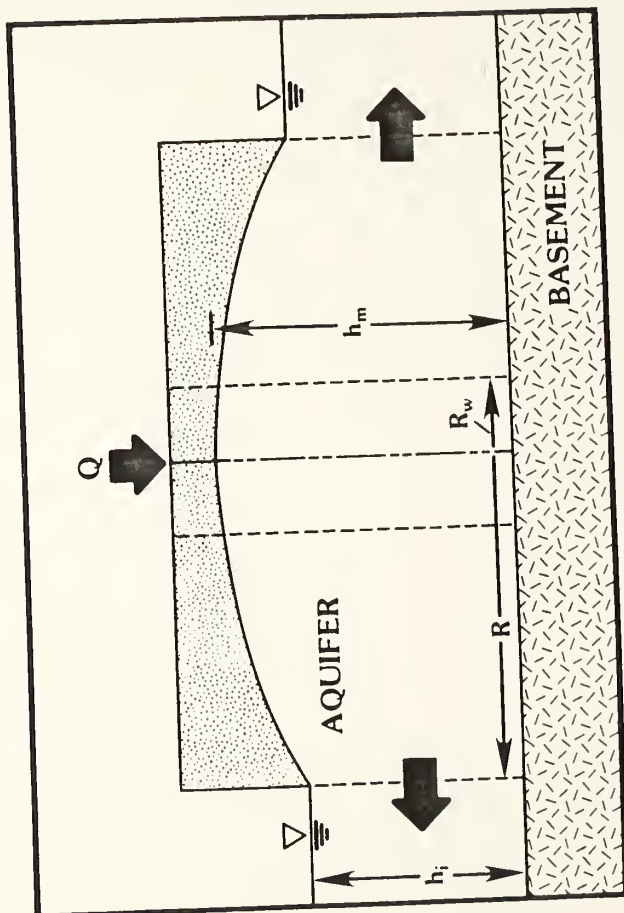


Figure 5.8

Figure 5.9. A schematic diagram of confined steady-state well flow.

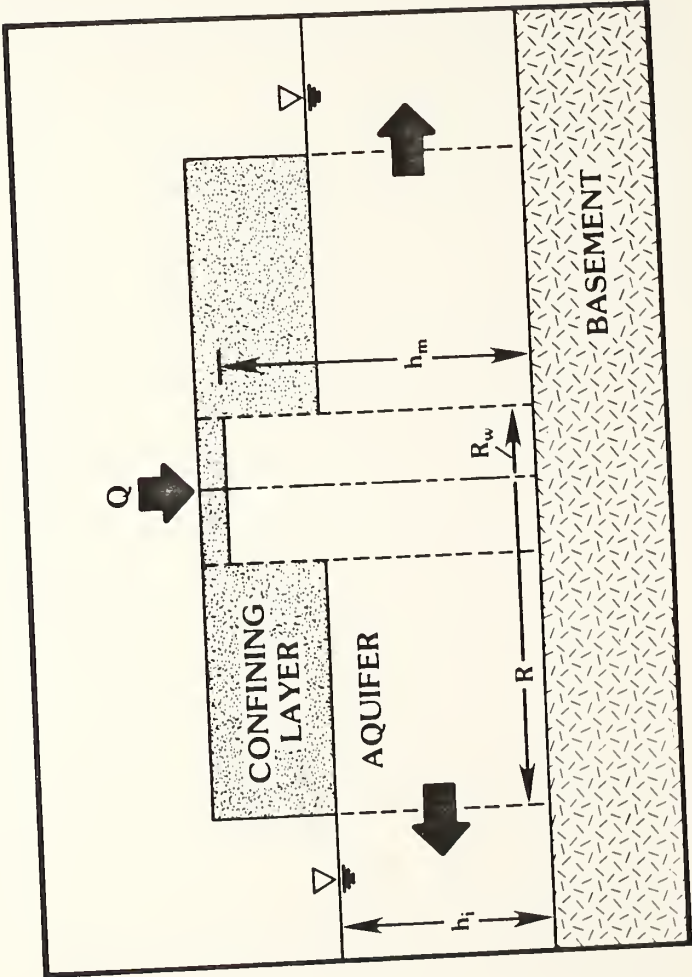


Figure 5.9

Solving Equation (V.7) in light of the above boundary conditions, we obtain:

$$h^2 = h_i^2 + \frac{Qv}{\pi kg} \ln(R/r) \quad (a \leq r) \quad (V.9)$$

Evaluated at $r=a$ Equation (V.9) yields an expression for the maximum hydraulic head:

$$h_m^2 - h_i^2 = \frac{Qv}{\pi kg} \ln(R/a) \quad (V.10)$$

Therefore the necessary permeability requirement for unconfined steady-state well flow is:

$$k = \frac{Qv}{\pi g (h_m^2 - h_i^2)} \ln(R/a) \quad (V.11)$$

Of course, the possibility exists that the groundwater mound of an initially unconfined aquifer could grow to the point of contact with the base of the polar cryosphere; in this event, the aquifer may undergo a transition between confined conditions at the poles to unconfined conditions closer to the equator. Indeed, the planetary inventory of H_2O on Mars may be sufficiently large that the subpermafrost aquifer has been confined at the poles from the very outset of basal melting. Given either case, the solution presented in Equation (V.11) will no longer apply.

To analyse the possibility of confined flow, we solve the steady

confined well equation, given by (Todd, 1959):

$$\frac{\partial}{\partial r} \left[r \frac{\partial h}{\partial r} \right] = 0 \quad (\text{V.12})$$

and which is subject to the boundary conditions:

$$h = h_i \quad (r=R)$$

$$Q = 2\pi r h_i v$$

Solving for the permeability in the same fashion as before, we find:

$$k = \frac{Qv}{2vh_i g(h_m - h_i)} \ln(R/a) \quad (\text{V.13})$$

In Table 5.4, permeabilities calculated from Equations (V.11) and (V.13) are presented for a reasonable range of polar recharge volumes and net hydraulic heads. The results indicate that a recharge volume of 1 km^3 of H_2O per Martian year, introduced into a 1 km thick aquifer at the Martian poles, could drive the flow of a similar volume of water to the Martian equator, given a regolith permeability of 25 darcies and a groundwater mound height of 100 m. If the recharge volume is lowered to 10^{-2} km^3 of H_2O per Martian year, and if we permit a net hydraulic head equivalent to the lithostatic pressure exerted by a 3 km thickness of ice-rich permafrost (i.e., we assume that the aquifer system is confined at the Martian poles such that the flow of groundwater is governed by artesian pressure), then the minimum

Table 5.4. Minimum regolith permeability requirements for steady-state flow.

	Q (km ³ /yr)	Mound Height (m)	k (darcies)
UNCONFINED:	1 10 ⁻²	10 ² 10 ²	25 2.5x10 ⁻¹
CONFINED:	1 10 ⁻² 10 ⁻²	10 ² 10 ² 10 ⁴	26 2.6x10 ⁻¹ 2.6x10 ⁻³

permeability of the regolith required to support a global groundwater flow system falls to approximately 10^{-3} darcies, a value which lies within the lower extreme of permeabilities for fractured igneous and metamorphic rock (Figure 5.10) (Freeze and Cherry, 1979). Yet, even this low value of regolith permeability will permit the pole-to-equator subsurface cycling of some 50 million cubic kilometers of H_2O over the course of Martian geologic history; the equivalent of cycling a 10 meter layer of water, averaged over the Martian surface, once every hundred million years.

The significance of these minimum regolith permeability requirements can be placed in perspective by comparing them with the regolith value assumed by Carr (1979) in his discussion of the possible role of confined aquifers in the formation of Martian flood features. Based on the measured permeability of a number of basalt aquifers on Earth, Carr (1979) concluded that a reasonable estimate for the permeability of the Martian megaregolith might be on the order of 10^3 darcies, a value which is roughly 10^2 to 10^6 times greater than the permeability required to support a Martian groundwater flow system driven by polar basal melting. It is important to note that these numbers represent effective permeabilities. Therefore, if only a very small fraction of the regolith possesses permeabilities as high as that estimated by Carr, then there will be no problem in meeting the minimum effective permeability requirements outlined here.

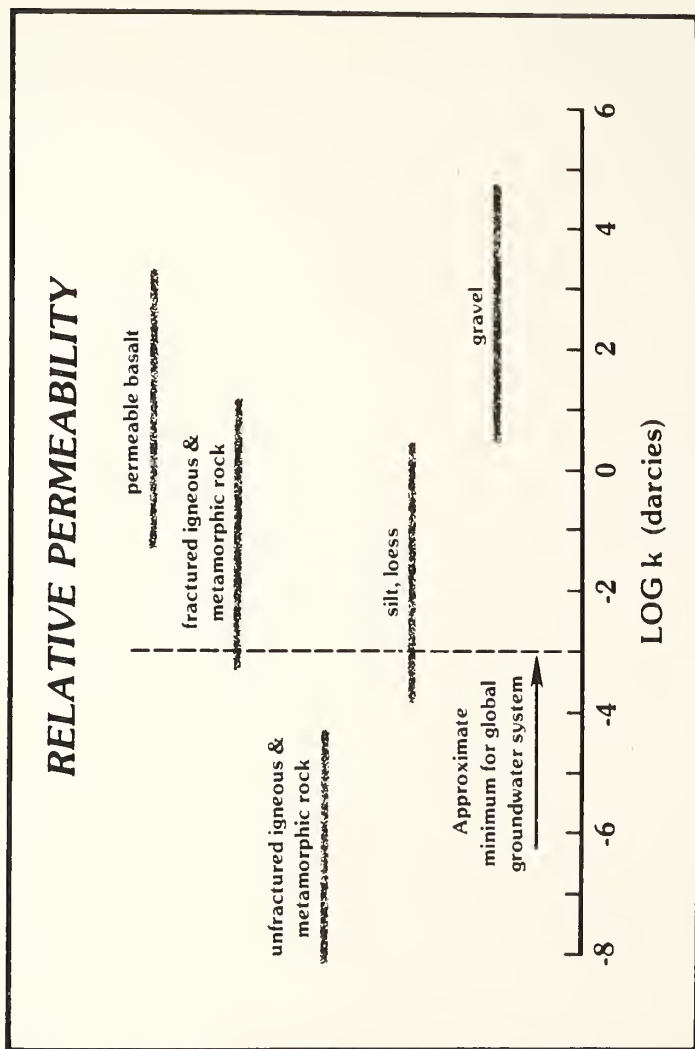


Figure 5.10

F. Conclusions

The calculations presented here, and elsewhere in this dissertation, lead to following conclusions:

1) If the inventory of H_2O on Mars exceeds by more than a few percent the quantity required to saturate the pore volume of the Martian cryosphere, then a subpermafrost groundwater system of global extent will necessarily result.

2) Under present climatic conditions, the inherent instability of equatorial ground ice will lead to a net atmospheric transport of H_2O from the hotter equatorial latitudes to the colder poles (Chapter II).

3) Based on the conditions postulated in (1), the deposition and retention of dust and H_2O in the Martian polar regions will result in basal melting. If the rate of melting balances the current rate of polar deposition on Mars, then as much as $.1-1 \text{ km}^3$ of groundwater may be introduced into the crust each Martian year (Chapter IV).

4) Given an effective regolith permeability typical of the lower extreme for fractured crystalline rock, the gradient in hydraulic head created by the presence of the polar groundwater mound may have lead to significant ($\sim 5 \times 10^7 \text{ km}^3 H_2O$) pole-to-equator subsurface transport over the course of Martian geologic history.

5) At equatorial latitudes, the presence of a geothermal gradient in the Martian crust will result in a net discharge of the groundwater system as H_2O vapor is transported from the warmer (higher vapor pressure) depths to the colder (lower vapor pressure) near surface

regolith. By this process a geothermal gradient of 25 K/km could replenish the equivalent of a 1 km thick layer of ground ice over the history of the planet (Chapter III).

While particular aspects of the climatic model presented in this dissertation may be debated (e.g., the actual porosity and permeability of the regolith, the magnitude of polar deposition, etc.), the occurrence of subsurface groundwater transport on Mars is essentially contingent on a single factor: Does the present planetary inventory of H_2O on Mars exceed, by more than a few percent, the quantity of water which is required to saturate the pore volume of the Martian cryosphere? If so, then basic physics suggests that the climatic model described here should naturally evolve. Given a geologically reasonable description of the Martian crust, the quantity of H_2O transported through the subsurface may then play an important role in the long-term cycling of H_2O between the Martian atmosphere, polar caps, and deep regolith.

G. Notation

a	radius of recharge area, cm.
d	depth to melting isotherm, cm.
g	gravitational acceleration, 371 cm/s^2 .
h	thickness of aquifer, cm.
h_i	initial thickness of aquifer, cm.
h_m	thickness of aquifer at center of groundwater mound, cm.
k	permeability of regolith, 1 darcy = $1 \times 10^{-8} \text{ cm}^2$.
k_{eff}	effective thermal conductivity of regolith, cal/cm-s-K.
K	porosity decay constant, 2.82 km.
Q	recharge volume, cm^3/s .
Q_g	geothermal heat flux, $22 \text{ cal/cm}^2\text{-sec}$.
r	radial distance, cm.
R	radial distance to region of minimum hydraulic head, cm.
R_w	well radius (equivalent to 'a'), cm.
t	time, s.
T_{mp}	melting point temperature, K.
T_{ms}	mean annual surface temperature, K.
u_o	$= a^2 v \epsilon / 4kgt$.
v	specific discharge, $\text{cm}^3/\text{cm}^2\text{-s}$.
w	rate of recharge, cm/s.
$W(u_o)$	well function.
z	depth, cm.
Z	$h_m^2 - h_i^2$.

Greek letters:

- ϵ effective porosity, cm^3/cm^3 .
- $\phi(0)$ surface porosity, cm^3/cm^3 .
- $\phi(z)$ porosity at depth 'z', cm^3/cm^3 .
- ν viscosity of water, cm^2/s .

B I B L I O G R A P H Y

- Adams, J. M., C. Breen, and C. Riekel, The diffusion of intralamellar water in 23.3 A Na-montmorillonite:pyridine/H₂O intercalate by quasielastic neutron scattering, Clays Clay Miner., 27, 140-144, 1979.
- Alkire, B. D. and O. B. Andersland, The effect of confining pressure on the mechanical properties of sand-ice materials, J. Glaciology, 12, 469-481, 1973.
- Allen, C. C., Areal distribution of Martian rampart craters, Icarus, 39, 111-123, 1979a.
- Allen, C. C., Volcano-ice interactions on Mars, J. Geophys. Res., 84, 8048-8059, 1979b.
- Alzaydi, A. A., C. A. Moore, and I. S. Rai, Combined pressure and diffusional transition region flow of gases in porous media, Amer. Inst. Chem. Eng. J., 24, 35-43, 1978.
- Anders, E. and T. Owen, Mars and Earth: Origin and abundance of volatiles, Science, 198, 453-465, 1977.
- Anderson, D. M., S. Gaffney, and P. F. Low, Frost phenomena on Mars, Science, 155, 319-322, 1967.
- Anderson, D. M., M. J. Schwarz, and A. R. Tice, Water vapor adsorption by sodium montmorillonite at -5°C, Icarus, 34, 638-644, 1978.
- Anderson, D. M., and A. R. Tice, The analysis of water in the Martian regolith, J. Mol. Evol., 14, 33-38, 1979.

- Arvidson, R. E., K. A. Goettel, and C. M. Hohenberg, A post-Viking view of Martian geologic evolution, Rev. Geophys. Space Phys., 18, 565-603, 1980.
- Baird, A. K., B. C. Clark, H. J. Rose, Jr., K. Keil, R. P. Christian, and J. L. Gooding, Minerological and petrological implications of Viking geochemical results from Mars: Interim Report, Science, 194, 1288-1293, 1976.
- Ballou, E. V., P. C. Wood, T. Wydeven, M. E. Lehwalt, and R. E. Mack, Chemical interpretation of Viking Lander 1 life detection experiment, Nature, 271, 644-645, 1978.
- Barker, E. S., R. A. Shorn, A. Woszczyk, R. G. Tull, S. J. Little, Mars: detection of atmospheric water vapor during the southern hemisphere spring and summer season, Science, 170, 1308-1310, 1970.
- Barrer, R. M., Surface and volume flow in porous media, in: The Solid-Gas Interface 2 (E. A. Flood, ed.), 557-609, Dekker, New York, 1967.
- Binder, A. B., On the internal structure of a Moon of fission origin, J. Geophys. Res., 85, 4872-4880, 1980.
- Binder, A. B. and M. A. Lange, On the thermal history, thermal state, and related tectonism of a Moon of fission origin, J. Geophys. Res., 85, 3194-3208, 1980.
- Blasius, K. R., J. A. Cutts and A. D. Howard, Topography and stratigraphy of Martian polar layered deposits, Icarus, 50, 140-160, 1982.
- Blasius, K. R., and J. A. Cutts, Global patterns of crater ejecta morphology on Mars, Bull. Amer. Astron. Soc., 13, 709, 1981.

- Blasius, K. R., J. A. Cutts, B. H. Lewis, and A. V. Vetrone, Three Simple Classes of Martian Crater Ejecta -- I. Global relationships of class abundance to latitude and terrain, Reports of Planetary Geology Program 1981, NASA TM 84211, 93-95, 1981.
- Bouyoucos, G. J., Effect of water vapor and capillary moisture in soils, J. Agr. Res., 5, 141-172, 1915.
- Brace, W. F., Permeability of crystalline and argillaceous rocks, Int. J. Rock Mech. Min. Sci. & Geomech Abstr., 17, 241-251, 1980.
- Brace, W. F., Resistivity of saturated crustal rocks to 40 km based on laboratory measurements in: The Structure and Physical Properties of the Earth's Crust, Geophysical Monograph Series, (J. G. Heacock, ed.), AGU, Washington, D.C. 243-255, 348p, 1971.
- Brass, G. W., Stability of brines on Mars, Icarus, 42, 20-28, 1980.
- Bredehoeft, J. D., A. W. England, D. B. Stewart, N. J. Trask, and I. J. Winograd, Geologic disposal of high-level radioactive wastes -- Earth-science perspectives, U. S. Geolog. Survey Circ. 779, 15 p, 1978.
- Breed, C. S., M. J. Grolier, and J. F. McCauley, Morphology and distribution of common 'sand' dunes on Mars: Comparison with the Earth, J. Geophys. Res., 84, 8183-8204, 1979.
- Bullock, P., and A. J. Thomasson, Rothamsted studies of soil structure II: Measurement and characterisation of macroporosity by image analysis and comparison with data from water retention measurements, J. Soil Sci., 30, 391-413, 1979.

- Cadle, R. D., Particle Size, Reinhold Publishing Corp., New York, 1965.
- Carr, M. H., The Surface of Mars, Yale University Press, New Haven, 232 pp., 1981.
- Carr, M. H., Formation of Martian flood features by release of water from confined aquifers, J. Geophys. Res., 84, 2995-3007, 1979.
- Carr, M. H. and G. G. Schaber, Martian permafrost features, J. Geophys. Res., 82, 4039-4055, 1977.
- Carr, M. H., L. S. Crumpler, J. A. Cutts, R. Greeley, J. E. Guest, and H. Masursky, Martian impact craters and emplacement of ejecta by surface flow, J. Geophys. Res., 82, 4055-44065, 1977.
- Carr, M. H. and G. D. Clow, Martian channels and valleys: Their characteristics, distribution, and age, Icarus, 48, 91-117, 1981.
- Carrier, W. D., III, Lunar soil grain size distribution, The Moon, 6, 250-263, 1973.
- Cary, J. W., Soil moisture transport due to thermal gradients: Practical aspects, Soil Sci. Soc. Amer. Proc., 30, 428-433, 1966.
- Cary, J. W., Onsager's relation and the non-isothermal diffusion of water vapor, J. Phys. Chem., 67, 126-129, 1963.
- Chamberlain, E. J. and A. J. Gow, Effect of freezing and thawing on the permeability and structure of soils, in: Int. Symp. on Ground Freezing, Ruhr University, Bochum, Germany, 1978.
- Chylek, P. and G. W. Grams, Scattering by nonspherical particles and optical properties of Martian dust, Icarus, 36, 198-203, 1978.
- Clark, B.C., Implications of abundant hygroscopic minerals in the Martian regolith, Icarus, 34, 645-665, 1978.

- Clark, B. C. and D. C. Van Hart, The salts of Mars, Icarus, 45, 370-378, 1981.
- Clark, B. C., A. K. Baird, H. J. Rose, P. Toulmin, K. Keil, A. J. Castro, W. C. Kelliher, C. D. Rowe, and P. H. Evans, Inorganic analysis of Martian surface samples at the Viking landing sites, Science, 194, 1283-1288, 1976.
- Claypool, G. E., A. H. Love, and E. K. Maughan, Organic geochemistry, incipient metamorphism, and oil generation in black shale members of phosphoria formation, western interior United States, The Amer. Assoc. Petrol. Geol. Bull., 62, 98-120, 1978.
- Clifford, S. M. and D. Hillel, The stability of ground ice in the equatorial region of Mars, J. Geophys. Res., 88, 2456-2474, 1983.
- Clifford, S. M., Mechanisms for the vertical transport of H₂O within the Martian regolith, in: Papers presented to the Conf. on Planet. Volatiles, LPI Contribution 488, 23-24, Alexandria, 1982a.
- Clifford, S. M., Polar basal melting on Mars, NASA TM 85127, 261-263, 1982b.
- Clifford, S. M., A model for the climatic behavior of water on Mars, in: Papers presented to the Third Int. Colloq. on Mars, LPI Contribution 441, 44-45, Pasadena, 1981a.
- Clifford, S. M., A pore volume estimate of the Martian megaregolith based on a lunar analog, in: Papers presented to the Third Int. Colloq. on Mars, LPI Contribution 441, 46-48, Pasadena, 1981b.

- Clifford, S. M., Mars: Polar cap basal melting as a recharge mechanism for a global groundwater system, Lunar Plan. Sci. Conf. XI, 165-167, 1980a.
- Clifford, S. M., Chasma Boreale (85 N, 0 W): Remnant of a Martian jokulhlaup? BAAS, 12, 678, 1980b.
- Clifford, S. M., A model for the removal and subsurface storage of a primitive Martian ice sheet, NASA TM 82385, 405-407, 1980c.
- Clifford, S. M., Mars: Ground ice replenishment from a subpermafrost groundwater system, in: Proc. 3rd Colloq. Planet. Water, 68-75, Niagara Falls, 1980d.
- Clifford, S. M., and R. L. Huguenin, The H₂O mass balance on Mars: Implications for a global subpermafrost groundwater flow system, NASA TM 81776, 144-146, 1980.
- Couture, R. A., M. G. Seitz, and M. J. Steindler, Sampling of brine in cores of Precambrian granite from northern Illinois, J. Geophys. Res., 88, 7331-7334, 1983.
- Cutts, J. A., Nature and origin of layered deposits of the Martian polar regions, J. Geophys. Res., 78, 4231, 1973a.
- Cutts, J. A., Wind erosion in the Martian polar regions, J. Geophys. Res., 78, 4211-4221, 1973b.
- Cutts, J. A. and B. H. Lewis, Models of climate cycles recorded in Martian polar layered deposits, Icarus, 50, 216-244, 1982.

- Cutts, J. A., K. R. Blasius and W. J. Roberts, Evolution of Martian polar landscapes: Interplay of long-term variations in perennial ice cover and dust storm intensity, J. Geophys. Res., 84, 2975-2993, 1979.
- Cutts, J. A., G. A. Briggs, M. H. Carr, R. Greeley and H. Masursky, North polar region of Mars: Imaging results from Viking 2, Science, 194, 1329-1337, 1976.
- Davies, D. W., The vertical distribution of Mars water vapor, J. Geophys. Res., 84, 2875-2879, 1979.
- Davies, D. W., C. B. Farmer, and D. D. LaPorte, Behavior of volatiles in Mars' polar areas: A model incorporating new experimental data, J. Geophys. Res., 82, 3815-3822, 1977.
- Davies, D. M. and L. A. Wainio, Measurements of water vapor in Mars' antarctic, Icarus, 45, 216-230, 1981.
- de Marsily, G., E. Ledoux, A. Barbreaux, and J. Margat, Nuclear waste disposal: Can the geologist guarantee isolation, Science, 197, 519-527, 1977.
- Dence, M. R., R. A. F. Grieve, and P. B. Robertson, Terrestrial impact structures: Principal characteristics and energy considerations, in: Impact and Explosion Cratering, (D. J. Roddy, R. O. Pepin, and R. B. Merrill, eds.), pp. 247-276, Pergamon Press, New York, 1977.
- de Vries, D. A., in: Physics of Plant Environment, (Van Wijk, W. R., ed.), Chpt. 7, North-Holland Publ. Co., Amsterdam, 1963.

- de Vries, D.A., in: Heat and Mass Transfer in the Biosphere, (de Vries, D.A. and N.H. Afgan, eds.), Chpt. 1, Scripta Book Co., Washington, D.C., 1975.
- Dewart, G., Seismic Evidence of a Wet Zone Under the West Antarctic Ice Sheet, J. Glaciology, 16, 73-88, 1976.
- Diamond, S., Pore size distribution in clays, Clays and Clay Minerals, 18, 7-23, 1970.
- Diamond, S., Microstructure and pore structure of impact-compacted clays, Clays and Clay Minerals, 19, 239-249, 1971.
- Diamond, S., and W. L. Dolch, Generalized log-normal distribution of pore sizes in hydrated cement paste, J. Colloid Interface Sci., 38, 234-244, 1972.
- Dickey, P. A., Patterns of chemical composition in deep subsurface waters, Am. Assoc. Petroleum Geologists Bull., 50, 2472-2478, 1966.
- Dzurisin, D. and K. R. Blasius, Topography of the Polar Layered Deposits of Mars, J. Geophys. Res., 80, 3286-3306, 1975.
- Eakin, T. E, A regional interbasin groundwater system in the White River area, southeastern Nevada, Water Resources Research, 2, 251-271, 1966.
- Eldridge, B. D., and L. F. Brown, The effect of cross sectional pore shape on Knudsen diffusion in porous material, AIChE J., 22, 942-944, 1976.
- Evans, R. B. III, G. M. Watson, and E. A. Mason, Gaseous diffusion in porous media at uniform pressure, J. Chem. Phys., 35, 2076-2083, 1961.

- Fanale, F. P., Mars: The role of the regolith in volatile storage and atmospheric evolution, in: Proc. Symp. on Plan. Atmos., 167-170, Ottawa, 1977.
- Fanale, F. P., Martian volatiles: Their degassing history and geochemical fate, Icarus, 28, 179-202, 1976.
- Fanale, F. P., J. R. Salvail, W. B. Banerdt and R. S. Saunders, Mars: The regolith-atmosphere-cap system and climate change, Icarus, 50, 381-407, 1982.
- Fanale, F. P. and W. A. Cannon, Adsorption on the Martian regolith, Nature, 230, 502-504, 1971.
- Fanale, F. P. and W. A. Cannon, Exchange of adsorbed H₂O and CO₂ between the regolith and atmosphere of Mars caused by changes in surface insolation, J. Geophys. Res., 79, 3397-3402, 1974.
- Fanale, F. P. and W. A. Cannon, Mars: CO₂ adsorption and capillary condensation on clays. Significance for volatile storage and atmospheric history, J. Geophys. Res., 84, 8404-8414, 1979.
- Farmer, C. B., Global exchange of water vapor on Mars, in: Proc. Symp. on Plan. Atmos., 151-157, Ottawa, 1977.
- Farmer, C. B., Liquid water on Mars, Icarus, 28, 279-289, 1976.
- Farmer, C. B. and P. E. Doms, Global and seasonal variation of water vapor on Mars and the implications for permafrost, J. Geophys. Res., 84, 2881-2888, 1979.
- Farmer, C. B., D. W. Davies, and D. D. LaPorte, Mars: Northern summer ice cap - water vapor observations from Viking 2, Science, 194, 1339-1340, 1976.

- Fetter, C. W. Jr., Applied Hydrology, Charles E. Merrill Publishing Co., Columbus, Ohio, 488 p., 1980.
- Flasar, M. F. and R. M. Goody, Diurnal behaviour of water on Mars, Planet. Space Sci., 24, 161-181, 1976.
- Foster, R. N. and J. B. Butt, A computational model for the structure of porous materials employed in catalysis, AIChE J., 12, 182-185, 1966.
- Freeze, R. A. and J. A. Cherry, Groundwater, Prentice-Hall, Toronto, 604 p., 1979.
- Fuller, A. O. and R. B. Hargraves, Some consequences of a liquid water saturated regolith in early Martian history, Icarus, 34, 614-621, 1978.
- Galfi, J. and G. Kovacs, Hydrology of Solid Rock Terrains, in: Subterranean Hydrology, Water Resources Publications, Littleton, Colorado, 801-966, 977 p., 1981.
- Gilliland, E. R., R. F. Baddour, G. P. Perkinson, and K. J. Sladek, Diffusion on surfaces. I. Effect of concentration on the diffusivity of physically adsorbed gases, Ind. Eng. Chem. Fundam., 13, 95-100, 1974.
- Gooding, J. L., Chemical weathering on Mars: Thermodynamic stabilities of primary minerals (and their alteration products) from mafic igneous rocks, Icarus, 33, 483-513, 1978.
- Graf, D. L., Chemical osmosis, reverse chemical osmosis, and the origin of subsurface brines, Geochimica et Cosmochemica Acta, 46, 1431-1448, 1982.

- Greeley, R., Silt-Clay aggregates on Mars, J. Geophys. Res., 84, 6248-6254, 1979.
- Greeley, R. and P. D. Spudis, Volcanism on Mars, Rev. Geophys. Space Phys., 19, 13-41, 1981.
- Grenfell, T. C. and G. A. Maykut, The optical properties of ice and snow in the Arctic basin, J. Glaciology, 18, 445-463, 1977.
- Gurnis, M., Martian cratering revisited: Implications for early geologic evolution, Icarus, 48, 62-75, 1981.
- Haimson, B. C. and T. W. Doe, State of stress, permeability, and fractures in the precambrian granite of northern Illinois, J. Geophys. Res., 88, 7355-7371, 1983.
- Hantush, M. S., Growth and decay of groundwater-mounds in response to uniform percolation, Water Resources Research, 3, 227-234, 1967.
- Hantush, M. S., Hydraulics of wells, in Advances in Hydroscience, (V.T. Chow, ed.), Academic Press, New York, 1964.
- Harris, H. J. H., K. Cartwright, and T. Torii, Dynamic chemical equilibrium in a polar desert pond: A sensitive index of meteorological cycles, Science, 204, 301-303, 1979.
- Hartmann, W. K., Martian surface and crust: Review and synthesis, Icarus, 19, 550-575, 1973.
- Hillel, D., Fundamentals of Soil Physics, Academic Press, New York, 1980.
- Hodges, C. A. and H. J. Moore, The subglacial birth of Olympus Mons and its aureoles, J. Geophys. Res., 84, 8061-8074, 1979.

- Hoffert, M. I., A. J. Callegari, C. T. Hsieh, and W. Ziegler, Liquid water on Mars: An energy balance climate model for CO₂/H₂O atmospheres, Icarus, 47, 112-129, 1981.
- Hotiguchi, Y., R. R. Hudgins, and P. L. Silveston, Effect of surface heterogeneity on surface diffusion in microporous solids, Can. J. Chem. Eng., 49, 76-87, 1971.
- Horz, F., R. Ostertag, and D. A. Rainey, Bunte breccia of the Ries: Continuous deposits of large impact craters, Rev. Geophys. Space Phys., 21, 1667-1725, 1983.
- Howard, A. D., Origin of the stepped topography of the Martian poles, Icarus, 34, 581-599, 1978.
- Howard, A. D., J. A. Cutts and K. L. Blasius, Stratigraphic relationships within Martian polar cap deposits, Icarus, 50, 161-215, 1982.
- Howard, A. D., Etched plains and braided ridges of the south polar region of Mars: Features produced by basal melting of ground ice? NASA TM 84211, 286-288, 1981.
- Hubbert, M. K. and W. W. Rubey, Role of fluid pressure in mechanics of overthrust faulting, Bull. Geol. Soc. Am., 70, 115, 1959.
- Huguenin, R. L., Mars: Chemical weathering as a massive volatile sink, Icarus, 28, 203-212, 1976.
- Huguenin, R. L., The formation of goethic and hydrated clay minerals on Mars, J. Geophys. Res., 79, 3895-3905, 1974.

- Hunt, C. B. and T. W. Robinson, Possible interbasin circulation of ground water in the southern part of the great basin, U. S. Geological Survey Prof. Paper 400-B, 273, 1960.
- Hyndman, R. D. and D. W. Hyndman, Water saturation and high electrical conductivity in the lower continental crust, in: Earth and Planetary Science Letters 4, North-Holland Publishing Co., Amsterdam, pp. 427-432, 1968.
- Ingersol, A. P., Mars: The Case Against Permanent CO₂ Frost Caps, J. Geophys. Res., 79, 3405-3410, 1974.
- Irani, R. R. and C. F. Callis, Particle Size: Measurement, Interpretation, and Application, John Wiley and Sons, Inc., New York, 1963.
- Jackson, R. D., D. A. Rose, and H. L. Penman, Circulation of water in soil under a temperature gradient, Nature, 205, 314-316, 1965.
- Jacobsen, S. B. and G. J. Wasserburg, The mean age of mantle and crustal reservoirs, J. Geophys. Res., 84, 7411-7426, 1979a.
- Jacobsen, S. B. and G. J. Wasserburg, Nd and Sr isotopic study of the Bay of Islands Ophiolite Complex and the evolution of the source of midocean ridge basalts, J. Geophys. Res., 84, 7429-7443, 1979b.
- Jaeger, J. C., Application of the theory of heat conduction to geothermal measurements, in: Terrestrial Heat Flow, pp. 7-23, Geophys. Monograph Series No. 8, AGU, 1965.

- Jakosky, B. M. and C. B. Farmer, The seasonal and global behavior of water vapor in the Mars atmosphere: Complete global results of the Viking atmospheric water detector experiment, J. Geophys. Res., 87, 2999-3019, 1982.
- James, P. B., G. Briggs, J. Barnes, and A. Spruck, Seasonal recession of Mars' south polar cap as seen by Viking, J. Geophys. Res., 84, 2889-2921, 1979.
- Johansen, L. A., Martian splash cratering and its relation to water, in: Proc. Second Colloq. on Plan. Water and Polar Processes, 109-110, Hanover, 1978.
- Johansen, L. A., Mud as a pseudo-rock magma, in: Proc. Third Colloq. on Plan. Water, 113-116, Niagara Falls, 1980.
- Johnson, M. F. L. and W. E. Stewart, Pore structure and gaseous diffusion in solid catalysts, J. Catalysis, 4, 248-252, 1965.
- Jones, K. L., R. E. Arvidson, E. A. Guinness, S. L. Bragg, S. D. Wall, C. E. Carlston, and D. G. Pidek, One Mars year: Viking lander imaging observations, Science, 204, 799-806, 1979.
- Jury, W. A. and J. Letey, Jr., Water vapor movement in soil: Reconciliation of theory and experiment, Soil Sci. Soc. Amer. J., 43, 823-827, 1979.
- Keihm, S. J. and M. G. Langseth, Lunar microwave brightness temperature observations reevaluated in the light of the Apollo program findings, Icarus, 24, 211-230, 1975.
- Kieffer, H. H., Mars south polar spring and summer temperatures: A residual CO₂ frost, J. Geophys. Res., 84, 8263-8288, 1979.

- Kieffer, H. H., Soil and surface temperatures at the Viking landing sites, Science, 194, 1344-1346, 1976.
- Kieffer, H. H., T. Z. Martin, A. R. Peterfreund, B. M. Jakosky, E. D. Miner, and F. D. Palluconi, Thermal and albedo mapping of Mars during the Viking primary mission, J. Geophys. Res., 82, 4249-4291, 1977.
- Kieffer, H. H., Chase, S. C., Jr., Martin, T. Z., Miner, E. D. and Palluconi, F. D., Martian north pole summer temperatures: Dirty water ice, Science, 194, 1341-1344, 1976.
- King, E. A., Jr., J. C. Butler, and M. F. Carman, The lunar regolith as sampled by Apollo 11 and Apollo 12: Grain size analysis, modal analysis, and origin of particles, Proc. Second Lunar Sci. Conf., 1, 737-746, 1971.
- King, E. A., Jr., J. C. Butler, and M. F. Carman, Chondrules in Apollo 14 samples and size analysis of Apollo 14 and 15 fines, Proc. Third Lunar Sci. Conf., 1, 673-686, 1972.
- Ladanyi, B. and F. H. Sayles, General report session II: Mechanical properties, Engineering Geology, 13, 7-18, 1979.
- Langseth, M. G., S. J. Keihm, and K. Peters, The revised lunar heat flow values, Lunar Sci. Conf. VII, 474-475, 1976.
- Laughlin, J., NMR investigation of mobility of water sorbed by clay minerals, North Dakota Water Resources Research Inst., Fargo, May, 1977.
- Lawrence, G. P., D. Payne, and D. J. Greenland, Pore size distribution in critical point and freeze dried aggregates from clay subsoils, J. Soil Sci., 30, 499-516, 1979.

- Lebofsky, L. A., Stability of frosts in the solar system, Icarus, 25, 205-217, 1975.
- Lederberg, J. and C. Sagan, Microenvironments for life on Mars, Proc. Nat. Acad. Sci., USA, 48, 1473-1475, 1962.
- Lee, W. H. K. and S. Uyeda, Review of heat flow data, in: Terrestrial Heat Flow, pp. 87-190, Geophys. Monograph Series No. 8, AGU, 1965.
- Legrand, H., Evaluation techniques of fractured-rock hydrology, J. of Hydrology, 43, 333-346, 1979.
- Leighton, R. B. and B. C. Murray, Behavior of CO₂ and other volatiles on Mars, Science, 153, 136-144, 1966.
- Leovy, C., Mars ice caps, Science, 154, 1178-1179, 1966.
- Luchitta, B. K., Mars and Earth: Comparisons of cold-climate features, Icarus, 45, 264-303, 1981.
- Mair, J. A. and A. G. Green, High-resolution seismic reflection profiles reveal fracture zones within a 'homogeneous' granite batholith, Nature, 294, 439-442, 1981.
- Malin, M. C., Salt weathering on Mars, J. Geophys. Res., 79, 3888-3894, 1974.
- Marino, M. A., Artificial groundwater recharge, I. Circular recharging area, J. of Hydrology, 25, 201-208, 1975.
- Mason, E. A., A. P. Malinauskas, and R. B. Evans III, Flow and diffusion of gasses in porous media, J. Chem. Phys., 46, 3199-3216, 1967.

- Masursky, H., J. M. Boyce, A. L. Dial, G. G. Schaber, and M. E. Strobell, Classification and time of formation of Martian channels based on Viking data, J. Geophys. Res., 82, 4016-4038, 1977.
- Matson, S. L. and J. A. Quinn, Knudsen diffusion through noncircular pores: Textbook errors, AIChE J., 23, 768-770, 1977.
- Maxwell, J. C., Influence of depth, temperature, and geologic age on porosity of quartzose sandstones, Bull. Amer. Assoc. Petrol. Geol., 48, 697-709, 1964.
- McElroy, M. B., T. Y. Kong, and Y. L. Yung, Photochemistry and evolution of Mars' atmosphere: A Viking perspective, J. Geophys. Res., 82, 4379-4388, 1977.
- McGaw, R., Heat Conduction in Saturated Granular Materials, Highway Res. Brd. - Special Rept. 103, 114-131, 1969.
- Mellor, M. and R. Testa, Effect of temperature on the creep of ice, J. Glaciology, 8, 131-145, 1969.
- Melosh, H. J., Cratering Mechanics - observational, experimental and theoretical, Ann. Rev. Earth Planet. Sci., 8, 65-93, 1980.
- Mifflin, M. D. and J. W. Hess, Regional carbonate flow systems in Nevada, J. of Hydrology, 43, 217-237, 1979.
- Miller, K. J., The effects of temperature and salinity on the phospholipid and fatty acid composition of a halotolerant, psychotolerant bacterium isolated from Antarctic Dry Valley soil, Ph.D. thesis, University of Massachusetts, Amherst, Massachusetts, 1984.

- Mooney, R. W., A. G. Kennen, and L. A. Wood, Adsorption of montmorillonite. I: Heat of desorption and application of BET theory, J. Am. Chem. Soc., 74, 1367-1374, 1952.
- Moore, H. J., C. R. Spitzer, K. Z. Bradford, P. M. Cates, R. E. Hutton, and R. W. Shorthill, Sample fields of the Viking Landers, physical properties, and aeolian processes, J. Geophys. Res., 84, 8365-8377, 1979.
- Moore, H. J., R. E. Hutton, R. F. Scott, C. R. Spitzer, and R. W. Shorthill, Surface materials of the Viking landing sites, J. Geophys. Res., 82, 4497-4523, 1977.
- Morris, D. A. and A. I. Johnson, Physical properties of rock and soil materials, as analyzed by the hydrologic laboratory of the U.S. Geological Survey 1948-60, Geological Survey Water-Supply Paper 1839-D, U.S.G.S., 1967.
- Morris, E. C., Recent (?) surface alterations from subsurface sources in the Olympus Mons area, Reports of Planetary Geology Program, 1979-1980, NASA TM 81776, 162-163.
- Mouginis-Mark, P., Ejecta emplacement and modes of formation of Martian fluidized ejecta craters, Icarus, 45, 60-76, 1981.
- Mouginis-Mark, P., Martian fluidized crater morphology: Variations with crater size, latitude, altitude, and target material, J. Geophys. Res., 84, 8011-8022, 1979.
- Murray, B. C., W. R. Ward, and S. C. Yeung, Periodic insolation variations on Mars, Science, 180, 638-640, 1973.

- Murray, B. C., L. A. Soderblom, J. A. Cutts, R. P. Sharp, D. J. Milton, and R. B. Leighton, Geological framework of the south polar region of Mars, Icarus, 17, 328-345, 1972.
- Mutch, T. A., R. E. Arvidson, J. W. Head, K. L. Jones, and R. S. Saunders, The Geology of Mars, Princeton University Press, Princeton, 400 p., 1976.
- Nekut, A., J. E. P. Connerney, and A. F. Kuches, Deep crustal electrical conductivity: Evidence for water in the lower crust, Geophys. Res. Let., 4, 239-242, 1977.
- Neukum, G. and D. U. Wise, Mars: A standard crater curve and possible new time scale, Science, 194, 1381-1387, 1976.
- Newman, A. C. D. and A. J. Thomasson, Rothamsted studies of soil structure III: Pore size distributions and shrinkage processes, J. Soil Sci., 30, 415-439, 1979.
- Nuegebauer, G., G. Munch, H. Kieffer, S. C. Chase Jr., and E. Miner, Mariner 1969 infrared radiometer results: Temperatures and thermal properties of the Martian surface, Astron. J., 76, 719-728, 1971.
- Nummedal, D., Clay aggregates on Earth, Mars and Io, NASA TM 84211, 216-218, 1981.
- Nye, J. F., The motion of ice sheets and glaciers, J. Glaciology, 3, 493-507, 1959.
- Nye, J. F., Water Flow in Glaciers: Jokulhlaups, Tunnels and Veins, J. Glaciology, 17, 181-207, 1976.

- Nye, J. F. and F. C. Frank, Hydrology of the intergranular veins in a temperate glacier, Symposium on the Hydrology of Glaciers, 157-161, Cambridge 1969.
- Nye, J. F. and S. Mae, The effect of non-hydrostatic stress on intergranular water veins and lenses in ice, J. Glaciology, 11, 81-101, 1972.
- O'Keefe, J. D. and T. J. Ahrens, Impact cratering: The effect of crustal strength and planetary gravity, Rev. Geophys. Space Phys., 19, 1-12, 1981.
- Orowan, E., Remarks at joint meeting of the British Glaciological Society, the British Rheologists Club and the Institute of Metals, J. Glaciol., 1, 231-236, 1949.
- Oswald, G. K. A. and G. de Q. Robin, Lakes beneath the Antarctic ice sheet, Nature, 245, 251-254, 1973.
- Pandey, G. N., M. R. Tek, and D. L. Katz, Diffusion of fluids through porous media with implications in petroleum geology, Amer. Assn. Petrol. Geol. Bull., 58, 291-303, 1974.
- Pang, K., J. M. Ajello, C. W. Hord, and W. G. Egan, Complex refractive index of Martian dust: Mariner 9 ultraviolet observations, Icarus, 27, 55-67, 1976.
- Parameswaran, V. R. and S. J. Jones, Triaxial testing of frozen sand, J. Glaciology, 27, 147-155, 1981.
- Paterson, W. S. B., The Physics of Glaciers, 2nd edition, Pergamon Press, New York, 380 p., 1981.

- Pettijohn, F. J., Sedimentary Rocks, 3rd edition, Harper & Row, New York, 1975.
- Philip, J. R. and deVries, D. A., Moisture movement in porous materials under temperature gradients, Trans. AGU, 38, 222-228, 1957.
- Pieri, D., Geomorphology of Martian valleys, Ph.D. Thesis, Cornell University, Ithaca, New York, 1979.
- Pieri, D., Martian valley morphology, distribution, age and origin, Science, 210, 895-897, 1980.
- Pohl, J., D. Stoffler, H. Gall, and K. Ernst, The Ries impact crater, in: Impact and Explosion Cratering, (D. J. Roddy, R. O. Pepin, and R. B. Merrill, Eds.), pp. 343-404, Pergamon Press, New York, 1977.
- Pollack, J. B. and D. C. Black, Implications of the gas compositional measurements of Pioneer Venus for the origin of planetary atmospheres, Science, 205, 56-59, 1979.
- Pollack, J. B., D. Colburn, F. M. Flasar, R. Kahn, C. E. Carlston, and D. Pidek, Properties and effects of dust particles suspended in the Martian atmosphere, J. Geophys. Res., 82, 2929-2945, 1979.
- Ponzi, M., J. Papa, J. B. P. Rivarola, and G. Zgrabich, On the surface diffusion of adsorbable gases through porous media, AIChE J., 23, 347-352, 1977.
- Puri, B. R., and K. Murari, Studies in surface area measurements of soils: 1. Comparison of different methods, Soil Sci., 96, 331-336, 1963.

- Quirk, J. P. and C. R. Panabokke, Pore volume-size distribution and swelling of natural soil aggregates, J. Soil Sci., 13, 71-81, 1962.
- Raymond, C. F. and W. D. Harrison, Some observations on the behavior of the liquid and gas phases in temperate glacier ice, J. Glaciology, 14, 213-233, 1975.
- Remick, R. R. and C. J. Geankoplis, Binary diffusion of gasses in capillaries in the transition region between Knudsen and molecular diffusion, Ind. Eng. Chem. Fund., 12, 214-220, 1973.
- Ricq-de Bouard, M., Migration of insoluble and soluble impurities in temperate ice: Study of a vertical ice profile through the Glacier du Mont de Lans (French Alps), J. Glaciology, 18, 231-238, 1977.
- Rieke, H. H., III, and G. V. Chilingarian, Compaction of Argillaceous Sediments, Elsevier Scientific Publishing Co., New York, 1974.
- Robin, G. deQ, D. J. Drewry, and D. T. Meldrum, International studies of ice sheet and bedrock, Phil. Trans. R. Soc. Land. B. 279, 185-196, 1977.
- Ross, W. D., Lognormal distribution functions for particle size, J. Colloid Interface Sci., 67, 181-182, 1978.
- Roszbacher, L. A., Models of ground ice distribution and landform evolution on Mars, presented at: The 14th Binghamton Geomorphology Symposium, Buffalo, 1983.
- Roszbacher, L. A. and S. Judson, Ground ice on Mars: Inventory, distribution, and resulting landforms, Icarus, 45, 39-59, 1981.
- Rothfield, L. B., Gaseous counterdiffusion in catalyst pellets, AIChE J., 9, 19-24, 1963.

- Rothlisberger, H., Water Pressure in Intra- and Subglacial Channels, J. Glaciology, 11, 177-203, 1972.
- Rowell, R. L., and A. B. Levit, Distribution functions for colloidal particles, J. Colloid Interface Sci., 34, 585-590, 1970.
- Sanger, F. J. and P. J. Hyde, Proceedings: USSR contribution, Permafrost, Second International Conference, NAS Wash. D.C. 866p, 1978.
- Sanger, F. J. and C. W. Kaplar, Plastic Deformation of Frozen Soils, Proceedings: Permafrost International Conference, NAS-NRC, Pub #1287, 305-315.
- Satterfield, C. N., Mass Transfer in Heterogeneous Catalysis, M.I.T. Press, Cambridge, 1970.
- Satterfield, C. N. and P. J. Cadle, Diffusion and flow in commercial catalysts at pressure levels about atmospheric, J. Ind. Eng. Chem. Fundam., 7, 202-209, 1968.
- Saunders, R. S. and L. A. Johansen, Latitudinal distribution of flow-ejecta morphology types on the ridged plains of Mars, Proc. of the 3rd Colloq. Planet. Water, 97-98, Niagara Falls, 1980.
- Schultz, P. H., Atmospheric effects on Martian ejecta emplacement, J. Geophys. Res., 84, 7669-7687, 1979.
- Schultz, P. H. and A. B. Lutz-Garihan, Equatorial paleo-poles on Mars, Proceedings of the Twelfth Lunar and Planetary Science Conference, 946-948, 1981.

- Schultz, P. H. and A. B. Lutz-Garihan, Ancient polar locations on Mars: evidence and implications, Proceedings of the Third International Colloquium on Mars, 229-231, 1981.
- Schultz, P. H. and A. B. Lutz-Garihan, Grazing Impacts on Mars: A record of lost satellites, Proceedings of the Thirteenth Lunar and Planetary Science Conference, Part I, J. Geophys. Res., 87, Supplement, A84-A96, 1982.
- Schultz, P. H. and H. Glicken, Impact crater and basin control of igneous processes on Mars, J. Geophys. Res., 84, 8033-8047, 1979.
- Schwartz, F. A. and J. E. Brow, Diffusivity of H₂O vapor in gasses, J. Chem. Physics, 19, 640-646, 1951.
- Scott, D. H. and M. H. Carr, Geologic map of Mars, U. S. Geol. Survey, Misc. Inv. Map I-1083, 1978.
- Scott, D. S. and F. A. L. Dullien, Diffusion of ideal gasses in capillaries and porous solids, AIChE J., 8, 113-117, 1962.
- Seeburger, D. A. and M. D. Zoback, The distribution of natural fractures and joints at depth in crystalline rock, J. Geophys. Res., 87, 5517-5534, 1982.
- Shankland, T. J. and M. E. Ander, Electrical conductivity, temperatures, and fluids in the lower crust, J. Geophys. Res., 88, 9475-9484, 1983.
- Sharp, R. P., Ice on Mars, J. Glaciology, 13, 173-185, 1974.
- Sharp, R. P., Mars: Troughed terrain, J. Geophys. Res., 78, 4063-4072, 1973a.

- Sharp, R. P., Mars: Fretted and chaotic terrains, J. Geophys. Res., 78, 4073-4083, 1973b.
- Sharp, R. P., Mars: South polar pits and etched terrain, J. Geophys. Res., 78, 4222-4230, 1973c.
- Sheldon, R. P., Long-distance migration of oil in Wyoming, The Mountain Geologist, 4, 53-65, 1967.
- Shorthill, R. W., H. J. Moore II, R. F. Scott, R. E. Hutton, S. Liebes Jr., and C. R. Spitzer, The "soil" of Mars, Science, 194, 91-97, 1976a.
- Shorthill, R. W., H. J. Moore II, R. E. Hutton, R. F. Scott, and C. R. Spitzer, The environs of Viking 2 Lander, Science, 194, 1309-1318, 1976b.
- Shreve, R. L., Movement of water in glaciers, J. Glaciology, 11, 205-214, 1972.
- Sills, I. D., L. A. G. Aylmore, and J. P. Quirk, An analysis of pore size in illite-kaolinite mixtures, J. Soil Sci., 24, 480-490, 1973.
- Sladek, K. J., The surface mobility of hydrogen chemisorbed on platinum, Sc.D. thesis, Dept. Chem. Eng., Massachusetts Institute of Technology, Cambridge, Mass., 1967.
- Sladek, K. J., E. R. Gilliland, and R. F. Baddour, Diffusion on surfaces II: Correlation of diffusivities of physically and chemically adsorbed species, Ind. Eng. Chem. Fund., 13, 100-105, 1974.
- Smoluchowski, R., Water on Mars, in: Report of 1967 Summer "TYCHO" Meeting, TG #31, Hanover, New Hampshire, 1967.

- Smoluchowski, R., Mars: Retention of ice, Science, 159, 1348-1350, 1968.
- Snow, D. T., Rock fracture spacings, openings, and porosities, Journal of the Soil Mechanics and Foundations Division, ASCE, 94, 73-91, 1968.
- Soderblom, L. A. and D. B. Wenner, Possible fossil H₂O liquid-ice interface in the Martian crust, Icarus, 34, 622-637, 1978.
- Soderblom, L. A., C. D. Condit, R. A. West, B. M. Herman, and T. J. Kreidler, Martian planetwide crater distributions: Implications for geologic history and surface processes, Icarus, 22, 239-263, 1974.
- Soderblom, L. A., M. C. Malin, J. A. Cutts, and B. C. Murray, Mariner 9 observations of the surface of Mars in the north polar region, J. Geophys. Res., 78, 4197, 1973.
- Soderblom, L. A., T. J. Kreidler, and H. Masursky, Latitudinal distribution of a debris mantle on the Martian surface, J. Geophys. Res., 78, 4117-4122, 1973.
- Squyres, S. W., The evolution of dust deposits in the Martian north polar region, Icarus, 40, 244-261, 1979.
- Stacey, F. D., Physics of the Earth, 2nd ed., John Wiley & Sons, New York, 414 p. 1969.
- Streltsova, T. D., Hydrodynamics of groundwater flow in a fractured formation, Water Resources Research, 12, 405-414, 1976.
- Taylor, S. T. and J. W. Cary, Linear equations for the simultaneous flow of matter and energy in a continuous soil system, Soil Sci. Soc. Proc., 167-172, 1964.

- Thakur, S. C., L. F. Brown, and G. L. Haller, Gas-adsorbate collisional effects and surface diffusion in porous materials, AICHE J., 26, 355-363, 1980.
- Thomas, P., Present wind activity on Mars: Relation to large latitudinally zoned sediment deposits, J. Geophys. Res., 87, 9999-10,008, 1982.
- Thomas, P., North-south asymmetry of eolian features in Martian polar regions: analysis based on crater-related wind markers, Icarus, 48, 76-90, 1981.
- Thompson, B. G., A. Nekut, and A. F. Kuckes, A deep crustal electromagnetic sounding in the Georgia Piedmont, J. Geophys. Res., 88, 9461-9473, 1983.
- Tittman, B. R., Brief note for consideration of active seismic exploration on Mars, J. Geophys. Res., 84, 7940-7942, 1979.
- Todd, D., K., Groundwater hydrology, John Wiley & Sons, New York, 336 p. 1959.
- Toksoz, M. N., Planetary seismology and interiors, Rev. Geophys. Space Phys., 17, 1641-1655, 1979.
- Toksoz, M. N. and A. T. Hsui, Thermal history and evolution of Mars, Icarus, 34, 537-547, 1978.
- Toon, O. B., J. B. Pollack, W. Ward, J. A. Burns, and K. Bilski, The astronomical theory of climatic change on Mars, Icarus, 44, 552-607, 1980.

- Toulmin, P., III, A. K. Baird, B. C. Clark, K. Keil, H. J. Rose (Jr.), P. H. Evans, and W. C. Kelliher, Geochemical and mineralogical interpretation of the Viking inorganic chemical results, J. Geophys. Res., 82, 4625-4634, 1977.
- Wako, N. and J. M. Smith, Diffusion in catalyst pellets, Chem. Eng. Sci., 17, 825-834, 1962.
- Wall, S. D., Analysis of condensates formed at the Viking 2 lander site: The first winter, Icarus, 47, 173-183, 1981.
- Wallace, D. and C. Sagan, Evaporation of ice in planetary atmospheres: Ice-covered rivers on Mars, Icarus, 39, 385-400, 1979.
- Waller, R. M., Water-sediment ejections in: The Great Alaska Earthquake of 1964, Hydrology, Part A, 97-116, 1968.
- Walker, J. C. G., Evolution of the Atmosphere, Macmillan Publishing Co., New York, 318 p., 1977.
- Waltz, J. P., Groundwater, in: Introduction to Physical Hydrology, Chapter 6.1., (R. J. Chorley ed.), Methuen & Co. Ltd., Harper & Row Publishers, Inc., Great Britain, 122-130, 211 p., 1969.
- Ward, W. R., Climatic variations on Mars. 1. Astronomical theory of insolation, J. Geophys. Res., 79, 3375-3386, 1974.
- Ward, W. R., B. C. Murray, and M. C. Malin, Climatic variations on Mars. 2. Evolution of carbon dioxide atmosphere and polar caps, J. Geophys. Res., 79, 3387-3395, 1974.
- Wechsler, A. E., and P. E. Glaser, Pressure effects on postulated lunar materials, Icarus, 4, 335, 1965.

- Weeks, W. and A. Assur, The mechanical properties of sea ice, CRREL Report II-C3, 94 pg. 1967.
- Weertman, J., Creep of ice, in: Physics and Chemistry of Ice, (E. Whalley, S. J. Jones, and L. W. Gold, eds.), Royal Society of Canada, Ottawa, Canada, 320-337, 1973.
- Weertman, J., General theory of water flow at the base of a glacier or ice sheet, Rev. Geophys. Space Phys., 10, 287-333, 1972.
- Weertman, J., Effect of a basal water layer on the dimensions of ice sheets, J. Glaciology, 6, 191-207, 1966.
- Weertman, J., Mechanism for the formation of inner moraines found near the edge of cold ice caps and ice sheets, J. Glaciology, 3, 965-978, 1961a.
- Weertman, J., Equilibrium profile of ice caps, J. Glaciology, 3, 953-964, 1961b.
- Wheeler, A., Reaction rates and selectivity in catalyst pores, in: Catalysis, 2, (P. H. Emmett, ed.), Reinhold, New York, 105, 1955.
- Wilhelms, D. E., Comparison of Martian and lunar multiringed circular basins, J. Geophys., Res., 78, 4084-4095, 1973.
- Winograd, I. J., Interbasin movement of ground water at the Nevada test site, Nevada, U. S. Geological Survey Prof. Paper 450-C, 108-111, 1962.
- Wise, D. U., M. P. Golembeck, and G. E. McGill, Tharsis province of Mars: Geologic sequence, geometry, and a deformation mechanism, Icarus, 38, 456-472, 1979.

Woronow, A., Preflow stresses in Martian rampart ejecta blankets: A means of estimating water content, Icarus, 45, 320-330, 1981.

Youngquist, G. R., Diffusion and flow of gasses in porous solids, in: Flow Through Porous Media, pp. 58-69, Amer. Chem. Soc. Pub., 1970.

Do, or do not. There is no such thing as 'try'.

Yoda, The Empire Strikes Back

A human being should be able to change a diaper, plan an invasion, butcher a hog, conn a ship, design a building, write a sonnet, balance accounts, build a wall, set a bone, comfort the dying, take orders, give orders, cooperate, act alone, solve equations, analyze a new problem, pitch manure, program a computer, cook a tasty meal
Specialization is for insects.

Lazurus Long, Time Enough for Love

